IMPORTANCE OF SUBSTRATE RECOGNITION AND METAL IONS IN THE RIBONUCLEASE P CATALYSIS

by

Wan Hsin Lim

A dissertation submitted in partial fulfillment
of the requirements for the degree of
Doctor of Philosophy
(Chemical Biology)
in The University of Michigan
2011

Doctoral Committee:

Professor Carol A. Fierke, Chair
Professor David R. Engelke
Professor Anna K. Mapp
Professor Nil G. Walter
Associate Professor Bruce Allan Palfey

I dedicate my thesis to my parents.

I want to thank my father, Soo Kim Lim, who has taught me to do my best in anything I wish to accomplish. I also want to thank my mother, Khoo Eng Ching, for her endless love and patience.

ACKNOWLEGMENTS

First of all, I would like to thank Carol for being a great advisor and I truly enjoy working with you for the past few years. I have learned a great deal from you to be a critical thinking scientist and I hope to bring this knowledge with me to my next career path. I want to acknowledge the past and present members of Fierke group, including Dr. John Hsieh, Dr. Kristin J. Smith-Koutmou, Xin Liu, Mike Howard and Chen Yu, who provide a fun and stimulating learning environment. John and Kristin have been helpful colleagues and taught me a lot about RNase P when I first join the P group. Xin Liu, Mike and Chen Yu, thanks for your encouragement and support when I feel disappointed with my experiments. I also want to acknowledge RNase P subgroup members (Dr. David R. Engelke, Dr. Micheal Marvin, Dr. Scott Walker, Dr. John Hsieh, Dr. Kristin J. Smith-Koutmou, Xin Liu, Mike Howard and Chen Yu) for helpful discussion. I want to thank Dr. Jane Jackman for her MRPP1 protein plasmid, so I could move forward with my mitochondrial RNase P project. To my husband, Xiaoliang Yin, thank you for your love, patience and support. Most importantly, I want to thank my parents and siblings for loving and taking care of my daughter, Julia, while I was completing my thesis.

TABLE OF CONTENTS

LIST OF FIGURES

LIST OF TABLES

ABSTRACT

Ribonuclease P (RNase P) catalyzes the 5' maturation of precursor-tRNA (pre-tRNA). Bacterial RNase P is composed of a catalytic RNA subunit (P RNA) and one small protein subunit (P protein); both subunits contribute to substrate recognition. Previous studies suggest that RNase P recognizes the tertiary fold of the tRNA moiety and the leader of pre-tRNA interacts with the P protein subunit. Bioinformatics analyses of 5' leader sequences in 160 bacterial genomes demonstrated species-dependent sequence preferences near the pre-tRNA cleavage site, suggesting the formation of sequence-specific interactions with the 5' leader. Here we demonstrate that the affinity of *Bacillus subtilis* RNase P for pre-tRNA^{Asp} is modulated by the leader sequence; pre-tRNA^{Asp} with adenosine and uracil at the N(-2) and N(-3) positions in the leader, respectively, have the highest binding affinity. Mutagenesis data indicate that a non-conserved nucleotide, G319 at J18/2 of the P RNA, forms a trans Watson-Crick-sugar-edge interaction with the base at N(-2) of pre-tRNA. Additionally, N61, R62 and R65 residues at the "RNR" motif of the P protein indirectly affect the N(-3) sequence selectivity. Sequence alterations at the N(-3) nucleotide also modulate the Ca^{2+}-dependence of pre-tRNA affinity, suggesting that interactions with this nucleotide stabilize the active conformation of RNase P.

The newly identified human mitochondrial (mtRNase P) and chloroplast RNase P are “proteinaceous” RNase P enzymes that are proposed to consist of three (MRPP1, MRPP2 and MRPP3) and one (PRORP1) protein subunits, respectively. MRPP3 is homologous to the PRORP1 protein. Sequence alignments of MRPP3 homologs indicate eight conserved residues, including cysteine, aspartate and histidine residues, located in the C-terminal domain, which have been proposed to coordinate catalytic and/or structural metal ions. Here, we demonstrate that the MRPP3 subunit is catalytically active alone *in vitro*, and thereby is the catalytic subunit of the human mtRNase P. Introducing the MRPP1 and MRPP2 subunits to MRPP3 subunit moderately reduces the human mtRNase P catalytic activity. Furthermore, two essential metal ions have been identified in MRPP3, including a minimum of one Mg^{2+} that activates catalysis and a tightly bound zinc ion that could serve to stabilize the structure of MRPP3 required for catalysis.

CHAPTER 1

INTRODUCTION

The biogenesis of tRNA requires a complex set of processing events to convert the primary transcript precursor tRNA (pre-tRNA) to a mature functional tRNA (2). Mature tRNA is required by all organisms and plays an integral role in translation by carrying amino acids to the ribosome to make protein. The maturation of the pre-tRNA consists of removal of both the 5' and 3' termini of the RNA chain (Figure 1-1). Maturation of the 3' terminus of pre-tRNA in bacteria varies from species to species. In *Escherichia coli* (*E. coli*), at least five different endo- and exonucleases (RNase II, D, PH, BN, and T) are involved, while in *Bacillus subtilis* (*B. subtilis*) only a single endonuclease (RNase Z) is required to catalyze the maturation of the 3' terminus of pre-tRNA (3-5). Eukaryotes from *Drosophila* to humans also utilize tRNase Z to catalyze the 3' end maturation of pre-tRNA (6-8). However, the maturation of 5' terminus of pre-tRNA requires only a single enzyme, called ribonuclease P (RNase P), and this is the only conserved enzyme in the pre-tRNA maturation pathway (9-11).

RNase P is a ribonucleoprotein complex that catalyzes the 5' end maturation of pre-tRNA to form mature tRNA and 5' leader. RNase P is conserved in all domains of life but the composition of RNase P varies from Bacteria, to Achaea

and Eucarya (12-14). Most known RNase Ps have a single large catalytic RNA (~130 kDa, P RNA) component that associates with either one, ≥four and ≥nine proteins in Bacteria, Achaea and Eukarya, respectively. In the presence of high monovalent salt and magnesium concentrations, bacterial and some archeal P RNAs are catalytically active *in vitro* in the absence of P protein (15,16). In addition, some eukaryal P RNAs, such as *Homo sapiens* P RNA, have been suggested to have some catalytic activity *in vitro* (17). However, recent studies have demonstrated that RNase P in certain organelles, including human and *Arabidopsis thaliana* mitochondria, consists of only protein subunits (18,19). These protein-based organellar RNase P enzymes carry out a similar function as the RNA-based RNase P enzyme. It is of great interest to understand how a "proteinaceous RNase P" evolved to retain the catalytic and structural roles of the RNA-mediated RNase P.

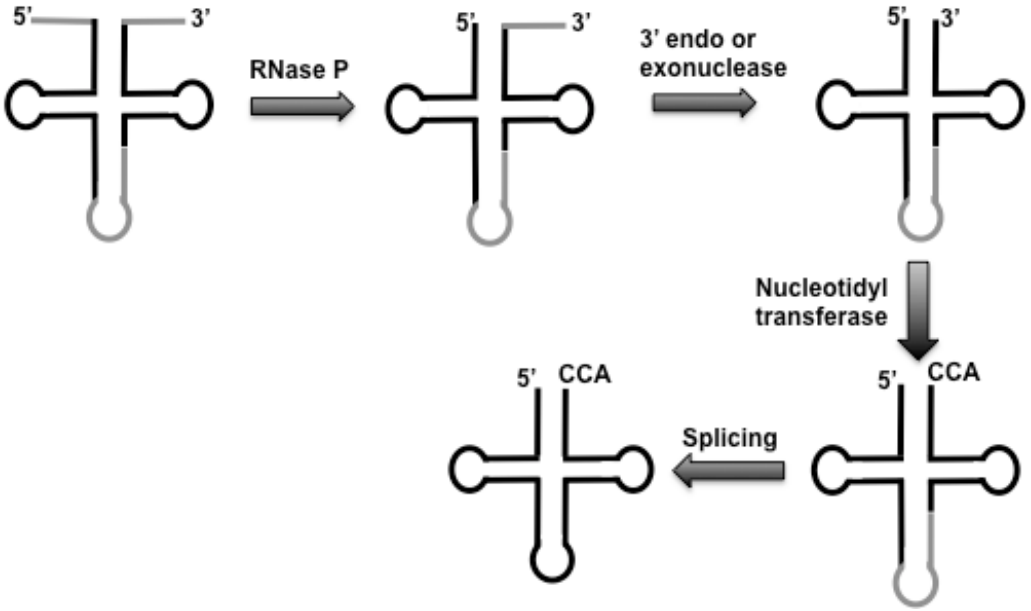

Figure 1-1: Model of pre-tRNA maturation pathway adapted from Hartmann R.K. et. al., 1999 (1). The mature tRNA is shown in black, while the 5' leader, 3' trailer and intervening sequences are in grey.

Bacterial RNase P

Structure of RNase P RNA

Bacterial RNase P RNA is encoded by the rnpB gene and is 300 to 400 nucleotides long. Based on phylogenetic comparative analysis, bacterial P RNA shows significant secondary structure diversity and has little sequence conservation among the 300 to 400 nucleotides (20). The secondary structure of the bacterial P RNA is broadly grouped into two archetypes, type A (ancestral-like) represented by *E. coli* and type B (*Bacillus*-like) represented by *B. subtilis*. X-ray crystal structures of both the type A (from *Thermotoga maritima*) and B (from *Bacillus stearothermophilus*) P RNAs have been solved (21,22). Both the type A and B P RNAs have a common core structure that is highly conserved in all three domains of life, including two independently folding domains, termed the specificity (S), and catalytic (C) domains (Figure 1-2). The conserved core structure of the S-domain is a non-helical structure that consists of the J11/12 and J12/11 connectors and the P9, P10 and P11 stems. The conserved core structure of the C-domain includes the coaxial stacks of P1/P4/P5, P2/P3 and P8/P9 (23). In the conserved core structures of the S and C-domains in bacterial P RNA, about half of the nucleotides are conserved.

Hydroxyl radical footprinting, crosslinking and affinity cleavage experiments illustrate that the C-domain of the *B. subtilis* P RNA contacts and forms a specific complex with the P protein, which is consistent with the crystal structure of *T. maritima* RNase P complex (24-27). This C-domain-P protein complex able to cleave the single stranded RNA and hairpin loop 3' end with similar efficiency as

the *B. subtilis* RNase P holoenzyme, suggesting that the active site is located at the C-domain of the P RNA (24). However, *B. subtilis* RNase P holoenzyme binds and cleaves pre-tRNA 100- to 500-fold better than the C-domain-P protein complex, indicating that the S-domain of the P RNA contributes to the pre-tRNA specificity and affinity (24). 21 of about 200 nucleotides in the universal core of all known P RNA sequences are conserved and situated at the J3/4-P4-J2/4, J15/2 and J11/12-J12/13 (Figure 1-3A) (28). Eleven of the 21 conserved nucleotides are located within helix P4, suggesting that the conserved nucleotides in helix P4 play important structural and/or functional roles in RNase P catalysis (20). Furthermore, the *E. coli* and *B. subtilis* RNase Ps are able to interchange their P protein subunits while retaining some catalytic activity *in vitro* (15). These results suggest that bacterial P RNAs retain a similar tertiary structural and the region of P RNA-P protein contacts is highly conserved (Figure 1-3B).

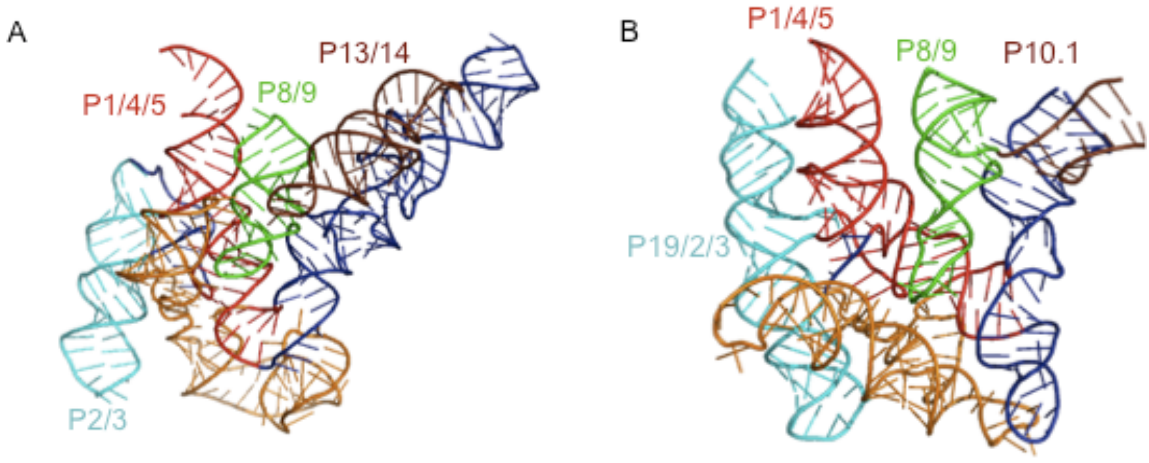

Figure 1-2: Crystal structures of bacterial RNase P RNAs adapted from Kazantsev, A.V. et. al., 2005 and Torres-Larios, A. et. al., 2005 (21,22). (A) *T. maritima* and (B) *B. stearothermophilus* P RNAs. The catalytic domain of P RNA is highlighted with red, orange and cyan stems. The specificity domain is highlighted with green, brown and blue stems.

Figure 1-3: Secondary structure of *T. maritima* RNase P RNA adapted from Reiter, N.J. et. al., 2010 (22,25). (A) Sequences that are conserved in all known bacterial P RNAs are shown in capital letters (20). The C-domain of *T. maritima* P RNA includes P2/P3, P1/P4/P5, P15/16, P17 and P18 which are shown in green, blue, yellow and purple, respectively. The S-domain of the *T. maritima* P RNA consists of P8/P9, P10, P11, P12 and P13/14 which are colored green, orange and pink, correspondingly. (B) Proposed sites of the P RNA contacts with the pre-tRNA and P protein based on the biochemical and crosslinking data as well as the recent crystal structural of the *T. maritima* RNase P·tRNA and RNase P·5' leader complex (25,26). The P RNA contacts with mature tRNA, 5' leader, 3'CCA and P protein are highlighted with in pink, orange, green and light blue, respectively.

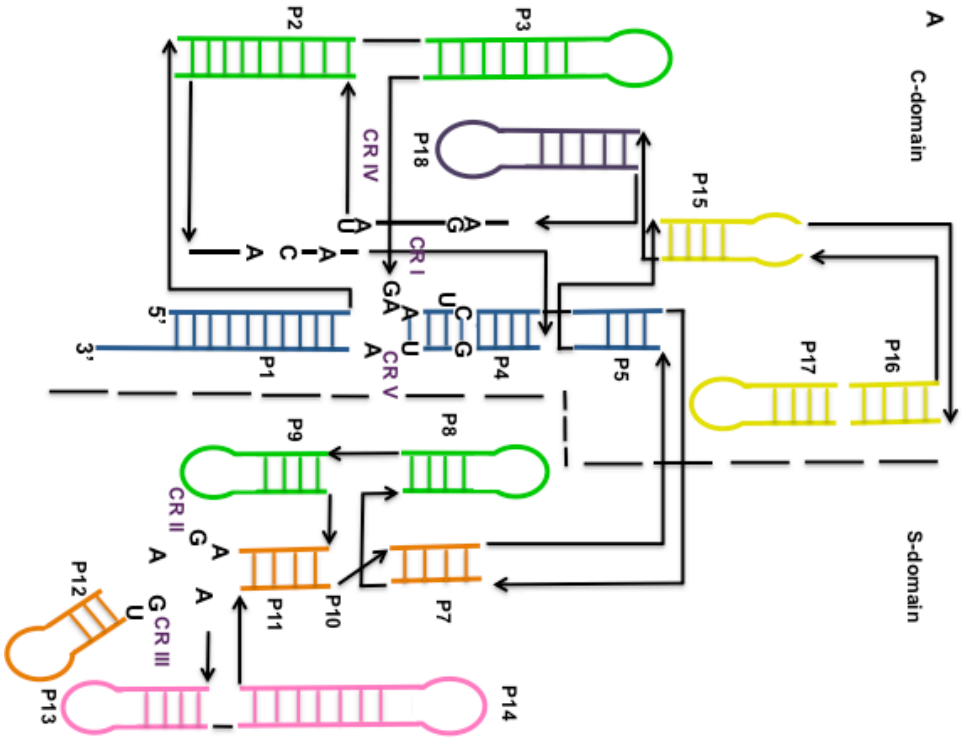
A
C-domain
S-domain
P1
P2
P3
P4
P5
P7
P8
P9
P10
P11
P12
P13
P14
P15
P16
P17
P18
CR I
CR II
CR III
CR IV
CR V
5'
3'

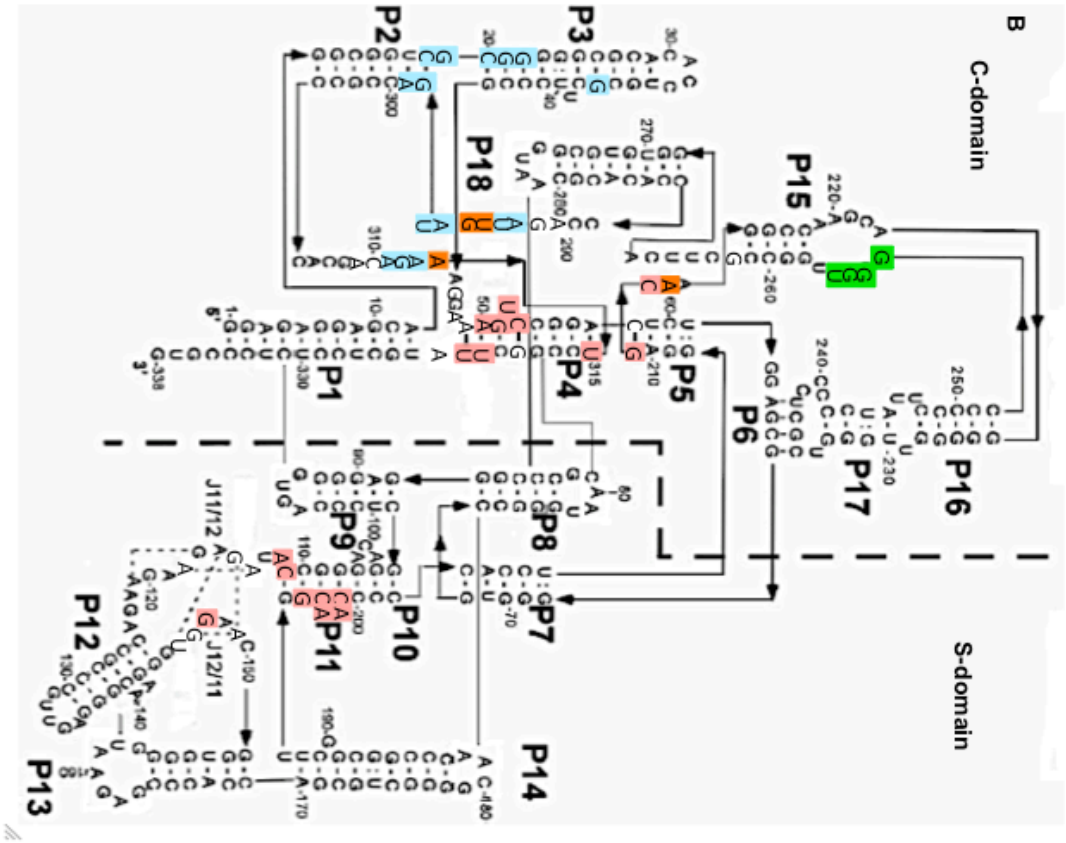
B
C-domain
S-domain
P1
P2
P3
P4
P5
P6
P7
P8
P9
P10
P11
P12
P13
P14
P15
P16
P17
P18

Indeed, based on the crystal structure of *T. maritima* RNase P, the region where P RNA contacts P protein is conserved in all bacterial species (25).

Structure of RNase P Protein

Bacterial RNase P is composed of only a single small P protein (~14 kDa) that associates with P RNA (130 kDa), which makes bacterial RNase P the simplest system for studying structure and function (29,30). Phylogenetic comparison analysis indicates low sequence similarity between the ancestral-like (type A) and *Bacillus*-like (type B) P proteins (31,32). However, X-ray crystal structures of P protein indicate a structural similarity between the homologous type A (from *T. maritima*) and type B (from *B. subtilis* and *S. aureus*) P proteins (33-35). Both type A and type B P proteins adopt an α-β sandwich fold with a topology $\alpha\beta\beta\beta\alpha\beta\alpha$ and have a highly conserved surface charge. There are three potential RNA binding motifs in the bacterial P protein, including an unusual βαβ crossover, a central β-cleft formed by four anti-parallel β strands flanked by an α-helix, and a putative "metal binding" loop (Figure 1-4). The βαβ crossover has a sequence termed the RNR motif (RNRXKRXXR) that binds proximal to the highly conserved elements of the helix P4 of P RNA, which is proposed to form the enzyme's active site (26,36).

Although the P protein does not play a direct role in catalysis, it is required for *in vivo* function of RNase P. Binding studies indicate that the P protein enhances the affinity of RNase P for pre-tRNA by 10^4 fold and increases the magnesium affinity of the RNase P·pre-tRNA complex (37,38). Cross-linking and time-

resolved fluorescence resonance energy transfer (trFRET) experiments have demonstrated that the central β-cleft of the P protein is located near the 5' leader from the third to the seventh nucleotide away from the cleavage site (27,39), consistent with the recent structure of the RNase P-tRNA-5" leader complex (25). The affinity of the RNase P·pre-tRNA complex for Mg^{2+} ions increases by > 2-fold as the 5' leader lengthens from 2 to 5 nucleotides, indicating that the P protein also enhances the Mg^{2+} binding site in the RNase P·pre-tRNA complex (40). Moreover, the highly conserved "RNR" sequence motif stabilizes the active conformation of RNase P by augmenting the affinity of the P protein for the P RNA by > 20-fold (41). The side chains in the RNA motif also increase the affinity of RNase P for pre-tRNA and reduce the concentration of metal ions required for RNase P catalysis *in vitro* (41,42).

Hartmann and coworkers also demonstrated that deletion of the *B. subtilis* P protein inhibits cell growth, however, substitution with other bacterial P proteins including those from Aquificae, Bacteroidetes, Cyanobacteria, α-Proteobacteria, β-Proteobacteria and γ-Proteobacteria, is able to rescue cell growth (43). Additionally, deletion of the α1 helix from *B. subtilis* P protein causes growth defects while deletion of the α3 helix impairs the cells vitality. Although the bacterial P proteins have < 30% sequence identity, replacement *B. subtilis* P protein by other bacterial RNase P proteins can rescue cells growth, suggesting that the bacterial P proteins have similar tertiary structures and are able to form functional heterologous RNase P *in vivo*. The β-central cleft of the P protein is flanked by the α1 helix, which cross-linked to the 5' leader of the pre-tRNA

(26,27). Therefore, deletion of the α1 helix could affect the pre-tRNA recognition by the RNase P *in vivo* and cause growth defects in cells. The α2 and α3 helices form a hydrophobic core with the interior of the β-central cleft, which could be crucial for P protein folding and structure stabilization. Therefore, deletion of the α3 helix could compromise the structure stability of P protein and impair the formation of RNase P holoenzyme complex and thereby inhibit cell growth. These results indicate that the P protein-pre-tRNA and P RNA-P protein interactions are important for enhancing the binding affinity of the RNase P·pre-tRNA complex for substrate and Mg^{2+} ions.

pre-tRNA Substrate Recognition

pre-tRNA is the primary substrate for RNase P which catalyzes hydrolysis to form a 5' phosphate and a 3' hydroxyl group (Figure 1-5) (15). However, RNase P is also capable of recognizing and cleaving multiple small, stable RNA molecules, termed non-tRNA substrates. For example, RNase P derived from *E.coli* catalyzes cleavage of precursor 4.5S RNA (pre-4.5S), and the intergenic region of polycistronic operon mRNAs (*his*, *tna* and *secG) in vitro* (15,44). Biochemical data indicate that the *B. subtilis* RNase P recognizes T stem-loop and acceptor stem of the pre-tRNA through coaxial stacking and backbone contacts with the S-domain of the P RNA (45-47). This interaction is mediated through the tertiary structure of the pre-tRNA (Figure 1-6). The crystal structure of the *T. maritima* RNase P·tRNA complex indicates that the S-domain of the P RNA base stacks with the TΨC and D loops of the pre-tRNA, consistent with the biochemical data (25). Moreover, *B. subtilis* RNase P holoenzyme binds pre-

tRNA 100-fold better than C-domain-P protein complex (24). These results suggest that contacts between the S-domain and the T-stem loop and acceptor stem enhance the specificity and affinity of the pre-tRNA for RNase P.

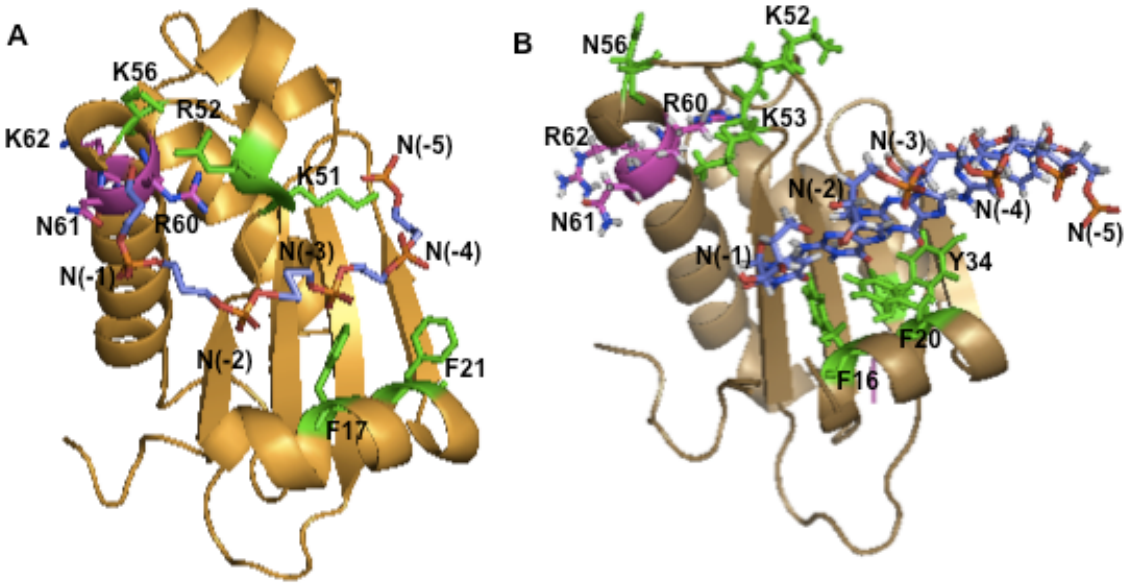

Figure 1-4: Structure of isolated bacterial RNase P proteins in contact with the 5' leader of the pre-tRNA. The "RNR" motif is highlighted in magenta, while the 5' leader of pre-tRNA highlighted in blue. (A) Crystal structure of the *T. maritima* P protein in contact with the 5' leader is adapted from Reiter, N.J. et. al., 2010 (25,33). Based on the crystal structure, the residues R52 and K56 contacts with the N(-1) nuceotide, the K51 contact with the N(-4) and N(-5) nucleotides, the F17 contact with N(-3) and N(-4) nucleotides and the F21 contact with N(-4) nucleotide. The distance between the P protein and the 5' leader contacts is ≤ ~ 4.5 Å. (B) The *B. subtilis* P protein in contact with the 5' leader (in red) based on trFRET data of the P RNA-P protein-pre-tRNA complex in Ca^{2+} buffers (48,49). Biochemical data have shown that N(-4) forms a direct contact with Y34 and stacks with F20. The F16, F20, K52, K53, N56, R60, N61 and R62 residues of *B. subtilis* P protein are corresponded to the F17, F21, K51, R52, K56, R60, N61 and K62 residues of T. maritima P protein.

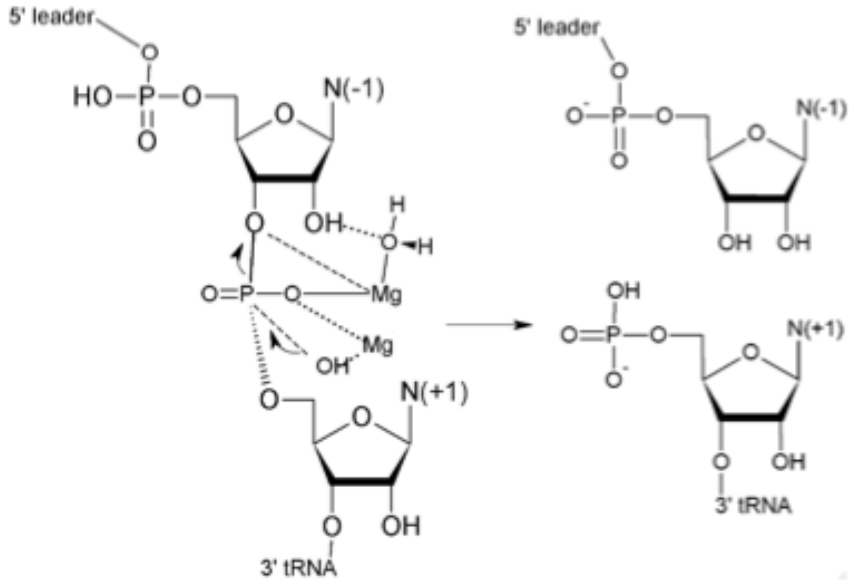

Figure 1-5: Schematic diagram of proposed cleavage reaction of the pre-tRNA by bacterial RNase P.

RNase P also recognizes pre-tRNA substrates through contacts with the CCA at the 3' end and with the 5' leader (50-52). The 3' RCCA motif forms a canonical Watson-Crick base pair with the G292, G293 and U294 from the P15 strand of the *E. coli* M1 RNA, consistent with the crystal structure of *T. maritima* RNase P·tRNA complex (53). The 3' end separates from the 5' end of the tRNA to enter a 20 Å tunnel pseudoknot formed by the P6/L17 of the P RNA (25). However, not all pre-tRNA transcripts encode the 3' RCCA; the tRNA nucleotidyltransferase catalyzes addition of CCA to many tRNAs (54,55).

Fierke and coworkers illustrated that the RNase P holoenzyme has a higher binding affinity and cleavage rate for pre-tRNA relative to tRNA that is dependent on the leader length; this preference is not observed for the P RNA subunit alone (37,39,48). These data suggest that the P protein enhances the

affinity and catalytic efficiency of the RNase P for pre-tRNA by interacting with the 5' leader. Harris and coworkers have demonstrated that this interaction with the 5' leader is important for the uniform binding affinity of *E. coli* RNase P for all pre-tRNAs, regardless of the sequence variation of the pre-tRNA; suboptimal tRNA sequences with decreased binding affinity for RNase P are compensated by a higher affinity interaction with the 5' leader (56). Similar phenomena are observed in the uniform substrate binding by the elongation factor Tu (57). Furthermore, crosslinking and trFRET data from *B. subtilis* RNase P as well as a recent crystal structure of the *T. maritima* RNase P·5' leader complex illustrate that the 5' leader of the pre-tRNA is located near the P RNA/P protein interface as well as at the central β-cleft of the P protein (25,27,39,51) (Figure 1-4). However, details of the molecular interaction between the 5' leader and RNase P are not fully elucidated. Thus, in Chapter 2 we analyze the molecular recognition of the 5' leader by the *B. subtilis* RNase P.

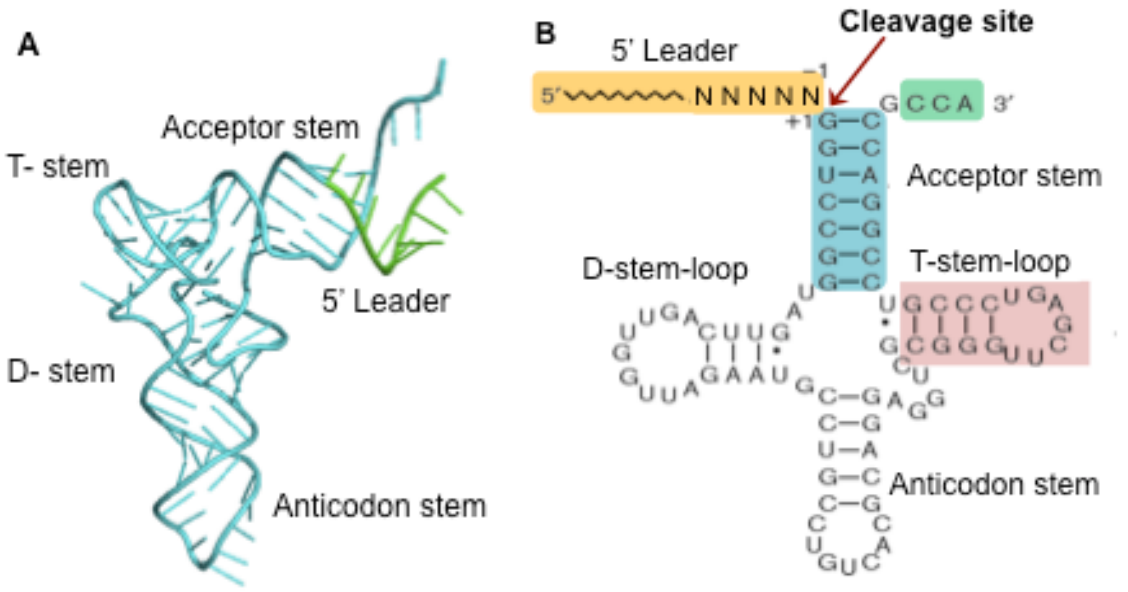

Figure 1-6: Tertiary and secondary structure of pre-tRNA. (A) Tertiary structure of canonical pre-tRNA with mature tRNA in cyan and 5' leader in green (25,58). (B) Secondary structure of the *B. subtilis* pre-tRNA^{Asp} with 5' leader highlighted in orange, 3' end of the CCA in green, acceptor stem in light blue and T-stem-loop in red (46,52,59,60). These pre-tRNA regions are essential substrate recognition by the bacterial RNase P.

Metal-dependent Catalysis of the RNase P

Bacterial RNase P is a metal-dependent enzyme that catalyzes the maturation of pre-tRNA in the presence of Mg^{2+} ions *in vitro* (61). The P RNA subunit catalyzes pre-tRNA cleavage in the presence of high concentration of monovalent and divalent ions (15). Cations play a crucial role in the RNase P catalysis by stabilizing the P RNA and pre-tRNA structures and enhancing the affinity of the P RNA for pre-tRNA. Divalent cations capable of inner sphere coordination are essential for stabilizing the transition state for pre-tRNA cleavage (62,63). Thus far, the specific Mg^{2+} ion binding sites that are essential

for RNase P catalysis are not clearly elucidated. Identification of specific Mg^{2+} ions binding sites is complicated by the large number of nonspecific Mg^{2+} ions (>100 ions) that interact with P RNA through Coulombic contacts. These cations stabilize the P RNA structure.

A highly conserved helix, P4, in P RNA has been proposed to contain specific Mg^{2+} binding sites important for catalysis. Eleven out of 21 conserved nucleotides in P RNA are located in helix P4 and deletion of this helix abrogates the catalytic activity of the RNase P (64-66). Sulfur substitution at the nonbridging oxygens of the phosphodiester bonds (phosphorothioate substitution) at A49 and U50 in helix P4 decreases the cleavage rate of the *B. subtilis* RNase P by 500-15000 fold in the presence of Mg^{2+}, without affecting pre-tRNA affinity. However, the catalytic activity of the *B. subtilis* RNase P is partially rescued by the addition of the manganese ions. The recent crystal structure of the *T. maritima* RNase P·tRNA complex illustrates that the 5' end of tRNA interacts with nucleotides in P4 (A49, A50, G51, U52) and heavy metal derivatives suggest that two Mg^{2+} binding sites are located in the helix P4; one interacts with the phosphodiester oxygens at A49/A50 and the other binds near the base of the bulged U52 (25). NMR and XAS data of metal binding to a stem-loop model of *B. subtilis* helix P4 identify an inner-sphere metal binding site formed by the bases of G378 and G379 (67,68). Nucleotide analog interference mapping (NAIM) data suggest that one or more Mg^{2+} binding site(s) important for function is clustered at the P1-P4 multihelix junction of *E. coli* RNase P (69). The Mg^{2+} ion bound to helix P4 have been proposed to function either as a metal-

hydroxide nucleophile to catalyze RNase P cleavage or as a cocatalytic metal ion that stabilizes the active P RNA conformation (68,70). Additionally interactions between helix P4 of P RNA and the RNR motif of P protein enhances the affinity of the Mg^{2+} binding site, as described previously, to facilitate RNase P catalysis at physiological metal ion concentrations.

Human Mitochondrial RNase P (mtRNase P) Protein Complex

The human mitochondrial genome is a single, closed circular DNA molecule of 16 kb (71). Except for a 1 kb non-coding region, the mitochondrial DNA (mtDNA) genome is tightly with packed with 37 genes, including 13 subunits of oxidative phosphorylation enzymes, mitochondria-specific tRNA and rRNA (72). Unlike the nuclear genome where RNA is frequently transcribed one gene at a time, mtDNA is transcribed into three long polycistronic RNA chains. This transcript is proposed to be cleaved by one or more endonucleases to release functional mRNA, rRNA and tRNA (73). Human mtDNA contains 22 tRNA genes that are dispersed through the genome and are transcribed into polycistronic RNA chains containing rRNA and protein-coding mRNA (74,75). Therefore, cleavage of tRNA genes from the primary transcript could also release mature mRNA and rRNA and be an important step in mitochondria biogenesis. Recently, two of the enzymes essential for tRNA processing in the human mitochondrial have been discovered: tRNase Z catalyzes the 3' end maturation of pre-tRNA *in vivo* and RNase P catalyzes the 5' end maturation of pre-tRNA (6,19).

Mutations in human mtRNase P and (mt)pre-tRNA have been associated

with numerous diseases, such as MELAS (mitochondrial myopathy, encephalopathy, lactic acidosis and stroke-like symptoms), progressive external opthalmoplegia and/or diabetes and coronary artery disease (76,77). Hence, investigating the structure and function of (mt)RNase P will provide insight into the role of tRNA biogenesis in dysfunctional mitochondria diseases.

Identification of the genes encoding human mitochondrial RNase P (mtRNase P) has been a great challenge because this enzyme has no sequence homology to the RNA-dependent RNase P found in Bacteria, Archaea and Eukarya. Furthermore, this enzyme is encoded by the nuclear genome rather than the mitochondrial genome (78). Initial biochemical experiments demonstrated the existence of two different RNase P enzymes in human cells with different properties (79). The human mtRNase P catalyzes cleavage of the mitochondrial substrates ((mt)pre-tRNA^{Tyr} and (mt)pre-tRNA^{Leu}) but not human nuclear substrates ((n)pre-tRNA^{Ser}), while the human nuclear RNase P catalyzes cleavage of (n)pre-tRNA^{Ser} and (mt)pre-tRNA^{Leu} but not (mt)pre-tRNA^{Tyr}. Many of the human (mt)pre-tRNAs have primary sequences and tertiary structures that deviate from the canonical cytoplasmic and bacterial tRNAs (80,81). Therefore, the mode of substrate recognition by the human mtRNase P could be different from the nuclear RNase P. However, (mt)pre-tRNA^{Leu} is cleaved by both mtRNase P and nuclear RNase P, presumably because this tRNA contains features from both the mitochondrial and cytoplasmic tRNAs. These biochemical data suggest that nuclear RNase P and mtRNase P are two distinct enzymes that have different but overlapping substrate specificity.

Density gradient centrifugation data also demonstrate that human mtRNase P has a protein-like density of 1.23 mg/mL, which differs from the *E. coli* RNase P, a ribonucleoprotein that has a density-like between RNA and protein (1.55 mg/mL) (82). Furthermore, the human mtRNase P activity is insensitive to micrococcal nuclease treatment that inactivates nuclear RNase P, suggesting that the human mtRNase P could be a "protein only" RNase P enzyme (79,82). Recently, Rossmanith and coworkers have successfully isolated proteins that catalyze mitochondrial pre-tRNA cleavage; they propose that the human mtRNase P is composed of an assembly of three protein subunits, without an RNA moiety (19). Partial purification, identification of protein subunits by mass spectrometry and reconstitution of the activity from recombinant subunits were employed to identify the human mtRNase P. The three different protein subunits proposed to form human mtRNase P, called MRPP1, MRPP2 and MRPP3, reconstitute to catalyze the 5' end maturation of the pre-tRNA.

RNA (guanine-9-)methyltransferase domain containing 1, MRPP1

RNA (guanine-9-) methyltransferase domain containing 1, termed MRPP1 in the human mtRNase P complex, is encoded by the RG9MTD1 gene on chromosome 3, has a molecular mass of ~46 kDa and contains an N-terminal mitochondrial localization sequence (19). MRPP1 is homologous to a yeast tRNA m^1G methyltransferase, Trm10p, that catalyzes the N^1 methylation of guanosine at position 9 of tRNA. Trm10p utilizes S-adenosylmethionine (SAM) as a methyl donor for this reaction (83). Based on the sequence homology with Trm10p, MRPP1 is proposed to function as a m^1G_9 methyltransferase as well.

Unpublished data from the Rossmanith laboratory suggest that MRPP1 catalyzes the methylation of G_9 of human (mt)tRNAs ((19), unpublished data). However, SAM is not an essential cofactor for cleavage of (mt)pre-$tRNA^{Tyr}$ catalyzed by mtRNase P, suggesting that methylation is not the sole function of this subunit.

To date, most known eukaryotic tRNA sequences have a purine at position 9, with the exception of four $tRNA^{Glu}$ from *Arabidopsis thaliana*, one $tRNA^{Arg}$ from *Caenorhabditis elegans,* two $tRNA^{His}$ from *Homo sapiens* and one $tRNA^{Glu}$ from *Plasmodium falciparum* (84). In yeast, 23 out of 34 tRNAs have guanosine at position 9. However, only 10 of these tRNAs contain the m^1G_9 modification *in vivo* (83). Trm10p orthologs from the archeal *Sulfolobus Acidocaldarius* (Saci_1677p) and *Thermococcus kodakaraensis* (TK0422p) also methylate adenosine and guanosine at position 9 of the tRNA (85). The yeast data indicate that a guanosine at position 9 of tRNA is not the defining recognition element for catalysis of the m^1G_9 modification. The crystal structure of yeast $tRNA^{Phe}$ visualizes the formation of a reverse-Hoogsteen-non-Watson-Crick base-triple interaction between the A at position 9 and U_{12}-A_{23} (86). It is possible that methylation of the nucleotide at position 9 of tRNA could be related to tRNA structure.

MRPP1, Trm10p and the Saci_1677p and TK0422p orthologs belong to the SAM-dependent tRNA methyltransferase (MTase) family. These MTases possess a fold similar to the Rossmann fold and are therefore called Rossmann fold MTases. This family of enzymes has been classified into five different classes based on their distinct structural features. Sequence homology indicates

that the archaeal Saci_1677p and TK0422p MTases belong to the SPOUT superfamily that is part of the class IV MTases (85). This class of MTases has a Rossmann fold consisting of a six-stranded β sheet core flanked by seven α helices (87-90). *Arabidopsis thaliana* fibrillarin, a nucleolar protein that involved in pre-rRNA and 2'-O-ribose methylation of rRNA and snRNAs, is part of the Rossmann fold SAM-dependent MTases family (91). Fibrillarin has two RNA binding sites that have Rossmann folds and mutation at the RNA binding site decrease the binding affinity for the U3 snoRNA and TMV RNA by > 5-fold, suggesting that Rossmann fold is involved in the RNA binding (91). Although MRPP1 is not yet classified due to the lack of high resolution structural information, sequence homology indicates that MRPP1 belongs to the MTase family and could contain a Rossmann fold that functions as a RNA-binding domain. Therefore, MRPP1 has been proposed to contain an RNA-binding domain that contributes to the substrate recognition of the mtRNase P complex. Furthermore, it has been suggested that m^1G modification by MRPP1 could be a novel type of substrate recognition by mtRNase P complex (19,78).

Hydroxysteroid (17-β) dehydrogenase 10, MRPP2

MRPP2 has also been identified as hydroxysteroid (17-β) dehydrogenase 10, a member of the short-chain dehydrogenase/reducatse (SDR) family (92). MRPP2 has ~260 amino acids (27kDa) and is encoded by HSD17B10 gene on chromosome X. MRPP2 has a N-terminal mitochondrial targeting signal and has also been identified as $HADH_2$, a hydroxyacyl-CoA dehydrogenase, because it catalyzes the β-oxidation of short chain fatty acids and steroids in the presence

of a NAD^+ cofactor *in vitro* (93). Numerous neurological diseases have been linked to the MRPP2 protein. For example, mutations in the HSD17B10 gene cause accumulation of 2-methyl-3-hydroxy-butyryl CoA, a metabolite in isoleucine metabolism, that leads to neurological abnormalities in patients (94). Moreover, MRPP2 was first discovered as an amyloid β-peptide-binding protein in patients with Alzheimer's Disease (95,96). The amyloid β-peptide has high affinity for MRPP2/$HADH_2$ and inhibits the $HADH_2$ activity of MRPP2 at micromolar concentrations (97). However, the dehydrogenase activity is not essential for RNase P activity since NAD^+ is not a required cofactor for pre-tRNA cleavage (19).

The SDR family of enzymes contain only 15 to 30% sequence similarity, including the conserved amino acids in the nucleotide cofactor binding motif and the active site (98). However, the SDR family has a conserved α/β sandwich structure and these enzymes normally form a functional tetramer complex. The α/β sandwich fold of the SDR family is composed of a central β-sheet flanked by several α helices (Figure 1-7), which is known as Rossmann-fold motif and is proposed to be a RNA-binding domain, as also proposed for MRPP1 (99). MRPP2 copurified with the MRPP1 subunit upon 6x His-tag affinity purification forming a MRPP1/MRPP2 complex (19). However, the role of MRPP2 in the mtRNase P catalysis is still unclear, although it has been proposed that MRPP2 could be important for (mt)pre-tRNA substrate recognition.

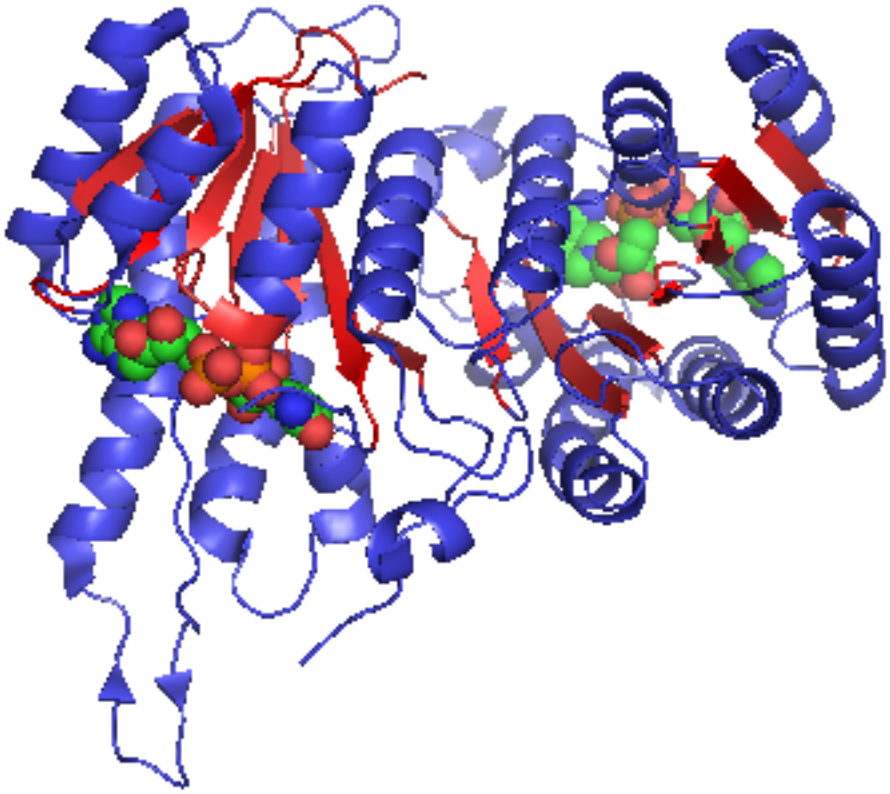

Figure 1-7: Crystal structure of human tetrameric $HADH_2$/MRPP2 (PDB code: pdb2o23). The β-strands are coloured in red, the α-helices and the loop region in blue. The $HADH_2$/MRPP2 is shown in complex with the NAD^+ cofactor, shown in sphere (100).

Unknown protein, MRPP3

In contrast to MRPP1 and MRPP2, MRPP3 was unannotated in the human genome with no known function before identification of human mtRNase P. Mass spectrometric analysis of partially purified mtRNase P identified MRPP3 as one of the 17 proteins (19). The role of MRPP3 in mtRNase P was confirmed when a mitochondrial fraction containing MRPP3 added to the MRPP1/MRPP2 complex catalyzed cleavage of (mt)pre-tRNA (19). MRPP3 is a protein containing 583 amino acids that is encoded by the KIAA0391 gene on chromosome 14.

Single nucleotide polymorphisms (SNPs) identified in the KIAA0391 gene have been linked to coronary artery diseases (76). How these sequence variations in the MRPP3 gene contribute to coronary artery diseases is not known but could be related to mitochondrial misfunction. MRPP3 has a N-terminal signal sequence that assists the localization of MRPP3 to the mitochondria. Sequence alignments of MRPP3 homologs reveal two pentatricopeptide repeat (PPR) motifs at the N-terminal end of the protein (19). PPR motifs have been identified in proteins in organelles and plants and are involved in post-transcriptional events, such as RNA processing, editing and splicing (101-103). PPR domains are a ~35 amino acid sequence motif with tandem arrays of 2 to 26 motifs per protein (103-106). Structural predictions of the PPR motif suggest the formation of two antiparallel α helices. The superhelix of PPR motifs could form a binding surface that includes hydrophilic and positively charge residues at the center and bottom portion of the groove, respectively (105,107,108). Based on gel mobility shift assays, PPR5 and CRP1 (a chloroplast PPR protein), bind preferentially to the single stranded RNA than the single stranded DNA or double stranded nucleic acids. PPR5 and CRP1 have high affinity for 31-mer RNA and unspliced trnG-UCC, a pre-tRNA that associate with a group II intron, respectively. Additionally, 9 to 6 nucleotides deletion from the 5' and 3' end of the unspliced trnG-UCC decreases the affinity for PPR5. Circular dichroism spectroscopy also indicates that PPR5 is a monomeric protein that has high α-helix content, which is similar to the TPR motifs (104). Together, these data suggested that the PPR

motif has a superhelix structure with RNA-binding domains that bind to RNA substrate.

In addition to the PPR motifs, sequence alignments of MRPP3 homologs reveal eight conserved cysteine, aspartate, and histidine residues in the C-terminal domain with spacing reminiscent of other metalloproteins. Metal-dependent protein nucleases generally include two or more highly conserved acidic active site residues that bind metal ions (109,110). Furthermore, the C-terminal of MRPP3 has been proposed to have homology to a NYN domain that is the catalytic motif of MRPP3. NYN domains are found in the eukaryotic Nedd4-binding protein 1 and bacterial YacP nucleases and have four conserved acidic residues (111). These conserved acidic residues are predicted to bind metal ions and could be part of the protein active site. However, the tertiary structure of the NYN domains remains to be elucidated. Furthermore, PFAM analysis of the MRPP3 indicates a zinc ribbon domain, suggesting a potential zinc binding site and could be involved in RNA binding and/or MRPP3 structural stabilization.

Giege and coworkers have isolated three proteins from *Arabidopsis thaliana* that are orthologs to MRPP3, called PRORP1, 2 and 3 (18). However, only PRORP1 has been shown to catalyze pre-tRNA cleavage *in vitro* and is localized to the mitochondria and chloroplast. Like MRPP3, PRORP1 has two PPR motifs and conserved acidic residues near the C-terminus. Mutation of two conserved aspartate side chains to alanine in PRORP1 eliminates the RNase P activity *in vitro* (18) suggesting that these conserved acidic residues are essential for RNase P catalysis, perhaps by binding catalytic metal ions. The proposed metal

ion binding sites and RNA-binding motifs (PPR motifs) in MRPP3 led to the speculation that this enzyme is a novel metal-dependent ribonuclease. In Chapter 4, we investigate the role of metal ions in activating human mtRNase P catalysis as well as the function of each of the three proposed mtRNase P subunits.

Objectives of this research

The overall goal of the research presented in this thesis is to advance our understanding of the function of RNase P, including determinants of substrate recognition and role of metal ions in catalysis. Chapter 2 will analyze molecular recognition of the 5' leader of pre-tRNA^{Asp} by *B. subtilis* RNase P. Bioinformatics analysis demonstrates sequence preferences in the 5' leader of the bacterial pre-tRNAs (49,60). Biochemical studies in chapter 2 indicate a sequence preference in the 5' leader for pre-tRNA affinity, which is consistent with predictions from the bioinformatics analysis. Complementary mutagenesis data indicate that the sequence preference at the second nucleotide from the cleavage site (-2 nt) in the 5' leader of the pre-tRNA is due to a trans Watson-Crick-sugar-edge base pairing with the G319 in the RNA subunit of RNase P. Furthermore, sequence preferences at the third position of the 5' leader from the cleavage site (-3 nt) enhance the metal-stabilized conformational change in RNase P coupled to pre-tRNA binding.

RNase P is a metal-dependent enzyme that catalyzes the 5' end maturation of the pre-tRNA. All known RNase P ribozyme require Mg^{2+} ions *in vivo* to stabilize the RNA structure and the transition state for pre-tRNA cleavage as well as

strengthen the affinity of the RNase P for pre-tRNA. However, the catalytic mechanism and catalytic role of metal ions in human mtRNase P, a protein-based enzyme, is not yet elucidated. Therefore, subsequent chapters describe the cloning and purification of human mtRNase P followed by analysis of the subunit content and role of metal ions in activating the human mtRNase P catalysis.

References

1. Hartmann, R. K., Gossringer, M., Spath, B., Fischer, S., and Marchfelder, A. (2009) *Prog Mol Biol Transl Sci* 85, 319-368
2. Apirion, D., and Miczak, A. (1993) *Bioessays* 15, 113-120
3. Li de la Sierra-Gallay, I., Mathy, N., Pellegrini, O., and Condon, C. (2006) *Nat Struct Mol Biol* 13, 376-377
4. Li, Z., and Deutscher, M. P. (1994) *J Biol Chem* 269, 6064-6071
5. Pellegrini, O., Nezzar, J., Marchfelder, A., Putzer, H., and Condon, C. (2003) *Embo J* 22, 4534-4543
6. Brzezniak, L. K., Bijata, M., Szczesny, R. J., and Stepien, P. P. (2011) *RNA Biol* 8
7. Dubrovsky, E. B., Dubrovskaya, V. A., Levinger, L., Schiffer, S., and Marchfelder, A. (2004) *Nucleic Acids Res* 32, 255-262
8. Rossmanith, W. (2011) *PLoS One* 6, e19152
9. Frank, D. N., and Pace, N. R. (1998) *Annu Rev Biochem* 67, 153-180
10. Gopalan, V., Vioque, A., and Altman, S. (2002) *J Biol Chem* 277, 6759-6762
11. Walker, S. C., and Engelke, D. R. (2006) *Crit Rev Biochem Mol Biol* 41, 77-102
12. Evans, D., Marquez, S. M., and Pace, N. R. (2006) *Trends Biochem Sci* 31, 333-341
13. Kazantsev, A. V., and Pace, N. R. (2006) *Nat Rev Microbiol* 4, 729-740
14. Marvin, M. C., and Engelke, D. R. (2009) *RNA Biol* 6, 40-42
15. Guerrier-Takada, C., Gardiner, K., Marsh, T., Pace, N., and Altman, S. (1983) *Cell* 35, 849-857
16. Pannucci, J. A., Haas, E. S., Hall, T. A., Harris, J. K., and Brown, J. W. (1999) *Proc Natl Acad Sci U S A* 96, 7803-7808
17. Kikovska, E., Svard, S. G., and Kirsebom, L. A. (2007) *Proc Natl Acad Sci U S A* 104, 2062-2067
18. Gobert, A., Gutmann, B., Taschner, A., Gossringer, M., Holzmann, J., Hartmann, R. K., Rossmanith, W., and Giege, P. (2010) *Nat Struct Mol Biol* 17, 740-744
19. Holzmann, J., Frank, P., Loffler, E., Bennett, K. L., Gerner, C., and Rossmanith, W. (2008) *Cell* 135, 462-474
20. Haas, E. S., Banta, A. B., Harris, J. K., Pace, N. R., and Brown, J. W. (1996) *Nucleic Acids Res* 24, 4775-4782
21. Kazantsev, A. V., Krivenko, A. A., Harrington, D. J., Holbrook, S. R., Adams, P. D., and Pace, N. R. (2005) *Proc Natl Acad Sci U S A* 102, 13392-13397
22. Torres-Larios, A., Swinger, K. K., Krasilnikov, A. S., Pan, T., and Mondragon, A. (2005) *Nature* 437, 584-587
23. Torres-Larios, A., Swinger, K. K., Pan, T., and Mondragon, A. (2006) *Curr Opin Struct Biol* 16, 327-335
24. Loria, A., and Pan, T. (2001) *Nucleic Acids Res* 29, 1892-1897

25. Reiter, N. J., Osterman, A., Torres-Larios, A., Swinger, K. K., Pan, T., and Mondragon, A. (2010) *Nature* 468, 784-789
26. Niranjanakumari, S., Day-Storms, J. J., Ahmed, M., Hsieh, J., Zahler, N. H., Venters, R. A., and Fierke, C. A. (2007) *Rna* 13, 521-535
27. Niranjanakumari, S., Stams, T., Crary, S. M., Christianson, D. W., and Fierke, C. A. (1998) *Proc Natl Acad Sci U S A* 95, 15212-15217
28. Chen, J. L., and Pace, N. R. (1997) *RNA* 3, 557-560
29. Hansen, F. G., Hansen, E. B., and Atlung, T. (1985) *Gene* 38, 85-93
30. Kole, R., and Altman, S. (1979) *Proc Natl Acad Sci U S A* 76, 3795-3799
31. Brown, J. W. (1999) *Nucleic Acids Res* 27, 314
32. Brown, J. W., and Pace, N. R. (1992) *Nucleic Acids Res* 20, 1451-1456
33. Kazantsev, A. V., Krivenko, A. A., Harrington, D. J., Carter, R. J., Holbrook, S. R., Adams, P. D., and Pace, N. R. (2003) *Proc Natl Acad Sci U S A* 100, 7497-7502
34. Spitzfaden, C., Nicholson, N., Jones, J. J., Guth, S., Lehr, R., Prescott, C. D., Hegg, L. A., and Eggleston, D. S. (2000) *J Mol Biol* 295, 105-115
35. Stams, T., Niranjanakumari, S., Fierke, C. A., and Christianson, D. W. (1998) *Science* 280, 752-755
36. Smith, J. K., Hsieh, J., and Fierke, C. A. (2007) *Biopolymers* 87, 329-338
37. Crary, S. M., Niranjanakumari, S., and Fierke, C. A. (1998) *Biochemistry* 37, 9409-9416
38. Kurz, J. C., Niranjanakumari, S., and Fierke, C. A. (1998) *Biochemistry* 37, 2393-2400
39. Rueda, D., Hsieh, J., Day-Storms, J. J., Fierke, C. A., and Walter, N. G. (2005) *Biochemistry* 44, 16130-16139
40. Kurz, J. C., and Fierke, C. A. (2002) *Biochemistry* 41, 9545-9558
41. Koutmou, K. S., Day-Storms, J. J., and Fierke, C. A. (2011) *RNA* 17, 1225-1235
42. Day-Storms, J. J., Niranjanakumari, S., and Fierke, C. A. (2004) *Rna* 10, 1595-1608
43. Gosringer, M., and Hartmann, R. K. (2007) *Mol Microbiol* 66, 801-813
44. Li, Y., and Altman, S. (2003) *Proc Natl Acad Sci U S A* 100, 13213-13218
45. Hansen, A., Pfeiffer, T., Zuleeg, T., Limmer, S., Ciesiolka, J., Feltens, R., and Hartmann, R. K. (2001) *Mol Microbiol* 41, 131-143
46. Loria, A., and Pan, T. (1997) *Biochemistry* 36, 6317-6325
47. Pan, T., Loria, A., and Zhong, K. (1995) *Proc Natl Acad Sci U S A* 92, 12510-12514
48. Hsieh, J., Koutmou, K. S., Rueda, D., Koutmos, M., Walter, N. G., and Fierke, C. A. (2010) *J Mol Biol* 400, 38-51
49. Koutmou, K. S., Zahler, N. H., Kurz, J. C., Campbell, F. E., Harris, M. E., and Fierke, C. A. (2010) *J Mol Biol* 396, 195-208
50. Christian, E. L., McPheeters, D. S., and Harris, M. E. (1998) *Biochemistry* 37, 17618-17628
51. Christian, E. L., Zahler, N. H., Kaye, N. M., and Harris, M. E. (2002) *Methods* 28, 307-322
52. Oh, B. K., and Pace, N. R. (1994) *Nucleic Acids Res* 22, 4087-4094

53. Kirsebom, L. A., and Svard, S. G. (1994) *Embo J* 13, 4870-4876
54. Shi, P. Y., Maizels, N., and Weiner, A. M. (1998) *EMBO J* 17, 3197-3206
55. Sprinzl, M., and Cramer, F. (1979) *Prog Nucleic Acid Res Mol Biol* 22, 1-69
56. Sun, L., Campbell, F. E., Zahler, N. H., and Harris, M. E. (2006) *Embo J* 25, 3998-4007
57. LaRiviere, F. J., Wolfson, A. D., and Uhlenbeck, O. C. (2001) *Science* 294, 165-168
58. Shi, H., and Moore, P. B. (2000) *RNA* 6, 1091-1105
59. Loria, A., Niranjanakumari, S., Fierke, C. A., and Pan, T. (1998) *Biochemistry* 37, 15466-15473
60. Zahler, N. H., Christian, E. L., and Harris, M. E. (2003) *Rna* 9, 734-745
61. Beebe, J. A., and Fierke, C. A. (1994) *Biochemistry* 33, 10294-10304
62. Beebe, J. A., Kurz, J. C., and Fierke, C. A. (1996) *Biochemistry* 35, 10493-10505
63. Smith, D., Burgin, A. B., Haas, E. S., and Pace, N. R. (1992) *J Biol Chem* 267, 2429-2436
64. Christian, E. L., Smith, K. M., Perera, N., and Harris, M. E. (2006) *RNA* 12, 1463-1467
65. Crary, S. M., Kurz, J. C., and Fierke, C. A. (2002) *RNA* 8, 933-947
66. Waugh, D. S., and Pace, N. R. (1993) *FASEB J* 7, 188-195
67. Getz, M. M., Andrews, A. J., Fierke, C. A., and Al-Hashimi, H. M. (2007) *RNA* 13, 251-266
68. Koutmou, K. S., Casiano-Negroni, A., Getz, M. M., Pazicni, S., Andrews, A. J., Penner-Hahn, J. E., Al-Hashimi, H. M., and Fierke, C. A. (2010) *Proc Natl Acad Sci U S A* 107, 2479-2484
69. Kaye, N. M., Zahler, N. H., Christian, E. L., and Harris, M. E. (2002) *J Mol Biol* 324, 429-442
70. Cassano, A. G., Anderson, V. E., and Harris, M. E. (2002) *J Am Chem Soc* 124, 10964-10965
71. Anderson, S., Bankier, A. T., Barrell, B. G., de Bruijn, M. H., Coulson, A. R., Drouin, J., Eperon, I. C., Nierlich, D. P., Roe, B. A., Sanger, F., Schreier, P. H., Smith, A. J., Staden, R., and Young, I. G. (1981) *Nature* 290, 457-465
72. Ojala, D., Merkel, C., Gelfand, R., and Attardi, G. (1980) *Cell* 22, 393-403
73. Ojala, D., Montoya, J., and Attardi, G. (1981) *Nature* 290, 470-474
74. Montoya, J., Gaines, G. L., and Attardi, G. (1983) *Cell* 34, 151-159
75. Montoya, J., Ojala, D., and Attardi, G. (1981) *Nature* 290, 465-470
76. Alsmadi, O., Muiya, P., Khalak, H., Al-Saud, H., Meyer, B. F., Al-Mohanna, F., Alshahid, M., and Dzimiri, N. (2009) *Ann Hum Genet* 73, 475-483
77. Wittenhagen, L. M., and Kelley, S. O. (2003) *Trends Biochem Sci* 28, 605-611
78. Rossmanith, W., and Holzmann, J. (2009) *Cell Cycle* 8, 1650-1653
79. Rossmanith, W., Tullo, A., Potuschak, T., Karwan, R., and Sbisa, E. (1995) *J Biol Chem* 270, 12885-12891

80. Putz, J., Dupuis, B., Sissler, M., and Florentz, C. (2007) *RNA* 13, 1184-1190
81. Sprinzl, M., Horn, C., Brown, M., Ioudovitch, A., and Steinberg, S. (1998) *Nucleic Acids Res* 26, 148-153
82. Rossmanith, W., and Karwan, R. M. (1998) *Biochem Biophys Res Commun* 247, 234-241
83. Jackman, J. E., Montange, R. K., Malik, H. S., and Phizicky, E. M. (2003) *RNA* 9, 574-585
84. Juhling, F., Morl, M., Hartmann, R. K., Sprinzl, M., Stadler, P. F., and Putz, J. (2009) *Nucleic Acids Res* 37, D159-162
85. Kempenaers, M., Roovers, M., Oudjama, Y., Tkaczuk, K. L., Bujnicki, J. M., and Droogmans, L. (2010) *Nucleic Acids Res* 38, 6533-6543
86. Kim, S. H., Suddath, F. L., Quigley, G. J., McPherson, A., Sussman, J. L., Wang, A. H., Seeman, N. C., and Rich, A. (1974) *Science* 185, 435-440
87. Anantharaman, V., Koonin, E. V., and Aravind, L. (2002) *J Mol Microbiol Biotechnol* 4, 71-75
88. Michel, G., Sauve, V., Larocque, R., Li, Y., Matte, A., and Cygler, M. (2002) *Structure* 10, 1303-1315
89. Nureki, O., Shirouzu, M., Hashimoto, K., Ishitani, R., Terada, T., Tamakoshi, M., Oshima, T., Chijimatsu, M., Takio, K., Vassylyev, D. G., Shibata, T., Inoue, Y., Kuramitsu, S., and Yokoyama, S. (2002) *Acta Crystallogr D Biol Crystallogr* 58, 1129-1137
90. Schubert, H. L., Blumenthal, R. M., and Cheng, X. (2003) *Trends Biochem Sci* 28, 329-335
91. Rakitina, D. V., Taliansky, M., Brown, J. W., and Kalinina, N. O. (2011) *Nucleic Acids Res*
92. Yang, S. Y., He, X. Y., and Schulz, H. (2005) *Trends Endocrinol Metab* 16, 167-175
93. He, X. Y., Yang, Y. Z., Peehl, D. M., Lauderdale, A., Schulz, H., and Yang, S. Y. (2003) *J Steroid Biochem Mol Biol* 87, 191-198
94. Ofman, R., Ruiter, J. P., Feenstra, M., Duran, M., Poll-The, B. T., Zschocke, J., Ensenauer, R., Lehnert, W., Sass, J. O., Sperl, W., and Wanders, R. J. (2003) *Am J Hum Genet* 72, 1300-1307
95. Yan, S. D., Fu, J., Soto, C., Chen, X., Zhu, H., Al-Mohanna, F., Collison, K., Zhu, A., Stern, E., Saido, T., Tohyama, M., Ogawa, S., Roher, A., and Stern, D. (1997) *Nature* 389, 689-695
96. Yan, S. D., Shi, Y., Zhu, A., Fu, J., Zhu, H., Zhu, Y., Gibson, L., Stern, E., Collison, K., Al-Mohanna, F., Ogawa, S., Roher, A., Clarke, S. G., and Stern, D. M. (1999) *J Biol Chem* 274, 2145-2156
97. Oppermann, U. C., Salim, S., Tjernberg, L. O., Terenius, L., and Jornvall, H. (1999) *FEBS Lett* 451, 238-242
98. Lukacik, P., Kavanagh, K. L., and Oppermann, U. (2006) *Mol Cell Endocrinol* 248, 61-71
99. Powell, A. J., Read, J. A., Banfield, M. J., Gunn-Moore, F., Yan, S. D., Lustbader, J., Stern, A. R., Stern, D. M., and Brady, R. L. (2000) *J Mol Biol* 303, 311-327

100. Kissinger, C. R., Rejto, P. A., Pelletier, L. A., Thomson, J. A., Showalter, R. E., Abreo, M. A., Agree, C. S., Margosiak, S., Meng, J. J., Aust, R. M., Vanderpool, D., Li, B., Tempczyk-Russell, A., and Villafranca, J. E. (2004) *J Mol Biol* 342, 943-952
101. Mili, S., and Pinol-Roma, S. (2003) *Mol Cell Biol* 23, 4972-4982
102. Robbins, J. C., Heller, W. P., and Hanson, M. R. (2009) *RNA* 15, 1142-1153
103. Yamazaki, H., Tasaka, M., and Shikanai, T. (2004) *Plant J* 38, 152-163
104. Delannoy, E., Stanley, W. A., Bond, C. S., and Small, I. D. (2007) *Biochem Soc Trans* 35, 1643-1647
105. Small, I. D., and Peeters, N. (2000) *Trends Biochem Sci* 25, 46-47
106. Williams-Carrier, R., Kroeger, T., and Barkan, A. (2008) *RNA* 14, 1930-1941
107. Jinek, M., Rehwinkel, J., Lazarus, B. D., Izaurralde, E., Hanover, J. A., and Conti, E. (2004) *Nat Struct Mol Biol* 11, 1001-1007
108. Wang, X., McLachlan, J., Zamore, P. D., and Hall, T. M. (2002) *Cell* 110, 501-512
109. Dokmanic, I., Sikic, M., and Tomic, S. (2008) *Acta Crystallogr D Biol Crystallogr* 64, 257-263
110. Dupureur, C. M. (2008) *Curr Opin Chem Biol* 12, 250-255
111. Anantharaman, V., and Aravind, L. (2006) *RNA Biol* 3, 18-27

CHAPTER 2

SUBSTRATE RECOGNITION OF THE 5' LEADER OF PRE-tRNA BY BACTERIAL RNASE P

Background

Ribonuclease P (RNase P) is an enzyme that catalyzes the maturation of the 5' end of a precursor-tRNA (pre-tRNA) to form a mature tRNA. This enzyme is a ribonucleoprotein composed of a conserved catalytic RNA subunit (P RNA) and a minimum of one protein subunit (P protein) (2,3). In Bacteria, the P RNA (~400 nucleotides) and P protein (~120 amino acids) function synergistically to enhance the efficiency of RNase P catalysis under physiological conditions; while the RNA is the catalytic subunit, both subunits contribute to substrate recognition. In addition to pre-tRNA cleavage, RNase P derived from *Escherichia coli* (*E. coli*) processes multiple small, stable RNA molecule, including precursor 4.5S RNA (pre-4.5S) and mRNA (4,5). RNase P from other sources, such as *Bacillus subtilis (B. subtilis)* show similar promiscuity (8). Although, tertiary structure has been proposed as a major feature of RNase P substrate recognition, biochemical data suggest that sequence-specific recognition may be important as well. However, the molecular details of many of these interactions remain to be elucidated. Characterization of the recognition and cleavage mechanisms

employed by RNase P will provide valuable insight into how this enzyme catalyzes processing of multiple RNA and pre-tRNA substrates *in vivo.*

Biochemical studies indicate that RNase P substrate recognition include a number of tRNA tertiary structural features, and specific contacts with the 5' leader, acceptor stem, T stem-loop and the RCCA motif at the 3' end of the pre-tRNA (9-12). The 2'-OH to 2'-H substitution studies indicate that P RNA make important backbone contact with at least four 2'-OH groups in the T stem-loop of pre-tRNA (12,13). Additionally, G292 and G293 (G258 and G259 in *B. subtilis*) of the *E. coli* P RNA form Watson-Crick base pairs with the 3' RCCA at the 3 'end of the pre-tRNA (10,11). The protein component of RNase P also enhances pre-tRNA affinity by interacting with the 5' leader (1,14-16). However, RNase P still binds and efficiently catalyzes cleavage of pre-tRNAs lacking some of these consensus sequences (17). These non-consensus sequences decrease the binding affinity of RNase P for mature tRNA. Surprisingly, the binding affinities of RNase P for the corresponding pre-tRNA are similar. Therefore, the 5' leaders of these pre-tRNAs have higher affinity interaction with RNase P protein, leading to uniform binding and catalysis of all pre-tRNAs by RNase P (14,17). The Harris group has demonstrated that the affinity of the leader and the tRNA modules are additive and combine to determine the overall substrate affinity. However, the details of the protein-leader recognition remain unclear. Bioinformatics analysis of pre-tRNA genes from 161 bacterial species reveal that more than 95% of the species show a sequence preference at one or more positions within the 5' leader (18). Furthermore, the percentage of bacterial species with a sequence

preference in the 5' leader increases near the pre-tRNA cleavage site. Together, the thermodynamic, kinetic and bioinformatics studies indicate that the 5' leader provides a significant contribution to the binding of pre-tRNA by RNase P, perhaps in a sequence-specific fashion.

The kinetics of pre-tRNA binding to RNase P has been analyzed by stopped flow fluorescence spectroscopy, demonstrating a two-step pre-tRNA binding mechanism that includes the initial formation of an ES complex (K_1), followed by a metal-stabilized conformational change (K_2) to form the ESM^{2+} moiety, as shown in Scheme 1 (19):

$$E + S \overset{K_1}{\rightleftharpoons} ES \overset{M^{2+},\, K_2}{\rightleftharpoons} ESM^{2+} \quad \text{(Scheme 1)}$$

The observed pre-tRNA dissociation constant, $K_{d,obs}$, reflects both the binding and conformational steps. The observed binding affinity of RNase P for pre-tRNA increases as the 5' leader length increases from 0 to 5 nucleotides. The first step in binding, reflected in the equilibrium constant K_1 (Scheme 1), is independent of the 5' leader length. However, the equilibrium constant for the conformational change step, K_2, increases significantly (28-fold) as the 5' leader length increases from 2 to 5 nucleotides (14,19,20). These measurements suggest that the protein-leader interaction forms during the second step, consistent with the enhanced FRET signal observed in this step between fluorophores located on the 5' end of pre-tRNA and P protein (20,21). Furthermore, addition of Ca^{2+} ions or Mg^{2+} ions to the E·S complex, preformed in cobalt hexammine ($Co(NH_3)_6^{3+}$), substantially increases the overall binding affinity of pre-tRNA through formation of the ESM^{2+} complex. Therefore, the conformational change is stabilized both by

the interaction between the 5' leader and the P protein and by binding divalent cations (Mg^{2+} and Ca^{2+}) and this, in turn, enhances the observed pre-tRNA affinity.

A variety of data, including crystallography, NMR spectroscopy, trFRET and crosslinking demonstrates that the 5' leader of the pre-tRNA interacts with the central β-cleft of the P protein and is positioned near the J5/15 and J18/2 helices of P RNA in the RNase P-substrate complex (6,7,22-24). Nucleotides at the first, second, third and fourth positions in the 5' leader from the pre-tRNA cleavage site are named N(-1), N(-2), N(-3) and N(-4). *B. subtilis* and *E. coli* RNase P show a strong sequence preference for binding pre-tRNA containing uracil and adenosine at N(-1) and N(-4) positions, respectively, consistent with the predictions of the bioinformatics analysis (1,18). The U(-1) is the most conserved nucleotide within the 5' leader and is proposed to form a canonical Watson-crick with the A248 (A246 in *B. subtilis*) at J5/15 of the *E. coli* P RNA (18). This U(-1) and A248 base pair contact is also observed in the crystal structure of *T. maritima* RNase P-substrate complex (6). The A(-4) substrate at the 5' leader of the *B. subtilis* pre-$tRNA^{Asp}$ forms a hydrogen bond and base stack with the Tyr34 and Phe20 at the central β-cleft of the P protein (1,6). Interactions between RNase P and uracil and adenosine at the N(-1) and N(-4) positions of pre-tRNA play a crucial role in increasing binding affinity and maintaining cleavage fidelity of the RNase P catalysis. Therefore, the sequence-specific interaction between the 5' leader and the RNase P is important for substrate recognition and catalysis. Bioinformatics analyses of the 5' leader sequences from 161 bacterial pre-tRNA

genes also illustrate a significant sequence preferences at N(-2) and N(-3) positions (1,18). However, the significance of these sequences preferences for RNase P function has not yet been examined. Here, we demonstrate that the sequence positions of pre-tRNA modulate pre-tRNA recognition by *B. subtilis* RNase P; mutagenesis and binding affinity measurements indicate a sequence preference for adenosine and pyrimidine at the N(-2) and N(-3) positions, respectively. Compensatory mutations suggest that the A(-2) nucleotide forms a direct contact with the G319 nucleotide at the J18/2 helix of the PRNA and this contact is formed in the initial encounter complex (ES). In contrast, the nucleotide preference at N(-3) affects the stability of the metal-dependent conformational change. Furthermore mutations in the highly conserved RNR motif of the P protein (N61, R62, and R65) that contact the P RNA affects the binding affinities and sequence selectivity at N(-3) (1,18,25). In summary, these data demonstrate that sequence-specific contacts with the N(-2) and N(-3) nucleotides in pre-tRNA modulate substrate selectivity *in vitro*, consistent with the bioinformatics analyses of *in vivo* substrates.

Materials and Methods

RNA and protein preparation

B. subtilis P RNA and *B. subtilis* pre-tRNA^{Asp} substrates with a 5-nucleotide leader were prepared by *in vitro* transcription from linearized DNA templates using T7 RNA polymerase as described previously (50). A318 and G319 P RNA mutants were prepared using QuikChange site-directed mutagenesis kit (Stratagene). *B. subtilis* pre-tRNA^{Asp} was 5'-end-labeled using [γ-^{32}P]ATP (MP Biomedical) and T4 polynucleotide kinase (New England Biolabs). P RNA and pre-tRNA were purified by 6% and 12% denaturing polyacrylamide gel electrophoresis (PAGE), respectively, followed by washing with TE buffer (10 mM Tris-HCl, pH 8.0 and 1 mM EDTA) (15). The 5'-end-labeled substrate was gel-purified, eluted and extracted with an equal volume of chloroform/phenol followed by ethanol precipitation.

P protein was expressed in BL21(DE3)pLysS *E. coli* by growth at 37^{o}C to an OD_{600} of 0.6 to 0.8 followed by induction by 1 mM isopropylthio-β-D-galactopyranoside. P protein was purified from the soluble fraction of the cell lysate by CM-Sepharose ion-exchange chromatography in the presence of urea (26). Variants of the *B. subtilis* protein with site-specific cysteine and alanine mutations were prepared as described previously (26). Before use, P protein was dialyzed overnight at 4^{o}C in the proper reaction buffer, and final concentrations were determined by absorbance at 280 nm (ε_{280} = 5120 M^{-1} cm^{-1}) (26).

Before use, P RNA and pre-tRNA were heat denatured at 95^{o}C for 3 min in water, then incubated at 37^{o}C for 10 min. To fold the RNAs, 50 mM Tris/MES,

and an appropriate final concentration of monovalent and divalent metal ions were added to the RNAs and incubated at 37°C for 30 min. After renaturation, P RNA was buffer exchanged and reconcentrated in the reaction buffer using an Amicon ultracentrifugal filter unit (10,000 MWCO) for three times to ensure the correct $[Ca^{2+}]_f$.

Substrate affinity, $K_{d,obs}$ measurements

Substrate affinities were measured by centrifuge gel filtration using a spin column (Spin-X, Corning Incorporated) with Sephadex G-75 resin (Sigma-Aldrich). The total substrate concentration ($[S_{tot}]$) was maintained at < 20% of the total RNase P concentration ($[E_{total}]$). Buffer conditions used for $K_{d,obs}$ measurements were: 50 mM Tris/MES, ~ 400 mM KCl, pH 6.0, varying (0 to 10 mM $CaCl_2$) concentrations of $[Ca^{2+}]_f$ with ionic strength maintained at 410 mM by varying the KCl concentration (~400 mM KCl). RNase P holoenzyme (1.2 nM to 2.7 μM) was reconstituted by adding a 1:1 ratio of dialyzed P protein and folded P RNA and incubating at 37°C for 30 min. These concentrations are significantly higher than the P RNA-P protein affinity under all conditions (27,28). Pre-tRNA substrates were renatured as described above. RNase P and pre-tRNA were mixed and incubated at 37°C for 5 min prior to loading onto preequilibrated gel filtration spin columns. Columns were centrifuged at 6000 rpm for 15 sec, and the radioactivity in the filtrate (bound substrates) and retentate (unbound substrates) was measured by Cerenkov scintillation counting. Dissociation constants, $K_{d,obs}$ were determined by fitting a single binding isotherm to the dependence of the fraction bound on the RNase P concentration (Eq.1).

Equation 1

$$\frac{[ES]}{[S_{total}]} = \frac{1}{1 + \frac{K_{d,obs}}{[E_{total}]}}$$

K_1 and $K_{1/2Ca}$ measurements

The Ca^{2+}-dependence of the affinity of RNase P for pre-tRNA was measured as described above except that the folding and binding buffer contained: 50 mM Tris-MES, 380 mM KCl, 2 mM $Co(NH_3)_6Cl_3$ (pH 6.0) and varying free $CaCl_2$ concentration (0 to 10 mM). The $K_{d,obs}$ for pre-tRNA was measured at various concentration of $[Ca^{2+}]_f$ using the centrifuge gel filtration columns. Equation 2 was fitted to the dependence of $K_{d,,obs}$ on the $[Ca^{2+}]_f$ to determine the values of K_1 (Scheme 1) and $K_{1/2}^{Ca}$.

Equation 2

$$K_{d,obs} = \frac{K_1(1 + \frac{[Ca^{2+}]^n}{K_2^n})}{1 + \frac{[Ca^{2+}]^n}{(K_{1/2}^{Ca})^n}}$$

Single turnover kinetic measurements

Single turnover experiments were performed in 50 mM MES/Tris, 191 mM KCl, and 5 mM $CaCl_2$ buffer (pH 8.0) at 37°C using excess RNase P holoenzyme concentrations ([E]/[S] >> 5; [E] 0.6 nM to 2 μM; [S] ≤ 0.1 nM) with limiting radiolabelled pre-$tRNA^{Asp}$. The 5' leader product was separated from the pre-$tRNA^{Asp}$ substrate on a 20% PAGE and quantified using a PhosphorImager (Amersham Bioscience Corp.). The observed rate constants, k_{obs} were determined by fitting a single-exponential equation to the data (Eq. 3).

Equation 3

$$[P] = [P]_\infty(1 - e^{-k_{obs}t})$$

Results

N(-2) and N(-3) sequences in the 5' leader of pre-tRNA contribute to the RNase P binding affinity.

Previous studies have shown that the 5' leader of pre-tRNA enhances the binding affinity and cleavage rate constants catalyzed by RNase P (1,7,9,14,15). Bioinformatics analyses of the sequences of the 5' leader of *B. subtilis* pre-tRNA indicate a sequence preference for adenosine at N(-2) position of the pre-tRNA (Figure 2-1). However, the sequence preference at the N(-3) position is not as strong as the N(-2) position in the *B. subtilis* 5' leader of the pre-tRNA. Bacterial species from *Chlamydophila, Clostridium* and *Streptomyces* indicate a high uracil and cytosine sequence preference at N(-3) position of the 5' leader of pre-tRNA (unpublished data). The sequence preferences observed by bioinformatics might reflect *in vivo* substrate recognition preferences for cleavage catalyzed by RNase P (1,18). To test this hypothesis and to evaluate the importance of N(-2) and N(-3) sequences for molecular recognition by RNase P, we measured the affinity of the *B. subtilis* RNase P for pre-tRNA^{Asp} with varying sequences at the N(-2) and N(-3) positions using centrifuge size-exclusion chromatography. In these binding experiments, the metal cofactor, Mg^{2+}, is replaced by Ca^{2+}, which stabilizes the formation RNase P-pre-tRNA complex by RNase P, but cleavage is slow ($t_{1/2} \approx 5$ hours) (29). These experiments were carried out in low mM (≤ 5 mM) concentrations of divalent cations to mimick *in vivo* conditions.

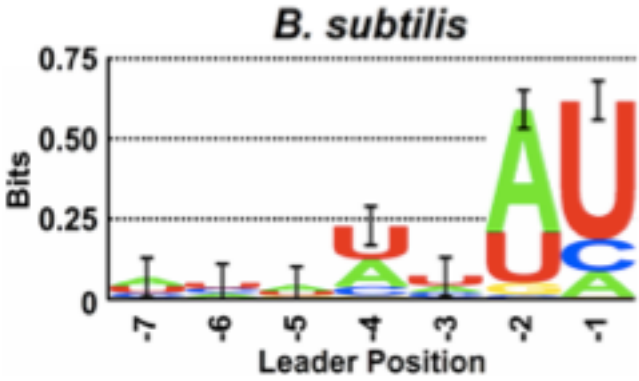

Figure 2-1: Genomic analysis of the conservation of the 5' leader sequence of *B.subtilis* pre-tRNAs by using sequence-Logos adapted from Koutmou K.S. et. al., 2010 (1).

The affinity measurements demonstrate a sequence preference at N(-2) for RNase P binding pre-tRNA; the substrate with A(-2) binds ~ 2-fold more tightly than C(-2) and U(-2) and ~ 10-fold more tightly than G(-2) (Figure 2-2A and Table 2-1). The preference for A and discrimination against G at N(-2) is consistent with the bio-informatics analysis. Similarly, the sequence at N(-3) also affects binding affinity where U(-3)- and C(-3)-pre-tRNA^{Asp} bind ~6.5 fold more tightly than substrates with an A or G at this position, suggesting that *B. subtilis* RNase P prefers a pyrimidine at N(-3). This is a larger discrimination than suggested by the bioinformatics. These data demonstrate that the sequences at N(-2) and N(-3) affects the affinity of RNase P for pre-tRNA.

To evaluate whether, the leader sequence of pre-tRNA affects RNase P catalysis, the single turnover cleavage rate constants were measured at saturating RNase P. The sequence at N(-2) has affects this rate constant < 2-fold with a maximal k_{obs} of 0.09 ± 0.01 min^{-1} for A(-2)-pre-tRNA and a minimum k_{obs} of 0.05 ± 0.01 min^{-1} for C(-2)-pre-tRNA (Table 2-1). Thus, the leader sequence preference affect the stability but not the reactivity of the ES complex, consistent with the direct interaction of the leader with the non-catalytic protein subunit.

Table 2-1. Sequence of N(-2) and N(-3) nucleotides in the 5' leader of pre-tRNA^{Asp} affect recognition by RNase P

Substrate	$K_{d,\,obs}$ (nM)		k_{obs} (min^{-1})
	N(-2)[a]	N(-3)[b]	N(-2)[c]
Adenosine	4 ± 1	26 ± 6	0.09 ± 0.01
Cytosine	9 ± 1	4 ± 1	0.05 ± 0.01
Guanosine	39 ± 6	23 ± 4	0.086 ± 0.002
Uracil	10 ± 2	4 ± 0.6	0.071 ± 0.004

[a] Dissociation constants, $K_{d,obs}$ measurements of pre-tRNA^{Asp} with a 5 nucleotide leader of the sequence containing 5' GAANU with varying sequence at N(-2). Conditions: 50 mM MES/Tris (pH 6.0) at 37°C, 5 mM $CaCl_2$, and [KCl] was adjusted to maintain ionic strength at 410 mM KCl.

[b] Dissociation constants, $K_{d,obs}$ measurements of pre-tRNA^{Asp} with a 5 nucleotide leader of the sequence containing 5' GANAU with varying sequence at N(-3). Conditions: Same as ([a]) except with 3 mM $CaCl_2$.

[c] Single turnover rate constant measured at saturating enzyme concentration for cleavage of N(-2)-pre-tRNA^{Asp}. Conditions: 50 mM MES/Tris (pH 8.0) at 37°C, 191 mM KCl and 5 mM $CaCl_2$.

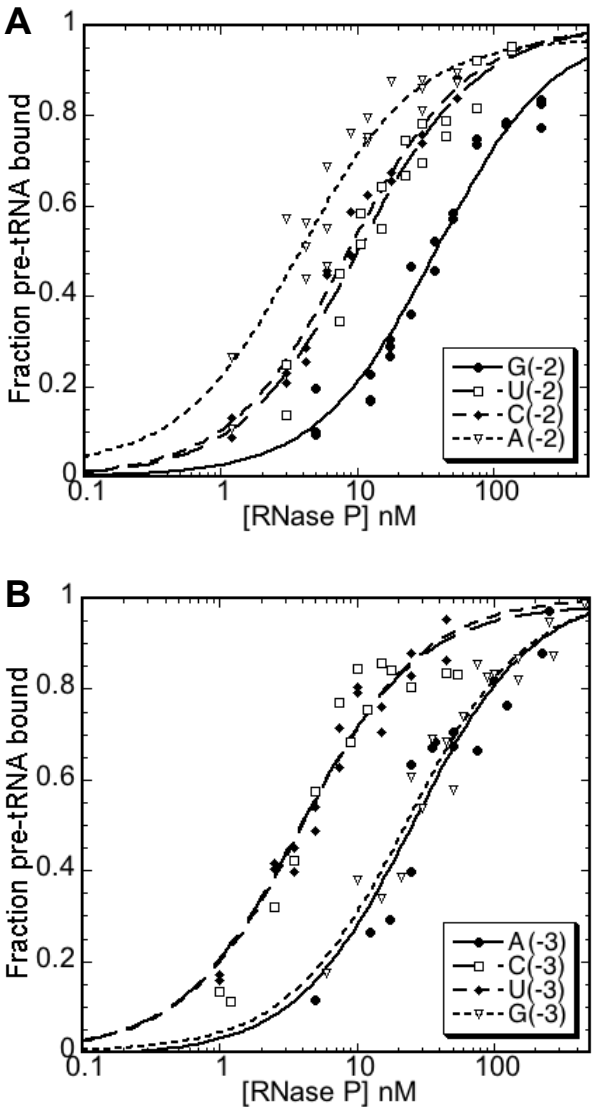

Figure 2-2: Sequence preference of N(-2) and N(-3) positions at 5' leader of the pre-tRNA^{Asp}. (A) Dissociation constants, $K_{d,obs}$ measurements of RNase P with pre-tRNA^{Asp} with adenosine, cytosine, uracil and guanosine at N(-2) position of the 5' leader in 50 mM Tris/MES, 395.5 mM KCl, 5 mM $CaCl_2$, pH 6.0. (B) Dissociation constants, $K_{d,obs}$ measurement of RNase P with pre-tRNA^{Asp} containing adenosine, cytosine, uracil and guanosine at N(-3) position of the 5' leader in 50 mM Tris/MES, 401.5 mM KCl, 3 mM $CaCl_2$ at pH 6.0. Dissociation constants ($K_{d,obs}$) are calculated from a fit of a binding isotherm to these data.

Compensatory mutations suggest base pairing between N(-2) of pre-tRNA leader and G319.

Crosslinking and affinity cleavage assays indicate that the N(-2) and N(-3) nucleotides in the RNase P-pre-tRNA complex in solution are located near the J5/15 and J18/2 helices in *B. subtilis* P RNA, while N(-3) through N(-7) are positioned near the central β-cleft of the P protein (Figure 2-3A) (7,16,22). In addition, current crystal structure of the *T. maritima* RNase P·5' leader complex suggests that the N(-2) and N(-3) nucleotides form contacts with the G295 and U294, respectively, (corresponding to G319 and A318 in *B. subtilis* P RNA) at the J18/2 helix of the P RNA (Figure 2-5) (6,30). To test the functional significance of contacts between these nucleotides in P RNA and the N(-2) and N(-3) nucleotides in pre-tRNA, we employed a compensatory mutation approach.

Wild type RNase P preferentially binds to pre-tRNA containing A(-2) in the leader (Figure 2-1). The A nucleotide at N(-2) cannot form a Watson-crick base pair with either G319 or A318 in P RNA. However, the NMR and crystal structures of RNA demonstrate the formation of a variety on non-Watson-Crick base pairing (31,32). To test for the formation of one of these alternative structure we measured the affinity of RNase P with mutations at A318 and G319 with pre-tRNA containing variable sequence at N(-2) and N(-3) (Table 2-2). Mutation of A318 to G, C, or U decreases the binding affinity for A(-2)-pre-tRNA by 4- to 20-fold, (Table 2-2) suggesting a possible base pairing interaction. To test this proposal, we assessed the effect of compensatory mutations at A318 and N(-2)-pre-tRNA on binding affinity. All of the nucleotide substitutions at 318

decrease the binding affinity of pre-tRNA by 2- to 75-fold, regardless of the nucleotide at N(-2) in pre-tRNA. Therefore no compensatory rescue is observed, suggesting that A318 does not base pair with the N(-2) nucleotide in pre-tRNA^{Asp}.

Nucleotide substitution at G319 lead to more modest changes in affinity with both enhanced (< 3-fold) and diminished (< 10-fold) affinity (Table 2-3). Furthermore, compensatory substitutions are observed. The binding affinity of A319 RNase P for G(-2)-pre-tRNA^{Asp} ($K_{d,obs}$ of 5 ± 1 nM) is comparable to the affinity of wild type (G319) RNase P for A(-2)-pre-tRNA^{Asp} ($K_{d,obs}$ of 4 ± 0.7 nM), suggesting that the A319/G(-2) and G319/A(-2) are equivalent. Likewise, the following pairs have similar binding affinities: (a) C319/U(-2) and U319/C(-2) ($K_{d,obs}$ of 5 ± 0.8 nM and 4.8 ± 1 nM); (b) C319/G(-2) and G319/C(-2) ($K_{d,obs}$ of 12 ± 1 nM and 9 ± 1 nM); and (c) U319/G(-2) and G319/U(-2) ($K_{d,obs}$ of 7 ± 1 nM and 10 ± 2 nM). These compensatory mutations suggest that the N(-2) nucleotide forms direct contact with G319. In contrast, single turnover measurements of the G319A, G319C and G319U RNase P mutants at saturating enzyme concentration demonstrate that the k_{obs} of ≤ 2-fold relative to that of wild type RNase P (Figure 2-3B). These results indicate that mutation at G319 has little effect on the RNase P cleavage. In summary, these data suggest that the N(-2) nucleotide forms a direct contact with G319, and not A318, in the J18/2 helix of the P RNA, consistent with the crystal structure of the *T. maritima* RNase P·tRNA·5'leader complex (6).

To examine possible base pairing between A318 and N(-3) nucleotide as visualized in the crystal structure, we measured the binding affinity of RNase P

mutants at A318 with the N(-3) substrates. Mutations at the A318 nucleotide decrease the binding affinity of the RNase P for C(-3) substrate, by 3- to 100-fold, suggesting a possible interaction. The binding affinities of A318G for A(-3), C(-3) and G(-3)-pre-tRNA^{Asp} are similar ($K_{d,obs}$ ~ 300 nM). While the U(-3)-pre-tRNA^{Asp} has a higher affinity ($K_{d,obs}$ ~100 nM). However, substitution of the C(-3) substrate with various nucleotides at N(-3) pre-tRNA does not rescue the binding affinity of the A318C and A318U mutants (Table 2-2). The affinity of A318C RNase P with A(-3) pre-tRNA (C/A pair) is 50-fold weaker than the affinity of wild type RNase P with C(-3) pre-tRNA (A/C pair). Similarly the affinity of A318U RNase P for A(-3)-pre-tRNA (U/A pair) is 10-times weaker than wild type RNase P with U(-3)-pre-tRNA (A/U pair). Additionally, binding affinity of the mature tRNA for A318C, A318U and A318G RNase P mutants are > 5-fold ($K_{d,obs}$ > 500 nM) relative to the wild type RNase P ($K_{d,obs}$ ~ 200 nM), suggesting that mutation at A318 nucleotide perturb the local structure stability of P RNA. Therefore, no compensatory mutations are observable in the binding data between A318 and, N(-3) nucleotide in pre-tRNA, providing no evidence for base pairing.

Table 2-2. Binding affinity, $K_{d,obs}$ of the N(-2), N(-3) and mature tRNA substrates for A318 mutants

	Dissociation Constant, $K_{d,obs}$ (nM)			
Substrate	**WT A318**	**A318C**	**A318G**	**A318U**
A(-2)	4 ±0.7	23 ± 6	84 ± 18	18 ± 5
C(-2)	9 ± 1	139 ± 23	130 ± 21	21 ± 4
G(-2)	39 ± 6	183 ± 25	318 ± 53	40 ± 8
U(-2)	10 ± 2	95 ± 28	246 ± 50	38 ± 6
A(-3)	26 ± 6	204 ± 31	349 ± 80	41 ± 7
C(-3)	4 ± 0.8	10 ± 3	307 ± 64	8 ± 2
G(-3)	25 ± 4	66 ± 11	337 ± 160	18 ± 6
U(-3)	4 ± 0.6	45 ± 14	107 ± 26	16 ± 3
tRNA	230 ± 112	> 500	> 500	> 500

[a] Dissociation constants, $K_{d,obs}$ measurements of N(-2) pre-tRNA^{Asp} for different nucleotide at A318 of the P RNA in 50 mM MES/Tris (pH 6.0) at 37^{o}C, 5 mM $CaCl_2$, and [KCl] was adjusted to maintain ionic strength. The leader sequence is: 5' GAANU

[b] Same as ([a]) except with N(-3) substrates and 3 mM $CaCl_2$. The leader sequence is: 5' GANAU.

[b] Same as ([a]) except with mature tRNA substrate.

Table 2-3. Binding affinity, $K_{d,obs}$ of the G319[a] mutants for N(-2) substrates.

		Sugar-Edge			
	N(-2) \ 319	A	C	G[b]	U
Watson-Crick	A	1.3 ±0.1	3.3 ± 0.3	4 ± 0.7	1.3 ±0.2
	C	4 ± 1	4.6 ± 0.8	9 ± 1	4.8 ± 1
	G	5 ± 1	12 ± 1	39 ± 6	7 ± 1
	U	4.6 ± 0.6	5 ± 0.8	10 ± 2	5.6 ± 1

[a] Dissociation constants, $K_{d,obs}$ (nM) measurement of N(-2) pre-tRNA for different nucleotide at 319 position of the P RNA in 50 mM MES/Tris (pH 6.0) at 37°C, 5 mM $CaCl_2$, and [KCl] was adjusted to maintain ionic strength. The leader sequence is: 5' GAANU.

[b] The G at position 319 is the wild type sequence of *B. subtilis* P RNA.

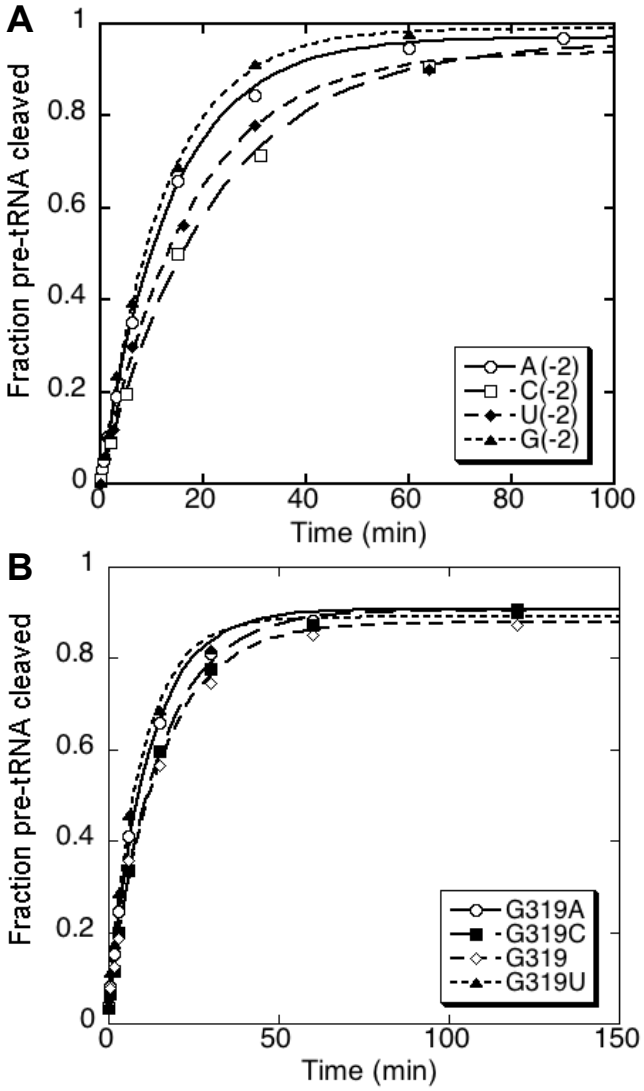

Figure 2-3: (A) Single turnover measurement of the RNase P catalyzed hydrolysis of N(-2) substrates. ^{32}P-labeled pre-tRNA^{Asp} (~0.01 nM) was incubated with saturating enzyme concentration (40 – 360 nM) in 50 mM MES/Tris, pH 8.0, 191 mM KCl and 5 mM $CaCl_2$ at 37^{o}C. (B) Single turnover reaction of the A(-2) substrate by various nucleotide at G319 of the PRNA. ^{32}P-labeled pre-tRNA^{Asp} (~0.01 nM) was incubated with saturating enzyme concentration (0.25 – 1 μM) in 50 mM MES/Tris, pH 8.0, 191 mM KCl and 5 mM $CaCl_2$ at 37^{o}C. The reaction was quenched by addition of 50 mM EDTA and the products were separated by PAGE and analyzed using a phosphoimager. The fraction of pre-tRNA cleaved by the RNase P as a function of time was plotted and fitted using Eq. 3 to obtain the observed rate constants, k_{obs}.

Mutations in P protein affect Sequence preference at N(-3) pre-tRNA.

Structural and biochemical data suggest that the N(-3) nucleotide of pre-tRNA is located near the P protein-P RNA interface and may therefore be sensitive to alterations in either subunit. Mutations in the central cleft and highly conserved RNR motif of the P protein have previously been shown to alter the N(-4)-pre-tRNA affinity and selectivity (1). Therefore, we tested whether these mutations also affect selectivity at the N(-3) position. As shown in Table 2-4, mutations in RNase P protein decrease pre-tRNA binding affinity substantially (2- to 30-fold). The F16A mutation, located in the first strand of the central β sheet, where the leader binds (16,33), and the K64C and R68A mutations in the RNR motif do not significantly affect the binding selectivity. The selectivity ratio ($K_{D,\ A(-3)}/K_{D,\ C(-3)}$) in the F16A, K64C and R68A mutation is comparable to that of wild type RNase P. In contrast, the N(-3) selectivity virtually disappears ($K_{D,\ A(-3)}/K_{D,\ C(-3)}$ ~ 1.4) in the R62 mutation located in the RNR motif. Furthermore, selectivity decreases in the R65A and N61C mutations in the RNR motif by ≤ 2-fold. The R65A and N61A also affect the N(-4) sequence selectivity by ≤ 2-fold. Based on the crystal structure of *T. maritima* RNase P·tRNA·5' leader complex and our current model of *B. subtilis* RNase P·pre-tRNA complex, the R62 is ≥ 10 Å away from the N(-3) nucleotide. Therefore, the R62A, R65A and N61C mutations in the RNR motif indirectly affect the N(-3) sequence selectivity.

Table 2-4. Binding affinities of the P protein mutants for N(-3) substrates.

	$K_{d,obs}$ (nM)[a]		$K_{d,mutants}/K_{d,native}$
Protein	A(-3)	C(-3)	A(-3)/C(-3)
Native	26 ± 6	4 ± 1	6.5 ± 2.2
F16A	147 ± 34	27 ± 5	5.4 ± 1.6
R65A	102 ± 20	34 ± 6	3.0 ± 0.8
R68A	61 ± 15	13 ± 3	4.7 ± 1.6
N61C	380 ± 81	109 ± 68	3.5 ± 2.3
R62C	171 ± 40	120 ± 61	1.4 ± 0.8
K64C	168 ± 47	22 ± 3	7.6 ± 2.4

[a] Dissociation constants, $K_{d,obs}$ of the P protein mutants for A(-3) and C(-3) substrates were measured at 50mM MES/Tris (pH 6.0) at 37^{o}C, 3 mM $CaCl_2$, and [KCl] was adjusted to maintain ionic strength.

Interaction of RNase P with N(-2) and N(-3) pre-tRNA differentially stabilize the encounter complex and the metal-dependent conformational change.

Pre-tRNA binds to RNase P in a two-step mechanism: the formation of an E·S encounter complex followed by a metal-stabilized conformational change in which the pre-tRNA leader contacts the P protein (scheme 1) (19). Therefore pre-tRNA affinity depends on the concentration of divalent cations. Additionally, the binding selectivity for the nucleotide at N(-4) in the pre-tRNA^{Asp} varies with Ca^{2+} concentration. Therefore, to further investigate recognition of the N(-2) and N(-3) nucleotides in the pre-tRNA leader we measured the calcium-dependence of binding affinity for A(-2)-, G(-2)-, A(-3)-, and C(-3)-pre-tRNA in $Co(NH_3)_6^{3+}$. Cobalt hexammine is an outer sphere metal ion that mimics $Mg(OH_2)_6^{2+}$ by stabilizing folded RNase P and pre-tRNA. Under these conditions the observed binding affinity of RNase P for each of the pre-tRNA substrate has a hyperbolic dependence on the Ca^{2+} concentration with a $K_{1/2}^{Ca}$ varying from 19 to 420 μM.

The pre-tRNA binding affinity in cobalt hexamine approximates the equilibrium constant for the formation of the initial encounter complex (K_1, Scheme 2) (19,34-36). Substitution of G for A at N(-2) in pre-tRNA decreases the value of K_1 from 90 ± 21 nM to 236 ± 60 nM, indicating formation of an interaction with this nucleotide in the encounter complex (Figure 2-4A). In contrast, the binding affinity of RNase P for A(-3) and C(-3) pre-tRNA in cobalt hexammine are comparable (90 ± 20 nM and 154 ± 27 nM), suggesting little contact in the initial encounter complex (Figure 2-4B). The calcium dependence of the binding affinity ($K_{1/2}^{Ca}$) reflects a combination of calcium affinity and the equilibrium constant for

the conformational changes. The value of $K_{1/2}^{Ca}$ is unaffected by the identity of the nucleotide at N(-2) indicating little influence on the metal-dependent conformational change (Figure 2-4A). However, the $K_{1/2}^{Ca}$ for A(-3) pre-tRNA is 20-fold higher (420 ± 30 μM) compared to that of the C(-3) pre-tRNA (19 ± 3 μM) suggesting that the interaction with this nucleotide occurs at the conformational change step (Figure 2-4B). The equation 2 is fitted to the dependence of $K_{d,obs}$ on calcium concentration and has a n ~ 1 for A(-2), G(-2), C(-3) and A(-3) pre-tRNAs.

(A)

$$\begin{array}{ccc} E + S + nCa^{2+} & \xleftrightarrow{K_1} & ES + nCa^{2+} \\ K_2 \updownarrow & & \updownarrow K_{1/2}^{Ca} \\ ECa_n^{2+} + S & \xleftrightarrow[K_3]{} & ES^*Ca_n^{2+} \end{array}$$

(B)

$$ES + nCa^{2+} \xleftrightarrow{K_4} ESCa_n^{2+} \xleftrightarrow{K_5} ES^*Ca_n^{2+}$$

(C)

$$K_{d,obs} = \frac{K_1(1 + \frac{[Ca^{2+}]^n}{K_2^n})}{1 + \frac{[Ca^{2+}]^n}{(K_{1/2}^{Ca})^n}}$$

$$K_1 = [E][S]/[ES]$$

$$K_2 = [E][Ca^{2+}]^n / [ECa_n^{2+}]$$

$$K_3 = [ECa_n^{2+}][S]/[ES^*Ca_n^{2+}]$$

$$K_4 = [ES][Ca^{2+}]^n / [ESCa_n^{2+}]$$

Scheme 2. (A) Metal dependence of pre-tRNA binding mechanism by the RNase P. **(B)** The expanded minimal metal-stabilized conformational change mechanism. **(C)** Equilibrium constant expressions to define the parameters in (A) and (B).

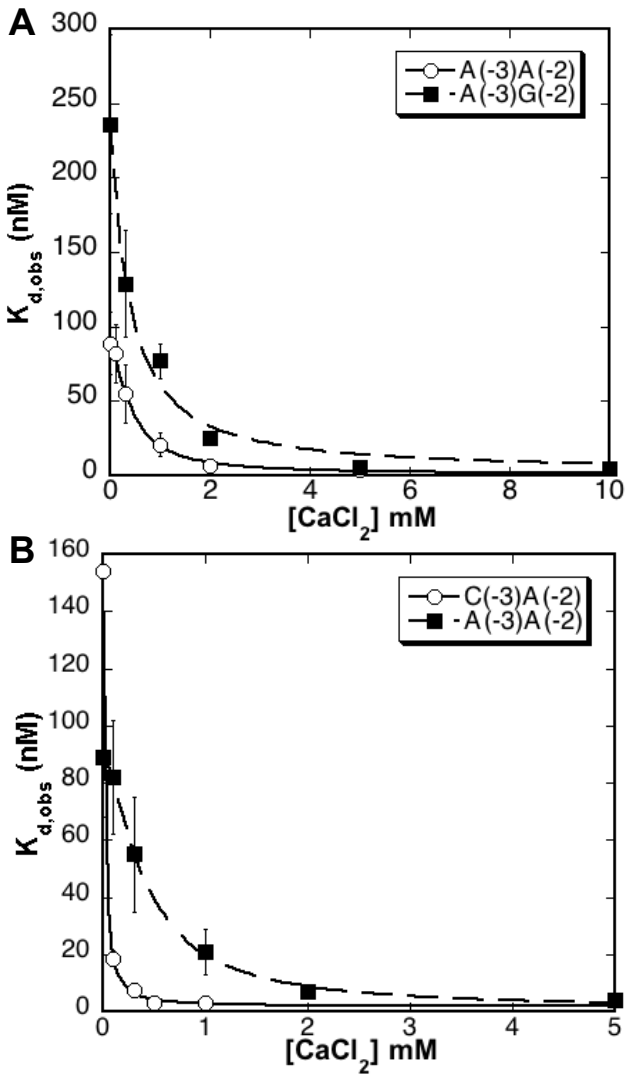

Figure 2-4. Metal dependence of pre-tRNA^{Asp} binding affinity by RNase P. (A) Metal dependent measurements of A(-2) (■) and G(-2) (▲) substrates binding affinity by RNase P. 0 to 10 mM of $CaCl_2$ was titrated into the 2 mM $Co(NH3)_6^{3+}$ to obtain the $K_{d,obs}$ of the RNase P for N(-2) substrates at various [$CaCl_2$] (see materials and methods). $K_{d,obs}$ values as a function of [$CaCl_2$] was plotted and fitted using Eq. 2 to obtain the initial formation of ES complex, K_1 and the metal stabilized conformation change step, $K_{1/2}^{Ca}$. The K_1 and $K_{1/2}^{Ca}$ for A(-2) and G(-2) substrates are K_1: 90 ± 21 nM and 235 ± 60 nM, $K_{1/2}^{Ca}$: 416 ± 27 μM and 387 ± 73 μM, respectively. (B) The K_1 and $K_{1/2}^{Ca}$ for A(-3) (■) and C(-3) (●) substrates are K_1: 90 ± 20 nM and 154 ± 27 nM, $K_{1/2}^{Ca}$: 416 ± 27 μM and 19 ± 3 μM, correspondingly.

Discussion

Specific contact between G319 in P RNA and N(-2) in pre-tRNA

Recent bioinformatics and biochemical studies have demonstrated sequence-specific contact between the N(-1) and N(-4) positions of the 5' leader and the 3' RCCA motif of pre-tRNA for *B. subtilis* and *E. coli* RNase P (1,18). Bioinformatics data suggest a sequence preference for RNase P at the N(-2) position of the 5' leader of the *B. subtilis* pre-tRNA^{Asp}. Here we have confirmed the bioinformatics prediction, demonstrating that *B. subtilis* RNase P preferentially binds A(-2) pre-tRNA relative to G(-2) pre-tRNA by 1.4 kcal/mole at 5 mM $CaCl_2$ *in vitro* (Table 2-1). While substitution of the A(-2) nucleotide with C, U or G decreases the binding affinity, the single turnover rate constant for pre-tRNA cleavage catalyzed by RNase P is unchanged. These data indicate that the nucleotide substitution alters an interaction with RNase P but does not change the structure of the RNase P·pre-tRNA complex.

Compensatory mutations implicate a sequence specific interaction between the N(-2) position of pre-tRNA and the G319 nucleotide at the J18/2 helix of the P RNA. The binding affinity of wild type RNase P for pre-tRNA is disrupted by 1.4 kcal/mole when the A nucleotide at the -2 position is replaced by G. However, high affinity binding between the RNase P and pre-tRNA is recovered when the G(-2) substrate binds to the G319A RNase P mutant, suggesting a compensatory base-pairing interaction between G319/A(-2) and A319/G(-2). In the same manner, a compensatory base-pairing substitution is observed for the following pairs: C319/A(-2) and A319/C(-2); C319/G(-2) and C319/G(-2); C319/U(-2) and

U319/C(-2); and G319/U(-2) with U319/G(-2). These results strongly suggest a direct contact between G319 of P RNA and N(-2) of pre-tRNA.

Interestingly, the affinity of most of these base-pairing substitutions are within 2 to 3-fold of each other, with the exception of G319/G(-2) base pair decreases binding affinity 10 to 40-fold different in $K_{d,obs}$ relative to the G319/A(-2) and A319/A(-2) base pairs respectively (Table 2-3). It is possible that this interaction was selected to minimize the sequence-specific interaction to enhance cleavage of a wide variety of substrates. To further examine this phenomenon, genomic sequences at the 319 position of P RNA and the N(-2) position of the 5' leader from 40 bacterial RNase P and pre-tRNA species were compiled and aligned to ascertain whether the P RNA sequence at position 319 co-varies with the nucleotide preference at the N(-2) position (Table 2-5). The sequence alignments of P RNA from 40 species indicate that the sequence at position 319 is split equally between A (21/40) and G (19/40). The majority of RNase P species have a modest preference for A(-2) pre-tRNA (28/40) although preference for G and U are also observed (Table 2-5). These comparisons indicate that the G-A (14/40) and A-A (15/40) pairs at 319/N(-2) are the most frequent combination.

Based on the NMR and crystal structures of the RNA, Leontis and coworkers have proposed 13 possible non-Watson-Crick RNA base pairing motifs (31,32). Each motif is characterized by a unique isosteric matrix indicating pairs of nucleotides that can form a similar geometry and glycosidic bond orientations, suggesting possible base pair substitutions for each base-pairing motif. A comparison between the isotericity matrices and the identification of

A

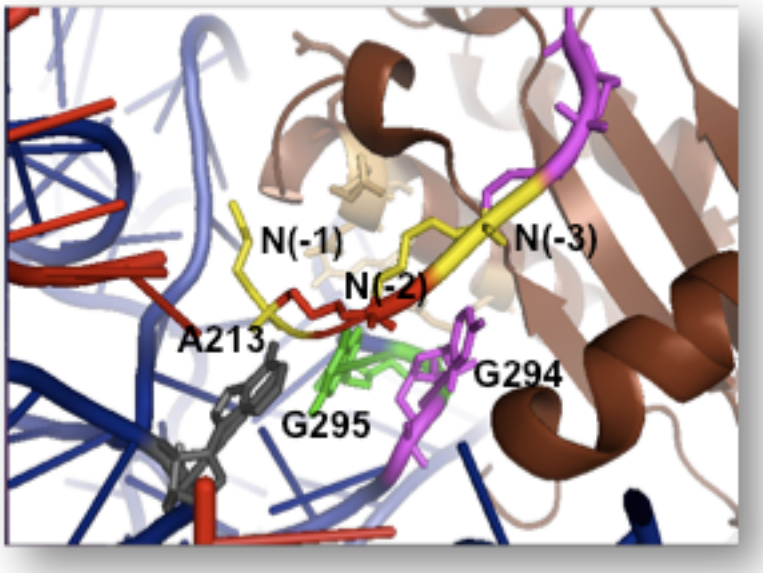

B

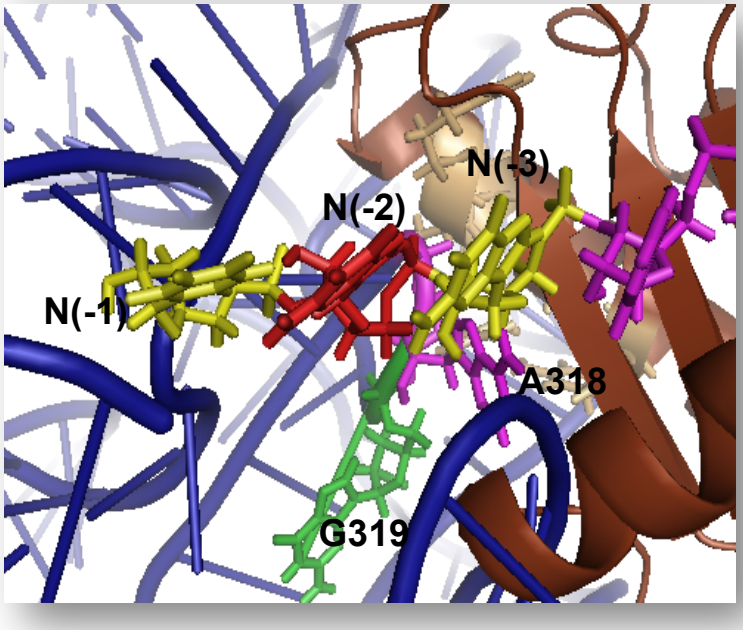

Figure 2-5: Structure of RNase P with bound pre-tRNA is generated using the Pymol program. (A) The crystal structure of *T. maritima* RNase P·tRNA·5' leader complex with 4.2 Å resolution (6). The N(-1) and N(-3) nucleotides, shown in yellow, are proposed to contact the A213 (gray) and U294 (magenta) nucleotides, respectively, while the N(-2) nucleotide, indicated in red, is proposed to be in contact with G295 (green). (B) The structural model *B. subtilis* RNase P is based on photocrosslinking and affinity cleavage data with 10 Å resolution (7). The N(-2) nucleotide, shown in red, is proposed to base pair with the G319 nucleotide (green). The N(-1) and N(-3) nucleotides are shown in yellow. The N(-3) nucleotide is proposed to base pair with A318 nucleotide (magenta). These contacts are not included in this model.

compensatory mutations at the G319 and N(-2) nucleotide from the binding affinity data, suggests the formation of a trans-Watson-Crick-sugar-edge interaction between the G319 and the N(-2) nucleotide (Figure 4-5). Because the sequence preference at the N(-2) position varies depending on the species while in bacteria is either A or G, we propose that the sugar-edge side of G319 directly contacts with the Watson-Crick side of the N(-2) nucleotide (Figure 4-5). This type of interaction allows G319 to directly contact various N(-2) nucleotides with different Watson-Crick structure, which allows bacterial RNase P to recognizes RNA substrates with variable sequence at N(-2) and maintains comparable binding affinity for the majority of nucleotide pairs between 319 and N(-2).

Sequence at N(-3) affect binding affinity

Bioinformatics analysis of the 5' leader of *B. subtilis* pre-tRNA shows no substantial sequence preference at the N(-3) position (1). However, the binding affinity data indicate a sequence preference for C(-3)- and U(-3)-pre-tRNA relative to the A(-3)- and G(-3)- by 1.2 kcal/mole (5' GANAU-pre-tRNA^{Asp}). Sequence preference for U and C at the N(-3) position is likely due to a combination of factors, including the structure of the 5' leader in unbound pre-tRNA and interaction with P RNA and/ or P protein and in the metal-stabilized conformational change occurs after pre-tRNA binding. From a structural perspective, addition of a purine at the N(-3) position in the 5' GANAU creates 5'-GAAAU and 5'-GAGAU sequences that enables base stacking of the three purine nucleotides. This could decrease the flexibility of the 5' leader sequences in unbound pre-tRNA and increase the energy barrier for contacting the P protein

in RNase P. Disruption of this base stacking upon binding to RNase P could explain the decreased affinity of pre-tRNA with A or G at N(-2) (Table 2-1). This explanation is also consistent with the observed effect of the N(-3) substitutions on the decreased stability of the metal-dependent conformational change, where the 5' leader docks into the binding cleft of the P protein (1,7,16). Pyrimidines (C and U) at the N(-3) position will decrease base stacking in unbound pre-tRNA and thus enhance the overall binding affinity.

Wild type RNase P preferentially binds to C(-3) pre-tRNA^{Asp} relative to the A(-3) substrate by 1.2 kcal/mole. However, the binding affinity of pre-tRNA and the specificity ratio of the A(-3) substrate relative to the C(-3) substrate for RNase P is altered by mutations in the RNR motif (N61C, R62C and R65A) up to 0.9 kcal/mole (Table 2-4). While a mutation in the central cleft of P protein (F16A) has little effect on selectivity, these results demonstrate that side chains in the RNR motif of the P protein effect recognition of the N(-3) nucleotide of pre-tRNA. Whether this is a direct or indirect effect is not clear. Affinity cleavage assays suggest that the N(-3) nucleotide is located within 15 Å of the RNR motif and the first β-strand of central β-cleft of the P protein (7,16). However, the *T. maritima* crystal structure of the RNase P·tRNA·5' leader complex positions the -3 nucleotide 6.5 Å away from the RNR motifs and the first β-strand of central β-cleft of the P protein (6). Furthermore, the R60 and R62 mutations that alter recognition of the N(-4) position in pre-tRNA also affect tRNA affinity, suggesting an indirect interaction (1,25). Nonetheless, selectivity at the N(-3) position is

altered by changes in both P RNA and P protein, suggesting that it is located near the P RNA/Pprotein subunit interface.

The crystal structure of the *T. maritima* RNase P·tRNA·5' leader (leader sequence of 5' GGCGU) positions the N(-3) nucleotide near U294 of P RNA (A318 in *B. subtilis* P RNA) and ≥ 10 Å from the protein subunit. However, compensatory mutations at the A318 and N(-3) nucleotides do not rescue the RNase P binding affinity, providing no evidence for direct contact between the A318 and N(-3) nucleotides. There are numerous explanations for these results. Based on the metal-dependent pre-tRNA binding mechanism, recognition of the N(-3) nucleotide of pre-tRNA is coupled to the metal stabilized conformational change step that occurs after binding to RNase P (Figure 2-4B). Since the crystal structure visualizes the RNase P·tRNA·5' leader product complex, it is possible that the position of N(-3) is altered. Alternatively, mutations at A318 in *B. subtilis* P RNA may alter the structure such that compensatory affects are not observed.

Bioinformatic analysis products RNase P substrate preferences

The binding affinity data for RNase P to pre-tRNAs with varying sequence at N(-2) correlate well with the preferences observed in the bioinformatics analysis (A>, C, U >G). This correlation suggests that molecular recognition between the N(-2) nucleotide of pre-tRNA and G319 of P RNA contribute to the observed preferences in the genomic sequences. Furthermore, the observed sequence preferences in the pre-tRNA leaders likely co-evolve with the binding preferences of RNase P. Therefore, the observed species-specific alterations in the genomic

sequences of pre-tRNA leaders likely also indicate alterations in RNase P substrate selectivity.

While the bioinformatics data correlate well with the RNase P substrate preferences at N(-1), N(-2) and N(-4) (1), no genomic preferences are observed for N(-3) despite clear binding affinity preferences in RNase P. This discrepancy could suggest that interactions between RNase P and the N(-3) nucleotide are key for tuning the affinity of the leader relative to the tRNA affinity to obtain the observed uniform binding of all pre-tRNA substrates that is important for maintaining effective concentrations of all processed cellular tRNAs.

Table 2-5. Sequence alignments of J5/15 and J18/2 helix of the P RNA and the N(-2) nucleotide.

Bacterial PRNA	J5/15[a]	J18/2[a]	N(-2)[b]
Agrobacterium tumefaciens	CAA	AGA UGA AU	G
Bacillus anthracis	AAA	AGA UAG AU	A
Bacillus subtilis	AAA	AGA UAG AU	A
Bacillus Halodurans	AAA	AGA CAG AU	A
Bacteroides thetaiotaomicron	UAA	AGA UAA AU	A
Bordetella pertussis	CAA	AGA GGA AU	C/U
Borrelia burgdorferi	CAA	AGA GAG AU	U
Caulobacter crecentus	CAA	AGA GGA AU	G
Clostridium acetobutylicum	CAA	AGA UAG AU	A
Chlamydia trachomatis	CAA	AGA UGA AU	A
Chlorobium tepidum	CAA	AGA UAA AU	A
Deinococcus radiodurans	CAA	AGA CAG AU	G
Enterococcus faecalis	CAA	AGA UAG AU	U
E. coli	CAA	AGA UGA AU	A
Haemophilus influenza	CAA	AGA GGA AU	A
Helicobacter pylori 26695	CAA	AGA UAA AU	A/U
Lactobacillus acidophilus	UAA	AGA UAG AU	A
Mycobacterium avium	CAA	AGA UGG AU	A
Mycobacterium bovis	CAA	AGA UGG AU	A/G
Mycobacterium leprae	CAA	AGA UGG AU	A
Mycobacterium tuberculosis	CAA	AGA UGG AU	A/G
Mycoplasma genitalium	AAA	AGA UAA AU	A
Mycoplasma hyopneumoniae	AAA	AGA UAA AU	A
Mycoplasma pneumoniae	AAA	ACA UAA AU	A
Neisseria gonnorhoeae	CAA	AGA GGA AU	A
Neisseria menigitidis	CAA	AGA GGA AU	A
Noctoc sp	CAA	AGA UAG AU	A
Pseudomonas Fluorescens	CAA	AGA CGA AU	A
Porphyromonas gingivalis	UAA	AGA UAA AU	A
Prochlorococcus marinus	CAA	AGA UAG AU	A
Rickettsia prowazekii	CAA	AGA UAA AU	A
Salmonella typhi	CAA	AGA UGA AU	A
Salmonella typhimurium	CAA	AGA UGA AU	A
Streptococcus pneumoniae	CAA	AGA CAG AU	U
Streptococcus pyogenes	CAA	AGA CAG AU	U
Thermotoga Maritima	CAA	AGA UUG AU	G
Thermus thermophilus	CAA	AGA GAG AU	G
Treponema pallidum	CAA	AGA CAG AU	U
Vibrio cholera	CAA	AGA GGA AU	G
Yersinia pestis	CAA	AGA GGA AU	A

[a] Sequences at J5/15 and J18/2 helices of P RNA were obtained from the RNase P database (37). The 319 nucleotide at the J18/2 helix from 40 bacterial P RNA genes is highlighted in yellow.

[b] Bioinformatics analysis of the N(-2) sequence preferences of the 5' leader from 40 bacterial pre-tRNA genes that were obtained from Genebank (38,39).

References

1. Koutmou, K. S., Zahler, N. H., Kurz, J. C., Campbell, F. E., Harris, M. E., and Fierke, C. A. (2010) *J Mol Biol* **396**, 195-208
2. Frank, D. N., and Pace, N. R. (1998) *Annu Rev Biochem* **67**, 153-180
3. Gopalan, V., Vioque, A., and Altman, S. (2002) *J Biol Chem* **277**, 6759-6762
4. Li, Y., and Altman, S. (2003) *Proc Natl Acad Sci U S A* **100**, 13213-13218
5. Peck-Miller, K. A., and Altman, S. (1991) *J Mol Biol* **221**, 1-5
6. Reiter, N. J., Osterman, A., Torres-Larios, A., Swinger, K. K., Pan, T., and Mondragon, A. (2010) *Nature* **468**, 784-789
7. Niranjanakumari, S., Day-Storms, J. J., Ahmed, M., Hsieh, J., Zahler, N. H., Venters, R. A., and Fierke, C. A. (2007) *Rna* **13**, 521-535
8. Seif, E., and Altman, S. (2008) *RNA* **14**, 1237-1243
9. Hansen, A., Pfeiffer, T., Zuleeg, T., Limmer, S., Ciesiolka, J., Feltens, R., and Hartmann, R. K. (2001) *Mol Microbiol* **41**, 131-143
10. Kirsebom, L. A., and Svard, S. G. (1994) *Embo J* **13**, 4870-4876
11. Oh, B. K., and Pace, N. R. (1994) *Nucleic Acids Res* **22**, 4087-4094
12. Pan, T., Loria, A., and Zhong, K. (1995) *Proc Natl Acad Sci U S A* **92**, 12510-12514
13. Loria, A., and Pan, T. (1997) *Biochemistry* **36**, 6317-6325
14. Crary, S. M., Niranjanakumari, S., and Fierke, C. A. (1998) *Biochemistry* **37**, 9409-9416
15. Kurz, J. C., Niranjanakumari, S., and Fierke, C. A. (1998) *Biochemistry* **37**, 2393-2400
16. Niranjanakumari, S., Stams, T., Crary, S. M., Christianson, D. W., and Fierke, C. A. (1998) *Proc Natl Acad Sci U S A* **95**, 15212-15217
17. Sun, L., Campbell, F. E., Zahler, N. H., and Harris, M. E. (2006) *Embo J* **25**, 3998-4007
18. Zahler, N. H., Christian, E. L., and Harris, M. E. (2003) *Rna* **9**, 734-745
19. Hsieh, J., Koutmou, K. S., Rueda, D., Koutmos, M., Walter, N. G., and Fierke, C. A. (2010) *J Mol Biol* **400**, 38-51
20. Rueda, D., Hsieh, J., Day-Storms, J. J., Fierke, C. A., and Walter, N. G. (2005) *Biochemistry* **44**, 16130-16139
21. Walter, N. G. (2001) *Methods* **25**, 19-30
22. Christian, E. L., and Harris, M. E. (1999) *Biochemistry* **38**, 12629-12638
23. Christian, E. L., Zahler, N. H., Kaye, N. M., and Harris, M. E. (2002) *Methods* **28**, 307-322
24. Koutmou, K. S., Casiano-Negroni, A., Getz, M. M., Pazicni, S., Andrews, A. J., Penner-Hahn, J. E., Al-Hashimi, H. M., and Fierke, C. A. (2010) *Proc Natl Acad Sci U S A* **107**, 2479-2484
25. Koutmou, K. S., Day-Storms, J. J., and Fierke, C. A. (2011) *RNA* **17**, 1225-1235
26. Niranjanakumari, S., Kurz, J. C., and Fierke, C. A. (1998) *Nucleic Acids Res* **26**, 3090-3096

27. Day-Storms, J. J., Niranjanakumari, S., and Fierke, C. A. (2004) *Rna* **10**, 1595-1608
28. Talbot, S. J., and Altman, S. (1994) *Biochemistry* **33**, 1399-1405
29. Smith, D., Burgin, A. B., Haas, E. S., and Pace, N. R. (1992) *J Biol Chem* **267**, 2429-2436
30. Haas, E. S., Banta, A. B., Harris, J. K., Pace, N. R., and Brown, J. W. (1996) *Nucleic Acids Res* **24**, 4775-4782
31. Leontis, N. B., Stombaugh, J., and Westhof, E. (2002) *Nucleic Acids Res* **30**, 3497-3531
32. Leontis, N. B., and Westhof, E. (2002) *Comp Funct Genomics* **3**, 518-524
33. Stams, T., Niranjanakumari, S., Fierke, C. A., and Christianson, D. W. (1998) *Science* **280**, 752-755
34. Beebe, J. A., and Fierke, C. A. (1994) *Biochemistry* **33**, 10294-10304
35. Beebe, J. A., Kurz, J. C., and Fierke, C. A. (1996) *Biochemistry* **35**, 10493-10505
36. Kurz, J. C., and Fierke, C. A. (2002) *Biochemistry* **41**, 9545-9558
37. Brown, J. W. (1999) *Nucleic Acids Res* **27**, 314
38. Benson, D. A., Karsch-Mizrachi, I., Lipman, D. J., Ostell, J., and Sayers, E. W. (2009) *Nucleic Acids Res* **37**, D26-31
39. Sayers, E. W., Barrett, T., Benson, D. A., Bryant, S. H., Canese, K., Chetvernin, V., Church, D. M., DiCuccio, M., Edgar, R., Federhen, S., Feolo, M., Geer, L. Y., Helmberg, W., Kapustin, Y., Landsman, D., Lipman, D. J., Madden, T. L., Maglott, D. R., Miller, V., Mizrachi, I., Ostell, J., Pruitt, K. D., Schuler, G. D., Sequeira, E., Sherry, S. T., Shumway, M., Sirotkin, K., Souvorov, A., Starchenko, G., Tatusova, T. A., Wagner, L., Yaschenko, E., and Ye, J. (2009) *Nucleic Acids Res* **37**, D5-15

CHAPTER 3

CLONING, EXPRESSION AND PURIFICATION OF HUMAN mtRNASE P PROTEINS

Background

Ribonuclease P (RNase P) is an essential enzyme that cleaves the 5' end of the precursor tRNA (pre-tRNA) to form a mature tRNA and 5' leader (1). All well-characterized RNase P enzymes to date are ribozymes, composed of a large catalytic RNA subunit (~400 nucleotides) that associates with one or more proteins in bacteria, archea and eukaryotes (2-4). In bacteria, the single RNase P protein reconstitutes with the RNase P RNA (P RNA) to strengthen the affinity of RNase P for substrates, to stabilize the RNase P holoenzyme complex, and to reduce the dependence of activity on the salt concentration as required for *in vivo* activity (5-9). However, the bacterial, archeal and eukaryal RNase P RNAs are homologous and proposed to be structurally related. Furthermore, the P RNA from bacteria and archea readily catalyzes cleavage of the 5' leader in the absence of protein under high salt conditions *in vitro* (1,10,11). Hence, RNase P was proposed as a universally conserved ribonucleoprotein retained from the primordial RNA world.

Unlike the RNA-dependent RNase P, human mitochondrial and spinach

chloroplast RNase Ps have been proposed to be protein-based enzymes because their densities are similar to protein rather than to RNA and their activities are insensitive to micrococcal nuclease treatment (12-15). However, a protein-based RNase P remained elusive to purification. In fact, the yeast mitochondrial RNase P is a protein-RNA complex (16,17) and one attempt at purification of the human mitochondrial RNase P suggested that the nuclear RNase P fulfilled this role (18). However, Rossmanith and colleagues recently discovered protein subunits containing RNase P activity purified from human mitochondria and *Arabidopsis thaliana* chloroplast; recombinant expression of these subunits in bacteria confirmed that these organellar RNase P are composed of proteins (19,20). These data suggest that the newly identified human mitochondrial RNase P is composed of three protein subunits (MRPP1, MRPP2 and MRPP3) that are nuclear encoded and imported into the mitochondria. These proteins were isolated and identified by a combination of partial protein purification, mass spectrometry and enzymatic activity approaches. The three protein subunits appear to have distinct functionalities and Rossmanith and colleagues demonstrated that the complex reconstituted from recombinant subunits catalyze the cleavage of the 5' end of (mt)pre-tRNA. In contrast, similar experiments to identify the chloroplast RNase P suggest that only a single subunit (PROP1, homologous to MRPP3) is essential for catalytic activity (19).

MRPP1 (*RG9MTD1*) is annotated as a RNA (guanosine-9-) methyltransferase domain that is homologous to yeast *TRM10*. Trm10p is a tRNA m^1G methyltransferases that catalyzes N^1 methylation of guanosine at position 9 of

tRNA using S-adenosyl methionine as a co-substrate (21). Unpublished data suggests that MRPP1 catalyzes the methylation of G_9 of human (mt)tRNAs (Holzmann J and Rossmanith W, unpublished data), Therefore, MRPP1 is proposed to function as a m^1G methyltransferase (20). Methylation of pre-tRNA could enhance the recognition of substrates by RNase P; however, the RNase P assays to date did not use methylated (mt)pre-tRNA substrates and no SAM was added to the assays. MRPP2 (*HSD17B10*) is a short-chain dehydrogenase/reductase that catalyzes β-oxidation of steroid and fatty acid substrates using NAD^+ as a co-substrate (22). This enzyme also belongs to the short chain dehydrogenase/reductase (SDR) family with a NAD^+ domain (Rossmann fold) that has been proposed to bind RNA (23-25). The third subunit, MRPP3 is a member of a novel domain family that is predicted to have metal-dependent nuclease activity (20). Sequence alignments of MRPP3 protein homologs indicate two pentatricopeptide repeat (PPR) motifs and four strictly conserved amino acids (3 aspartates and 1 histidine) that have been proposed to bind RNA and metal ions, respectively (20,26,27). Furthermore, the recently identified *Arabidopsis thaliana* RNase P, PRORP1, is an ortholog to MRPP3 (19). These data suggest that MRPP3 is a member of a new family of metal-dependent ribonucleases. However, the role of each of the proposed human mtRNase P subunits in catalysis is poorly understood. Additionally, the catalytic mechanism and the molecular recognition of this protein-based RNase P enzyme remain to be elucidated.

To investigate the roles of MRPP1, MRPP2 and MRPP3 in the human

mtRNase P catalysis, these proteins were individually cloned, recombinantly expressed and purified from *Escherichia coli (E. coli*) cells. This chapter will describe the cloning, expression and purification of the human mtRNase P subunits. The cDNA for these proteins was purchased from the American Type Culture Collection (ATCC), subcloned into the JEJ494 and pETM11 vectors and his-tagged versions of the proteins expressed in *E. coli* cells. Immobilized metal affinity (IMAC) and anion-exchange chromatography were employed to purify each of the subunits to reconstitute the human mtRNase P protein complex.

Materials and Methods

Subcloning of each of the human mtRNase P subunits

MRPP2 (cat. No. MGC-8345) and MRPP3 (cat. No. MGC-36741) cDNA clones were purchased from ATCC. The coding sequences of the putative MRPP2 were amplified using the polymerase chain reaction (PCR) with 0.004U/μL *PfuTurbo*® DNA polymerase, 0.2mM dNTP mix, 10x reaction buffer (Stratagene) and the following primers (0.4 μM) (forward primer, FP and reverse primer, RP): FP 5' GGG CCA TAT GGC AGC AGC GTG TCG G 3', RP 5' GGG CTC GAG TCA AGG CTG CAT ACG 3' (purchased from IDT). The PCR reaction cycle was as the following: (a) In the first cycle, the reaction was heated to 94^{o}C for 30 sec. (b) In the second cycle, the reaction was heated to 94^{o}C for 30 sec and annealed at 55^{o}C for 30 sec followed by elongation at 72^{o}C for 2 min. The second cycle was repeated for 26 times. (c) In the third cycle, reaction was heated to 94^{o}C for 30 sec and annealed at 55^{o}C for 30 sec followed by elongation at 72^{o}C for 11 min. MRPP2 PCR product and the pETM11 vector were both digested with NdeI and

XhoI restriction enzymes at unique restriction sites (New England Biolab, NEB). The MRPP2 gene was ligated to the pETM11 using the final concentration of 1X T4 DNA ligase buffer, 400U T4 DNA ligase (NEB), and 1:3 and 1:6 ratio of vector:insert in the 20 uL ligation reaction. The ligation reaction was incubated on ice overnight and transformed into the SmartCells™ (Genlantis) the following day. There are two NdeI sites in the MRPP3 sequence therefore site-directed mutagenesis was performed to remove the two NdeI sites (C to T at nucleotide 564 and 1680), while retaining the MRPP3 amino acid in sequence. PCR was performed on the MRPP3 gene by using 0.004U/μL Taq polymerase, 0.2 mM dNTP mix, 10x reaction buffer (Stratagene) and the following primers (0.4 μM); FP 5' GGA ACC AGC AGC ATA TGT TTT CTC TTA AAA CAA TGT CTC C 3', RP 5' GAG GTC AGA ACT CGA GTC ATG TCT TTT GGT GGA GGC 3'. The MRPP3 PCR product was ligated to pCR®4-TOPO® vector using the TOPO TA cloning® kit (Invitrogen). The PCR cycle used for MRPP3 was same as the PCR cycle for cloning MRPP2 gene. Both the ligated MRPP3 gene and the pETM11 vector were double digested with NdeI and XhoI restriction enzymes followed by ligation with Quick T4 DNA Ligase (NEB) as described in the Quick T4 DNA Ligase kit. The ligated reaction was transformed into SmartCells™. The plasmids encoding MRPP2 (pMR2-TEV-His) and MRPP3 (pMR3-TEV-His) were purified and the correct gene sequence confirmed by sequencing at the Michigan DNA Sequencing Center. A plasmid encoding recombinant MRPP1 (pMR1-3C-His) was a gift from Dr. Jane Jackman (Ohio State University) and is composed of an

N-terminal 6x His-tag, followed by a 3C protease cleavage site and then amino acids 40 to 403 of MRPP1, deleting a putative mitochondrial imported sequence.

Expression of human mtRNase P protein subunits

The MRPP1 plasmid (pMR1-3C-His) was transformed into BL21(DE3)pLysS *E. coli* and the cells grown in Luria broth (LB) media at 37°C to an OD_{600} ~ 0.8. Protein expression was induced by the addition of 1 mM isopropylthio-β-D-galactopyranoside (IPTG) and incubation at 16°C overnight. Plasmids encoding MRPP2 (pMR2-TEV-His) and MRPP3 (pMR3-TEV-His) were transformed into the Rosetta(DE3) *E. coli* strain (Novagen) and grown in the LB media at 37°C to an OD_{600} ~ 0.8. Protein expression was induced by the addition of 1 mM IPTG and incubation at 16°C overnight. The cells expressing MRPP1 and MRPP2 were resuspended in lysis buffer (20 mM Tris-HCl pH 7.5, 15% glycerol, 150 mM NaCl, 30 mM imidazole, 0.1 mM TCEP, 0.02% Tween 20, 0.1% proteinase inhibitor cocktail (Thermo Scientific) and 0.3 mg/mL phenylmethylsulfonyl fluoride (PMSF)). Cells expressing MRPP3 was resuspended in the same lysis buffer with 20 mM MOPs (pH 7.8) substituted for 20 mM Tris-HCl (pH 7.5). The resuspended cells were frozen at -80°C until ready to be purified.

Purification of recombinant MRPP1, MRPP2 and MRPP3

Cells expressing MRPP1, MRPP2 or MRPP3 were lysed by sonication and centrifuged at 16 000g for 30 minutes for clarification of the cell lysate. The cleared lysate was applied to an IMAC column (GE healthcare) that was charged with 50 mM $NiSO_4$. About 1 mL of IMAC resins for 1 L culture was used and the cleared lysate was run through the Ni(II)-charged column. The MRPP1 and

MRPP2 subunits were eluted using a linear gradient from 30 mM to 500 mM imidazole in buffer A (20 mM Tris-HCl pH 7.5, 15% glycerol, 150 mM NaCl, 0.1 mM TCEP and 0.02% Tween 20). MRPP3 was eluted with linear gradient from 30 mM to 300 mM imidazole with the buffer A containing 20 mM MOPS (pH 7.8), replacing the Tris-HCl (pH 7.5). About 1000 U of 6x His-tagged TEV protease (ProTEV Plus from Promega) was added to the MRPP2 and MRPP3 proteins, while about 500 U of 6x His-tagged 3C protease (Novagen) was added to the MRPP1 protein. The protease cleavage reactions were dialyzed against buffer A at 4^{o}C overnight. The cleaved proteins were applied to a second Ni-IMAC column; the his-tagged proteases and proteins and nucleic acids that interact non-specifically with the nickel resin should be retained on the column while the cleaved proteins should elute in the flow-through. MRPP3 was further purified using an anion or cation-exchange chromatography (DEAE or SP column from GE healthcare). MRPP3 was dialyzed against buffer B (20 mM MOP pH 7.8, 15% glycerol, 50 mM NaCl and 0.1 mM TCEP) at 4^{o}C overnight. ~ 0.1 mg/mL MRPP3 protein (10 mL of volume) was applied to a 5 mL DEAE column and eluted using a linear gradient from 50 mM and 500 mM NaCl. For the SP column, the MRPP3 was dialyzed in buffer C (20 mM Tris-HCl pH 7.5, 15% glycerol, 150 mM NaCl and 0.1 mM TCEP) at 4^{o}C overnight. ~ 1 mg/ mL of MRPP3 (15 mL of volume) was loaded onto the 5 mL SP column followed by elution with a linear gradient from 150 mM to 2 M NaCl. The MRPP proteins were concentrated using Vivopore concentrator or Ficoll treatment before EDTA dialysis.

To chelate co-eluting divalent metal ions, 0.7 mg/mL of MRPP1 (2.5 mL of volume) and 0.1 mg/mL of MRPP2 (2 mL of volume) were dialyzed once against 1 L of buffer C containing 1 mM EDTA, while 0.05 mg/mL of MRPP3 (3 mL of volume) was dialyzed once against 1 L of buffer D (30 mM MOP pH 7.8, 15% glycerol, 150 mM NaCl, 0.1 mM TCEP and 1 mM EDTA) at 4^{o}C overnight. The recombinant proteins were further dialyzed once against 1 L of metal free buffer, that was pre-incubated with CHELEX®100 resins (Bio-Rad) without EDTA at 4^{o}C overnight. The concentration of metal ions associated with each recombinant protein was determined by inductively coupled plasma mass spectrometry (ICP-MS) at the Department of Geological Sciences by Dr. Ted Hudson.

Results

cDNA clones of MRPP1, MRPP2 and MRPP3

The MRPP1 cDNA construct, subcloned into the JEJ494 vector, is composed of an N-terminal His_6-tag, a 3C protease cleavage site followed by the coding region of MRPP1 encoding amino acids 40 to 403 (the mitochondrial signaling sequence at the N-terminus of MRPP1 is removed, see Figure 3-1A). cDNA constructs of the MRPP2 and MRPP3 genes are cloned into the pETM11 vector. The MRPP2 and MRPP3 genes are composed of 783 and 1749 nucleotides, respectively, encoded between the NdeI and XhoI restriction sites of the pETM11 vector. Recombinant MRPP2 is comprised of an N-terminal 6x His-tag and a TEV-protease cleavage site followed by the full length coding sequence of MRPP2 (Figure 3-1B). Recombinant MRPP3 has an N-terminal 6x His-tag followed by a TEV-protease cleavage site and amino acid 46 to 583 (Figure 3-1C). The first 45 amino acids of MRPP3 encoding the mitochondrial signal localization sequence is removed.

Recombinant expression of MRPP1, MRPP2 and MRPP3 in *E. coli* cells

Recombinant MRPP1, MRPP2 and MRPP3 are expressed in the *E. coli* cells transformed with the respective T7 expression plasmid (2.5 to 6 mg protein/L cell culture). Overexpression of each of these proteins in *E. coli* cells was confirmed using His-tag western blot analysis (Figure 3-2B, Figure 3-5D and Figure 3-7C). The 45 kDa MRPP1 protein is solubly expressed in both BL21(DE3)pLysS and BL21(DE3) cells at 18^0C upon induction with 1 mM IPTG. The His-tag western blot analysis of MRPP1 indicates some protein degradation (Figure 3-2B).

A.

MAHHHHHHMGTLEAQT(Q/G)PGSMSSKIPAVTYPKNESTPPSEELELDKWKTT
MKSSVQEECVSTISSSKDEDPLAATREFIEMWRLLGREVPEHITEEELKTLMEC
VSNTAKKKYLKYLYTKEKVKKARQIKKEMKAAAREEAKNIKLLETTEEDKQKNFL
FLRLWDRNMDIAMGWKGAQAMQFGQPLVFDMAYENYMKRKELQNTVSQLLE
SEGWNRRNVDPFHIYFCNLKIDGALHRELVKRYQEKWDKLLLTSTEKSHVDLFP
KDSIIYLTADSPNVMTTFRHDKVYVIGSFVDKSMQPGTSLAKAKRLNLATECLPL
DKYLQWEIGNKNLTLDQMIRILLCLKNNGNWQEALQFVPKRKHTGFLEISQHSQ
EFINRLKKAKT

B.

MKHHHHHHPMSDYDIPTTENLYFQ(G/H)MAAACRSVKGLVAVITGGASGLGLA
TAERLVGQGASAVLLDLPNSGGEAQAKKLGNNCVFAPADVTSEKDVQTALALA
KGKFGRVDVAVNCAGIAVASKTYNLKKGQTHTLEDFQRVLDVNLMGTFNVIRLV
AGEMGQNEPDQGGQRGVIINTASVAAFEGQVGQAAYSASKGGIVGMTLPIARD
LAPIGIRVMTIAPGLFGTPLLTSLPEKVCNFLASQVPFPSRLGDPAEYAHLVQAII
ENPFLNGEVIRLDGAIRMQP

C.

MKHHHHHHPMSDYDIPTTENLYFQ(G/H)MFSLKTMSPQNTKATNLIAKARYLRK
DEGSNKQVYSVPHFFLAGAAKERSQMNSQTEDHALAPVRNTIQLPTQPLNSEE
WDKLKEDLKENTGKTSFESWIISQMAGCHSSIDVAKSLLAWVAAKNNGIVSYDL
LVKYLYLCVFHMQTSEVIDVFEIMKARYKTLEPRGYSLLIRGLIHSDRWREALLLL
EDIKKVITPSKKNYNDCIQGALLHQDVNTAWNLYQELLGHDIVPMLETLKAFFDF
GKDIKDDNYSNKLLDILSYLRNNQLYPGESFAHSIKTWFESVPGKQWKGQFTTV
RKSGQCSGCGKTIESIQLSPEEYECLKGKIMRDVIDGGDQYRKTTPQELKRFEN
FIKSRPPFDVVIDGLNVAKMFPKVRESQLLLNVVSQLAKRNLRLLVLGRKHMLR
RSSQWSRDEMEEVQKQASCFFADDISEDDPFLLYATLHSGNHCRFITRDLMRD
HKACLPDAKTQRLFFKWQQGHQLAIVNRFPGSKLTFQRILSYDTVVQTTGDSW
HIPYDEDLVERCSCEVPTKWLCLHQKT

Figure 3-1: Protein sequences of the three human mtRNase P subunits encoded in the JEJ494 and pETM11 vectors. (A) Sequence of the MRPP1 protein encoded by the pMR1-3C-His plasmid with the 6x His-tag highlighted in yellow, the 3C protease cleavage site sequence in red and the MRPP1 protein sequence from amino acid 40 to 403 underlined. (B) Sequence of the MRPP2 protein encoded by the pMR2-TEV-His plasmid with the 6x His-tag highlighted in yellow, TEV protease cleavage site sequence in green and the MRPP2 full length protein sequence underlined the TEV protease cleavage site sequence in green and the protein sequence underlined. (C) Sequence of the MRPP3 protein encoded by the pMR3-TEV-His plasmid with the 6x His-tag highlighted in yellow, TEV protease cleavage site sequence in green and the MRPP3 protein sequence starting from amino acid 46 to 583 underlined.

cells compared to BL21(DE3) pMR1-3C-His plasmid cells (Figure 3-2). To reduce the protein degradation by the cellular proteases, the temperature for expression of MRPP1 in BL21(DE3)pLysS pMR1-3C-His cells was lowered to 16°C since this decreases the proteolytic activity in *E. coli* cell lysates (28).

To optimize recombinant expression of the 28 kDa MRPP2 in *E. coli* the media (auto-induction and LB media), IPTG concentration (0 to 400 μM) and cell lines (BL21(DE3) and Rosetta(DE3) cells) were varied using the 96 well-plates. To evaluate expression levels of MRPP2, the cells were induced, incubated at 28^0C overnight, pelleted and then lysed by addition of the B-Per II bacterial protein extraction reagent (Thermo Scientific). The soluble and insoluble proteins were separated by centrifugation and fractionated on by SDS polyacrylamide gel electrophoresis (SDS-PAGE) (Figure 3-3). These data illustrate that the expression level of the MRPP2 is unaffected by the cell line (Rosetta(DE3) and BL21(DE3) cells) (Figure 3-3A and 3-3B) or the culture medium/induction method (auto-induction versus LB/IPTG medium). However, the majority of the expressed MRPP2 is insoluble (Figure 3-3C and 3-3D). Alternatively, the expression level of MRPP2 can be optimized by varying temperature, from 34^oC to 16^oC to increase in the MRPP2 solubility. Currently, to obtain sufficient MRPP2 protein for activity measurement, the MRPP2 is grown in Rosetta(DE3) cells at 37^oC followed by induction with 1 mM IPTG at OD_{600} ~0.8 and continued to grow at 16^oC (as described in (20)).

The 62 kDa MRPP3 was expressed in both the BL21(DE3)pLysS and Rosetta(DE3) cells, induced by addition of 1 mM IPTG and incubation for 16 to

18 hr at 16°C followed by SDS-PAGE analysis. Based on the SDS-PAGE analysis, the MRPP3 has higher expression level in the Rosetta(DE3) cells relative to BL21(DE3)plysS cells (Figure 3-5A and 3-5B). To examine the expression levels of MRPP3 in Rosetta(DE3) cells, the cells were induced, incubated at 16^0C overnight, pelleted and then lysed by addition of the B-Per II bacterial protein extraction reagent (Thermo Scientific). The soluble and insoluble proteins were separated by centrifugation and fractionated on by SDS polyacrylamide gel electrophoresis (SDS-PAGE) (Figure 3-4). These data illustrate that the expression level of MRPP3 does not increase after induction with 1 mM IPTG for 4 to 20 hr (Figure 3-4A) and MRPP3 protein is not in the insoluble form as well (Figure 3-4B). This could be due to the toxicity of the MRPP3 protein toward *E. coli* cells and cause cells death.

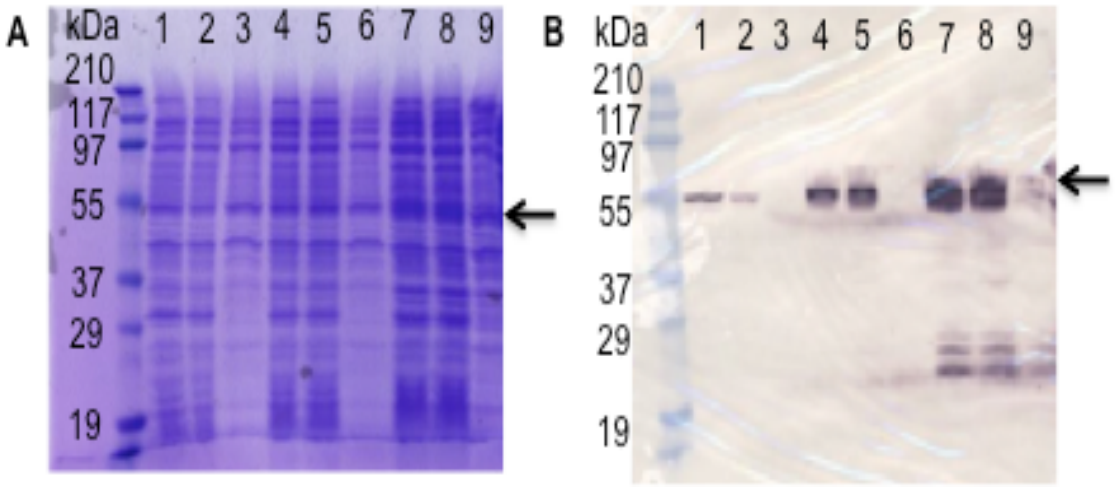

Figure 3-2: SDS-PAGE and Western blot analysis of recombinant expression of MRPP1 protein. (A) Expression level of MRPP1 (indicated by arrow) in the cleared lysates from BL21(DE3)pLysSpMR1-3C-His and BL21(DE3)pMR1-3C-His cells. The cleared lysates are the total expression from BL21(DE3)pLysSpMR1-3C-His and BL21(DE3)pMR1-3C-His cells. Lanes 1 and 2 are lysates from non-induced BL21(DE3)pLysSpMR1-3C-His cells, while lane 3 is the lysate from non-induced BL21(DE3)pMR1-3C-His cells. Lanes 4, 5 (duplicate samples) and 7, 8 (duplicate samples) are lysates from BL21(DE3)pLysSpMRP1-3C-His cells at 2 ½ and 20 hours, respectively, after induction with 1 mM IPTG and incubation at 18°C, correspondingly. Lane 6 and 9 are lysates from BL21(DE3)pMR1-3C-His cells at 2 ½ and 20 hours, respectively, after induction with 1 mM IPTG and incubation at 18°C, respectively. (B) His-tag western blot analysis of MRPP1 expressed in the lysates of BL21(DE3)pLysSpMR1-3C-His and BL21(DE3)pMR1-3C-His cells. The samples loaded in lanes 1 to 9 correspond to the samples in lanes 1 to 9 in (A).

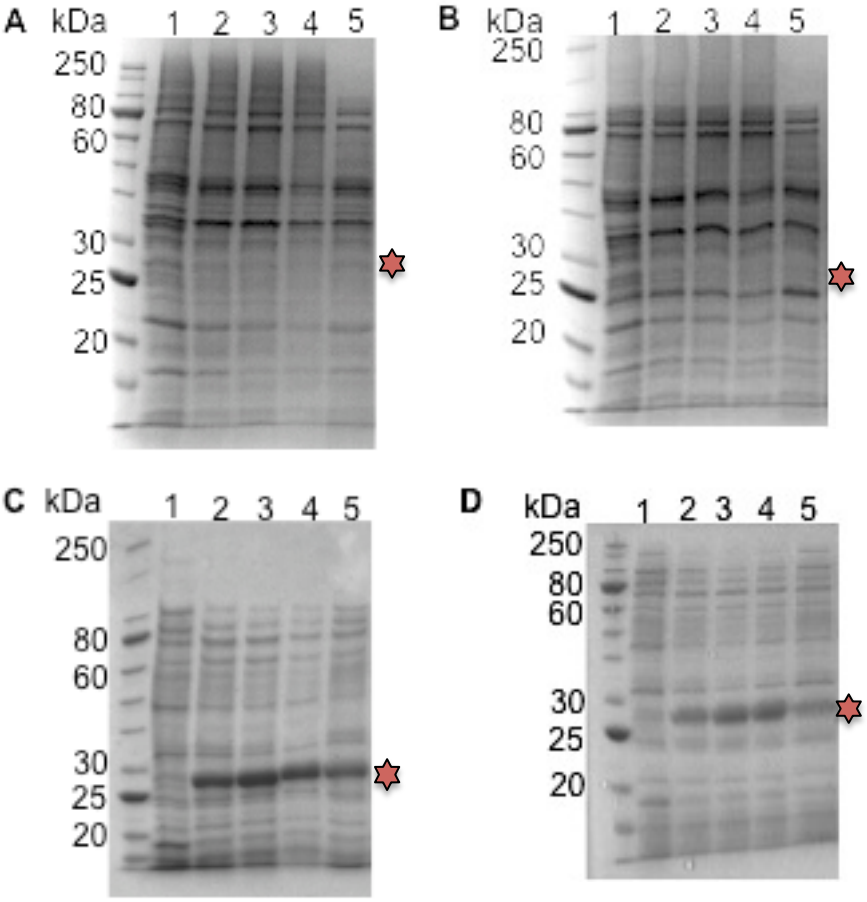
A
kDa
1 2 3 4 5
250
80
60
30
25
20
B
kDa
1 2 3 4 5
250
80
60
30
25
20
C
kDa
1 2 3 4 5
250
80
60
30
25
20
D
kDa
1 2 3 4 5
250
80
60
30
25
20

Figure 3-3: Level of MRPP2 (shown by red star) expression in BL21(DE3) and Rosetta(DE3) cells transformed with pMR2-TEV-His as indicated by fractionation on a SDS-PAGE gel. (A) Expression level of soluble MRPP2 in cell lysates from Rosetta(DE3)pMR2-TEV-His cells grown in auto-induction or LB media with varied IPTG concentrations at 28°C. Lane 1 is the lysate from non-induced cells, while lanes 2, 3, and 4 contain the lysates from Rosetta(DE3)pMR2-TEV-His cells induced with 50, 100 and 400 μM IPTG, respectively, in LB media while lane 5 is from the lysate from cells grown in auto-induction media. (B) The samples loaded onto the SDS-PAGE gel are the same as those in panel (A) except that the cell line is BL21(DE3)pMR2-TEV-His. (C) Expression level of the insoluble MRPP2 protein in Rosetta(DE3) cells. The samples loaded onto the SDS-PAGE gel are taken from the same cell growths as panel (A) but here the insoluble fraction is loaded onto the gel, rather than the soluble fraction shown in (A). (D) Same as (B) with exception that the insoluble fraction is loaded onto the gel.

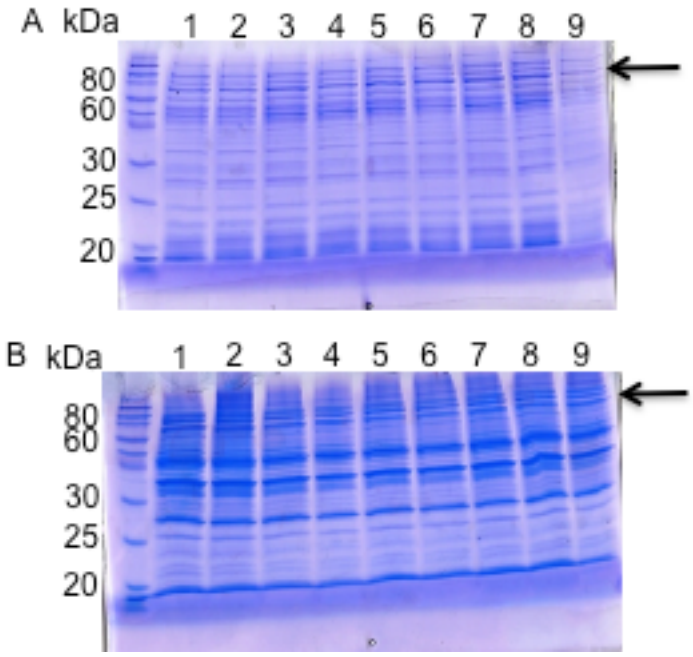

Figure 3-4: Level of MRPP3 (shown by arrow) expression in Rosetta(DE3) cells transformed with pMR3-TEV-His as indicated by fractionation on a SDS-PAGE gel. (A) Expression level of soluble MRPP3 in cell lysates from Rosetta(DE3)pMR3-TEV-His cells grown in LB media at 16^{o}C. Lane 1, 2, and 3 are the soluble MRPP3 from non-induced cells, while lanes 4, 5, and 6 contain the lysates from Rosetta(DE3)pMR3-TEV-His at 4 hr after induction with 1 mM IPTG and incubation at 16°C. Lanes 7, 8, and 9 contain the lysates from Rosetta(DE3)pMR3-TEV-His at 20 hr after induction with 1 mM IPTG and incubation at 16°C. (B) Expression level of insoluble MRPP3 in cell lysates from Rosetta(DE3)pMR3-TEV-His cells grown in LB media at 16^{o}C. The samples loaded onto the SDS-PAGE gel are the same as those in panel (A) except that the MRPP3 protein is insoluble.

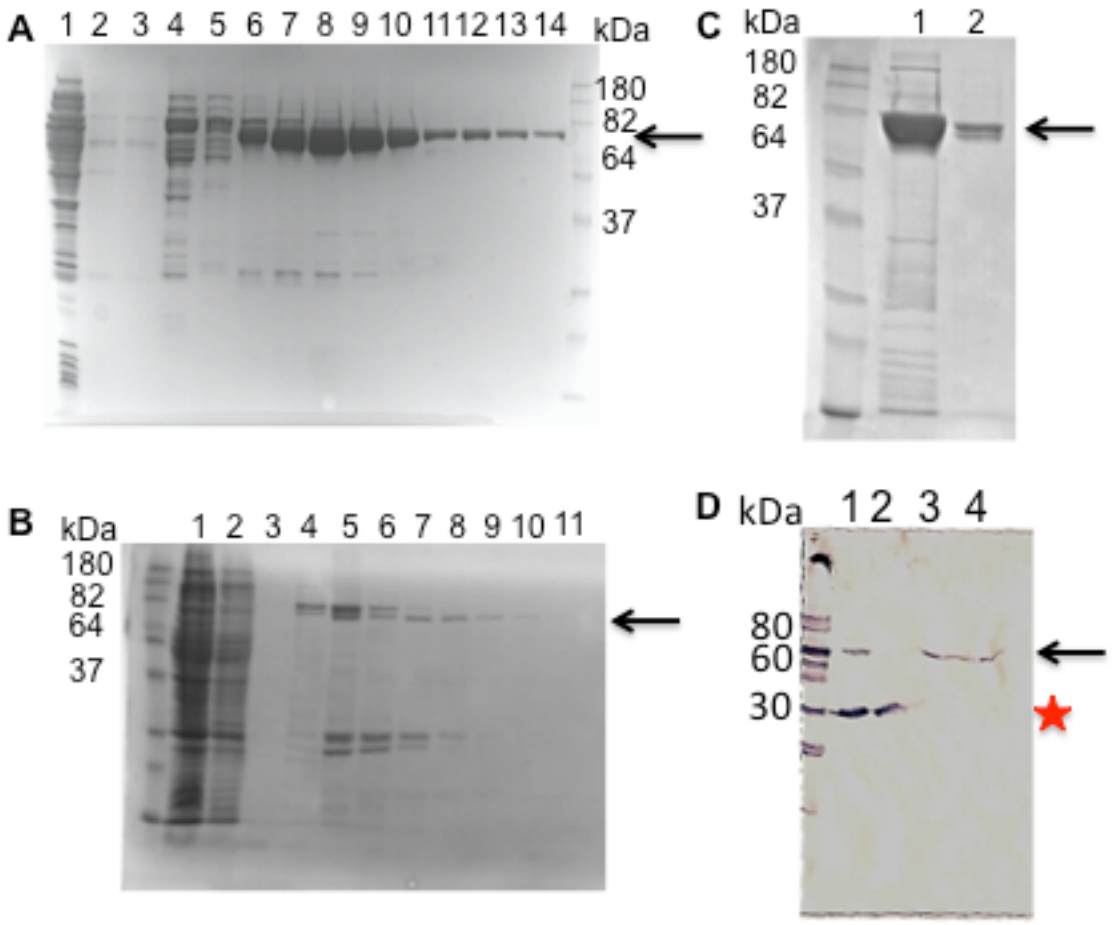
A
1 2 3 4 5 6 7 8 9 10 11 12 13 14
kDa
180
82
64
37
B
kDa
1 2 3 4 5 6 7 8 9 10 11
180
82
64
37
C
kDa
1 2
180
82
64
37
D
kDa
1 2 3 4
80
60
30

Figure 3-5: SDS PAGE analysis of MRPP3 (shown by arrow) protein purification from recombinant expression in either Rosetta(DE3)pMR3-TEV-His or BL21(DE3)pLysSpMR3-TEV-His cells. (A) SDS PAGE analysis of MRPP3 expressed in BL21(DE3)pLysSpMR3-TEV-His cells and fractionation using a Ni(II)-Chelating Sepharose with an imidazole gradient. Lane 1 is the cleared cellular lysate containing soluble MRPP3 that is loaded onto the column and lanes 2 and 3 are flow-through and first wash of the column. Lanes 4 to 14 show the protein elution profile; MRPP3 elutes from the Ni(II) column mainly in lanes 6 - 10. B) SDS PAGE analysis of MRPP3 expressed in Rosetta(DE3)pMR3-TEV-His cells and fractionation using a Ni(II)-Chelating Sepharose with an imidazole gradient. Lane 1 is the cleared cellular lysate containing soluble MRPP3 that is loaded onto the column and lane 2 is the flow-through from the column. Lanes 3 to 11 show the protein elution profile; MRPP3 elutes from the Ni(II) column mainly in lanes 4 – 6, although multiple bands are observed in this eluate. (C) SDS-PAGE analysis of MRPP3 from (A) after cleavage by TEV protease and fractionation on a second Ni(II) column. Lane 1 is the His-tagged MRPP3 before cleavage with TEV protease and Lane 2 is MRPP3 after cleavage and purification on a second Ni(II) column. This protein is estimated as 90% pure. (D) His-tag western blot analysis of MRPP2 and MRPP3 expressed in the lysates of Rosetta(DE3)pMR2-TEV-His and BL21(DE3)pLySpMR3-TEV-His cells. Lane 1 and 2 are MRPP2 protein (shown by red star) that serves as a positive control for His-tag western blots. Lane 3 is soluble MRPP3 protein and lane 4 is MRPP3 protein after first Ni(II) column.

Purification of MRPP1, MRPP2 and MRPP3 proteins

The His-tagged MRPP1, MRPP2 and MRPP3 proteins are purified using IMAC affinity chromatography with Chelating Sepharose matrix charged with $NiSO_4$. The His-tagged MRPP1, MRPP2 and MRPP3 each elute from the Ni(II)-charged IMAC column at about 100 mM imidazole. After proteolytic cleavage of the his-tag and purification using a second Ni(II)-IMAC column, MRPP1 and MRPP2 are ~95% pure, while the MRPP3 is > 90% pure based on SDS-PAGE analysis (Figure 3-6B, 3-7B, and 3-5C). The purified MRPP1, MRPP2 and MRPP3 contain a cleavable His-tag and are cleaved with the 3C and TEV proteases, respectively. The 3C protease cleaves the MRPP1 with ~ 90% efficiency, while the TEV protease cleaves the MRPP2 and MRPP3 with ~ 50% efficiency (Figure 3-6B, 3-7B and 3-5C).

For purification of MRPP3, precipitation observed when the protein is concentrated using the Amicon Ultra centrifugal filters. Therefore, gentle methods to concentrate the protein, such as Vivapore concentrator or Ficoll treatment is necessary. Additionally, the 260 nm/280 nm absorbance ratio of the MRPP3 protein was ~1.0, suggesting that nucleic acids co-eluted with this protein. Therefore, MRPP3 was further purified using either anion (DEAE-Sephacel™ Fast Flow) or cation (SP-Sepharose™ Fast Flow) exchange chromatography with a salt gradient to remove contaminating proteins and nucleic acids (Figure 3-8). MRPP3 is eluted from the DEAE and SP columns at ~150 mM NaCl and 700 mM NaCl, respectively. The DEAE column successfully removes nucleic acids, as indicated by a decrease in the 260/280 nm absorbance ratio of MRPP3 to 0.8.

However, after the SP column the 260/280 nm absorbance ratio of MRPP3 remains at ~ 1.0, suggesting that nucleic acids co-elute with MRPP3. After cation exchange chromatography the purity of MRPP3 is estimated as 95%. The activity measurement of the purified MRPP proteins will be alluded to Chapter 4.

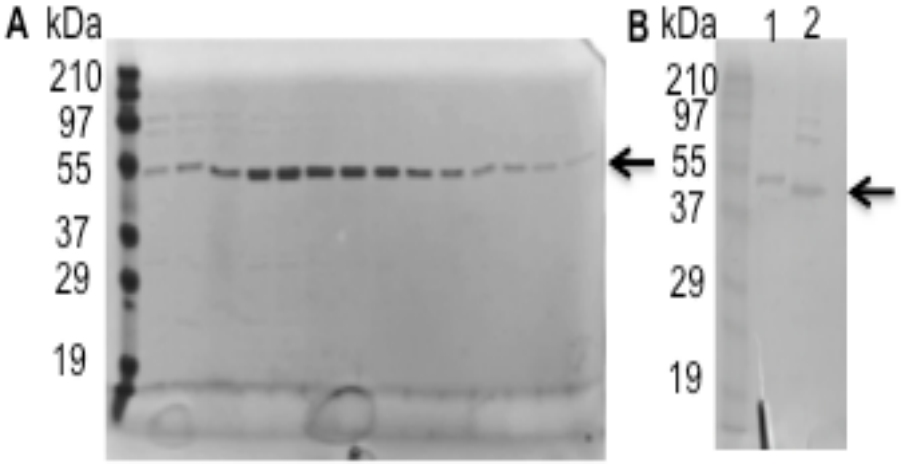

Figure 3-6: Purification of His-tagged MRPP1 by affinity chromatography. (A) SDS-PAGE analysis of MRPP1 fractionation on a Ni(II)-charged IMAC column. The His-tagged MRPP1 protein is applied to the Ni(II) column in 20 mM Tris-HCl pH 7.5, 15% glycerol, 150 mM NaCl, 0.1 mM TCEP, 30 mM imidazole buffer and 0.02% Tween 20 and is eluted with linear gradient from 90 to 500 mM imidazole. Lane 1 is molecular mass standards. MRPP1 (shown by the arrow) elutes from the NI(II) column upon addition of 90 mM imidazole (fractions 1 to 27). (B) The 6x His-tag attached to purified MRPP1 is cleaved by incubation with 3C protease. Lane 1 is the His-tagged MRPP1 before cleavage and lane 2 is the cleaved MRPP1 protein after purification on the second Ni(II) column.

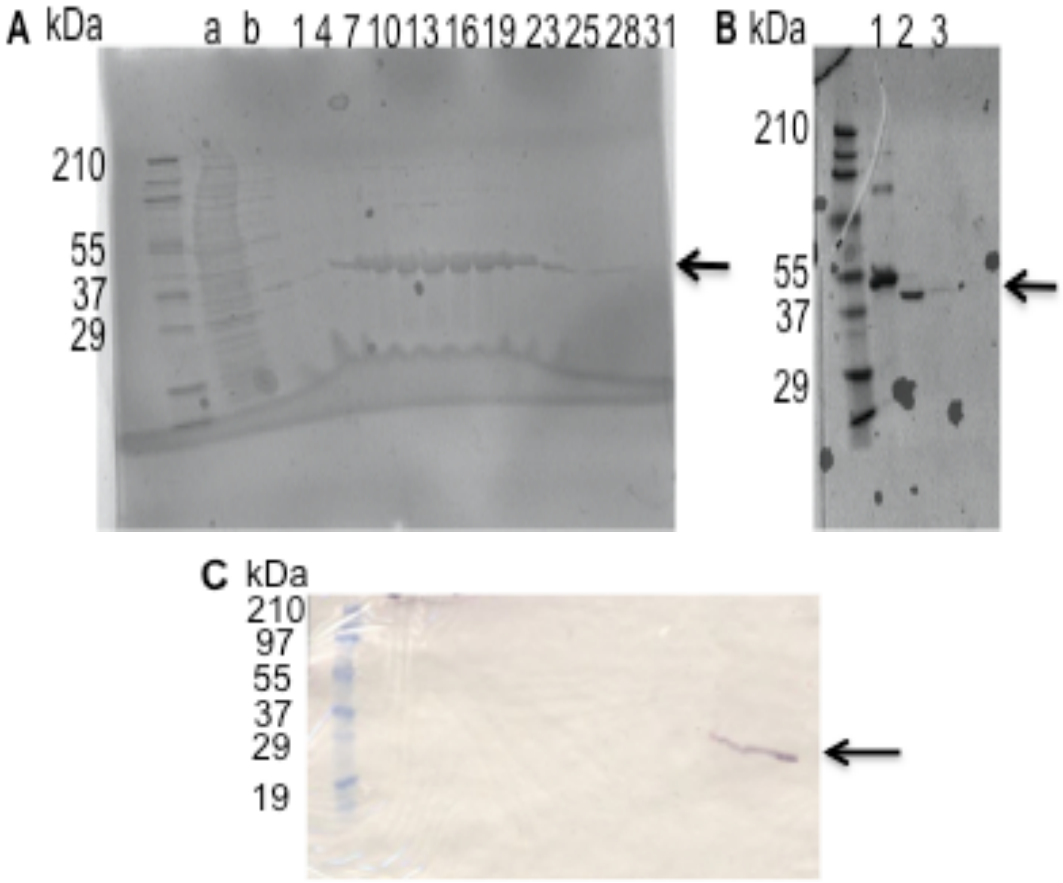

Figure 3-7: Purification of MRPP2 protein by Ni(II)-charged IMAC column. (A) SDS-PAGE analysis of MRPP2 fractionation on a Ni(II)-charged IMAC column. The His-tagged MRPP2 protein is applied to the Ni(II) column in 20 mM Tris-HCl pH 7.5, 15% glycerol, 150 mM NaCl, 0.1 mM TCEP, 30 mM imidazole and 0.02% Tween 20 buffer and is eluted with linear gradient from 100 to 500 mM imidazole. Lanes a and b are the protein flow-through and wash-flow-through of the column, respectively. MRPP2 (shown by the arrow) elutes from the NI(II) column at the start of the imidazole gradient (100 mM) (fractions 1 to 31). (B) The 6x His-tag attached to purified MRPP2 is cleaved by incubation with TEV protease. Lane 1 is the His-tagged MRPP2 before cleavage and lane 2 is the cleaved MRPP2 protein after purification on the second Ni(II) column. (C) His-tag western blot analysis of MRPP2 expressed in the lysates of Rosetta(DE3)pMR2-TEV-His cells. MRPP2 indicated in arrow is the total expression of MRPP2 after 18 hr induction by 1 mM IPTG at 16^{o}C.

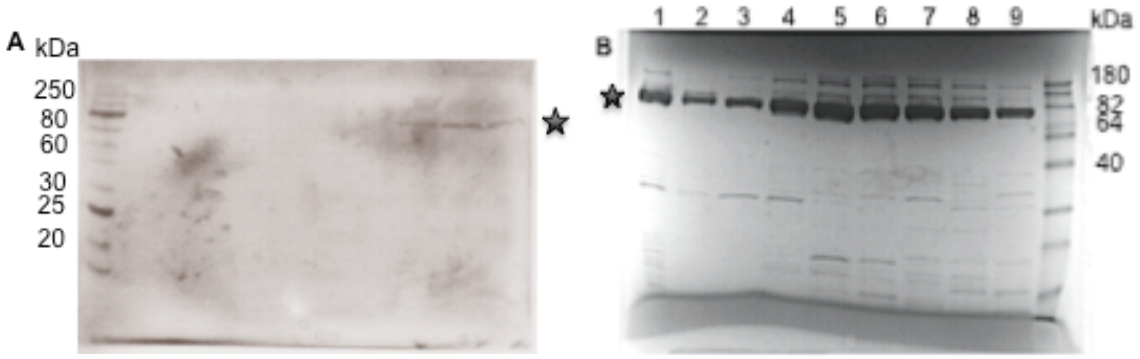

Figure 3-8: SDS PAGE analysis of MRPP3 protein fractionated by DEAE and SP column chromatography using a linear salt gradient. (A) MRPP3, shown by the star, is eluted from the DEAE column at ~150 mM NaCl in 20 mM MOPS pH 7.8, 15% glycerol, and 0.1 mM TCEP buffer. (B) Purification of MRPP3 using SP chromatography. Lane 1 is the MRPP3 protein after the first Ni(II) column and before applied to the SP column, lane 2 is the protein flow-through from the SP column and lanes 3 to 9 are the eluate fractions containing MRPP3 (~700 mM NaCl).

Discussion

The cDNAs encoding the MRPP1, MRPP2 and MRPP3 genes were sub-cloned into *E. coli* expression vectors with the addition of a His-tag and removal of mitochondrial localization sequences and recombinantly expressed in the *E. coli* cells. The MRPP1 expression is higher in the BL21(DE3)pLysS cells compared to BL21(DE3) cells transformed with the expression plasmid. This result suggests that expression of MRPP1 in *E. coli* affects cell growth and/or viability. MRPP1 expression is enhanced in the BL21(DE3)pLysS cells because the T7 lysozyme expressed from the pLysS plasmid inhibits T7 RNA polymerase to suppress the basal expression level of MRPP1 before IPTG induction (29).

MRPP2 expresses well in the Rosetta(DE3)pMR2-TEV-His cells, however, the majority of the MRPP2 protein is insoluble when growing at 28^{o}C. However, Rossmanith and coworkers, have grown the MRPP2 protein at 16^{o}C. Therefore, to obtain sufficient MRPP2 protein for the experiments carried out in Chapter 4, the pMR2-TEV-His plasmid was transformed and grown in the Rosetta(DE3) cells at 37^{o}C followed by induction with 1 mM IPTG at OD_{600} ~0.8 and continued to grow at 16^{o}C (Figure 3-7). In the future, soluble expression of recombinant MRPP2 could be enhanced by attaching a solubility-enhancing tag, such as SUMO, MBP or GST tag, to the N-terminus of the pMR2-TEV-His plasmid (30,31). Recombinant expression of MRPP3 is enhanced in the Rosetta(DE3)pMR3-TEV-His cells relative to BL21(DE3)pLysSpMR3-TEV-His cells. The Rosetta(DE3) cell line contains a plasmid containing “rare” tRNA genes that encode eukaryotic codons rarely used in the *E. coli* (31). The “rare”

tRNA genes can increase the expression level of the eukaryotic proteins by raising the concentrations of tRNAs that recognize the eukaryotic codon usage during protein translation in *E. coli*. Codon usage frequency analyzer indicate 11 out of 50 codons in the 5' end of the MRPP3 mRNA score low codon usage (< 20%) by the *E. coli* (Figure 3-9). Therefore, expression of Rosetta(DE3)pMR3-TEV-His cells with "rare" tRNA will support the transcription initiation of the MRPP3 mRNA (32). This phenomenum could explain the higher expression level of MRPP3 in the Rosetta(DE3) cells.

The His-tagged MRPP1, MRPP2 and MRPP3 proteins are each purified using IMAC affinity chromatography and MRPP3 is further purified using either anion or cation exchange chromatography. MRPP1, MRPP2 and MRPP3 each elute from the Ni(II) affinity column at ~100 mM imidazole with ≥ 70% purity. The His-tag attached to MRPP1, MRPP2, and MRPP3 is each cleaved by incubation with 3C or TEV protease with ≥ 50% efficiency. A second Ni(II) column is used to separate the non-cleaved and cleaved MRPP1, MRPP2 and MRPP3 proteins as well as to remove the His-tagged proteases and other proteins that bind nonspecifically to the resin; the cleaved proteins do not bind to the Ni(II) column. Since MRPP3 has a calculated pI of ~ 9 (33) and is a proposed to bind nucleic acids, this protein is further purified using ion exchange chromatography (DEAE-Sephacel™ Fast Flow) to eliminate contaminating nucleic acids.

In summary, MRPP1, MRPP2 and MRPP3 are three distinct proteins that are transported to the mitochondrial via the signal localization sequences and are proposed to form a complex that catalyzes cleavage of mitochondrial precursor

tRNAs in human mitochondria (20). The function of each of the MRPP1, MRPP2 and MRPP3 subunits in the human mtRNase P complex for catalysis of pre-tRNA is unclear and remains to be determined. Previous data suggested showed that the reconstituted human mtRNase P protein complex catalyzes cleavage of the 5' end of the (mt)pre-tRNA in a 2:4:1 ratio of MRPP1:MRPP2:MRPP3. However, the exact stoichiometry of the subunits in human mtRNase P protein complex needs to be clarified. To further explore the catalytic function of human mtRNase P each of the subunits was recombinantly expressed in *E. coli* and purified using IMAC and anion exchange chromatography. These proteins were successfully expressed in *E. coli* cells at a level of 2.5 – 6 mg protein/L culture medium. Each of these recombinant proteins was successfully purified to >95% purity using affinity and anion-exchange chromatography. This work has developed methods to produce quantities of pure, recombinant MRPP1, MRPP2 and MRPP3 to investigate the catalytic mechanism of human mtRNase P in processing the (mt)pre-tRNA, as described in Chapter 4. Further optimization of expression levels in the future will enhance the biochemical and structural studies of these proteins.

Prior studies have shown that point mutations in the human (mt)tRNAs have been associated with human mitochondrial dysfunction, such as mitochondrial myopathy, encephalopathy, lactic acidosis and stroke (MELAS) syndrome (34,35). Some of these (mt)pre-tRNA point mutations decrease the cleavage efficiency of the human mtRNase P (36). Furthermore, mutations in MRPP3 have been associated with myocardial infarction and coronary artery

disease (37). Hence, elucidating the catalytic mechanism and substrate recognition by the human mtRNase P in processing (mt)pre-tRNA will shed some light of how these pathogenic mutations affect the (mt)tRNA processing pathway and how this may contribute to pathogenesis.

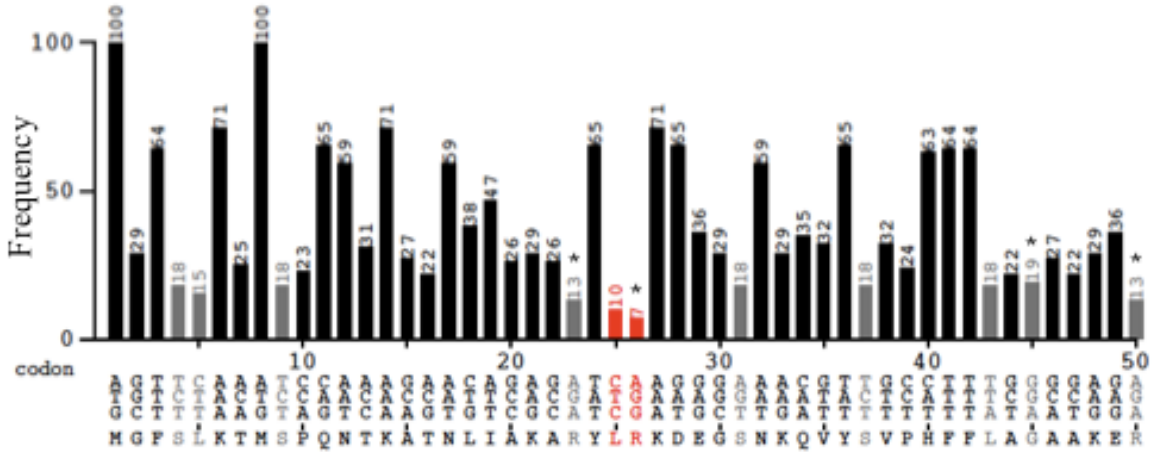

Figure 3-9: Codon usage frequency analyzer of MRPP3 coding sequences. The grey and red bars indicate the frequency of MRPP3 codon usage by *E. coli* that are < 20% and < 10%, respectively. The frequency of MRPP3 codon usage that will be enhanced by the “rare” tRNAs in the Rosetta(DE3) cell lines are shown in (*).

References

1. Guerrier-Takada, C., Gardiner, K., Marsh, T., Pace, N., and Altman, S. (1983) *Cell* **35**, 849-857
2. Evans, D., Marquez, S. M., and Pace, N. R. (2006) *Trends Biochem Sci* **31**, 333-341
3. Gopalan, V., Vioque, A., and Altman, S. (2002) *J Biol Chem* **277**, 6759-6762
4. Lai, L. B., Vioque, A., Kirsebom, L. A., and Gopalan, V. (2010) *FEBS Lett* **584**, 287-296
5. Beebe, J. A., and Fierke, C. A. (1994) *Biochemistry* **33**, 10294-10304
6. Beebe, J. A., Kurz, J. C., and Fierke, C. A. (1996) *Biochemistry* **35**, 10493-10505
7. Crary, S. M., Niranjanakumari, S., and Fierke, C. A. (1998) *Biochemistry* **37**, 9409-9416
8. Day-Storms, J. J., Niranjanakumari, S., and Fierke, C. A. (2004) *Rna* **10**, 1595-1608
9. Koutmou, K. S., Day-Storms, J. J., and Fierke, C. A. (2011) *RNA* **17**, 1225-1235
10. Kikovska, E., Svard, S. G., and Kirsebom, L. A. (2007) *Proc Natl Acad Sci U S A* **104**, 2062-2067
11. Pannucci, J. A., Haas, E. S., Hall, T. A., Harris, J. K., and Brown, J. W. (1999) *Proc Natl Acad Sci U S A* **96**, 7803-7808
12. Rossmanith, W., and Karwan, R. M. (1998) *Biochem Biophys Res Commun* **247**, 234-241
13. Rossmanith, W., Tullo, A., Potuschak, T., Karwan, R., and Sbisa, E. (1995) *J Biol Chem* **270**, 12885-12891
14. Salavati, R., Panigrahi, A. K., and Stuart, K. D. (2001) *Mol Biochem Parasitol* **115**, 109-117
15. Wang, M. J., Davis, N. W., and Gegenheimer, P. (1988) *Embo J* **7**, 1567-1574
16. Morales, M. J., Wise, C. A., Hollingsworth, M. J., and Martin, N. C. (1989) *Nucleic Acids Res* **17**, 6865-6881
17. Dang, Y. L., and Martin, N. C. (1993) *J Biol Chem* **268**, 19791-19796
18. Puranam, R. S., and Attardi, G. (2001) *Mol Cell Biol* **21**, 548-561
19. Gobert, A., Gutmann, B., Taschner, A., Gossringer, M., Holzmann, J., Hartmann, R. K., Rossmanith, W., and Giege, P. (2010) *Nat Struct Mol Biol* **17**, 740-744
20. Holzmann, J., Frank, P., Loffler, E., Bennett, K. L., Gerner, C., and Rossmanith, W. (2008) *Cell* **135**, 462-474
21. Jackman, J. E., Montange, R. K., Malik, H. S., and Phizicky, E. M. (2003) *RNA* **9**, 574-585
22. He, X. Y., Yang, Y. Z., Peehl, D. M., Lauderdale, A., Schulz, H., and Yang, S. Y. (2003) *J Steroid Biochem Mol Biol* **87**, 191-198

23. Ghosh, D., Weeks, C. M., Grochulski, P., Duax, W. L., Erman, M., Rimsay, R. L., and Orr, J. C. (1991) *Proc Natl Acad Sci U S A* **88**, 10064-10068
24. Lukacik, P., Kavanagh, K. L., and Oppermann, U. (2006) *Mol Cell Endocrinol* **248**, 61-71
25. Yang, S. Y., He, X. Y., and Schulz, H. (2005) *Trends Endocrinol Metab* **16**, 167-175
26. Delannoy, E., Stanley, W. A., Bond, C. S., and Small, I. D. (2007) *Biochem Soc Trans* **35**, 1643-1647
27. Dokmanic, I., Sikic, M., and Tomic, S. (2008) *Acta Crystallogr D Biol Crystallogr* **64**, 257-263
28. Jahic, M., Wallberg, F., Bollok, M., Garcia, P., and Enfors, S. O. (2003) *Microb Cell Fact* **2**, 6
29. Zhang, X., and Studier, F. W. (1997) *J Mol Biol* **269**, 10-27
30. Esposito, D., and Chatterjee, D. K. (2006) *Curr Opin Biotechnol* **17**, 353-358
31. Makrides, S. C. (1996) *Microbiol Rev* **60**, 512-538
32. Fuhrmann, M., Hausherr, A., Ferbitz, L., Schodl, T., Heitzer, M., and Hegemann, P. (2004) *Plant Mol Biol* **55**, 869-881
33. Gasteiger, E., Gattiker, A., Hoogland, C., Ivanyi, I., Appel, R. D., and Bairoch, A. (2003) *Nucleic Acids Res* **31**, 3784-3788
34. Levinger, L., Morl, M., and Florentz, C. (2004) *Nucleic Acids Res* **32**, 5430-5441
35. Wittenhagen, L. M., and Kelley, S. O. (2003) *Trends Biochem Sci* **28**, 605-611
36. Rossmanith, W., and Karwan, R. M. (1998) *FEBS Lett* **433**, 269-274
37. Alsmadi, O., Muiya, P., Khalak, H., Al-Saud, H., Meyer, B. F., Al-Mohanna, F., Alshahid, M., and Dzimiri, N. (2009) *Ann Hum Genet* **73**, 475-483

CHAPTER 4

IDENTIFICATION OF METAL ION ACTIVATION OF HUMAN MITOCHONDRIAL RNASE P CATALYSIS

Background

Ribonuclease P (RNase P) is an endonuclease that catalyzes the 5' end maturation of precursor tRNA (pre-tRNA) to form mature tRNA and 5' leader. Nuclear RNase P is highly conserved in all three kingdom of life (Bacteria, Archaea and Eukarya) and consists of a large catalytic RNA subunit and one or more protein subunits *in vivo* (1-3). In Bacteria, the RNase P RNA alone has comparable activity to the RNase P holoenzyme in the presence of high concentrations of salts (100 mM NH_4Cl and 60 mM $MgCl_2$) (4). In the absence of the protein subunits, some Archeal and Eukaryal RNase P RNAs are catalytically active *in vitro* only in the presence of very high salt (least 1 M monovalent and 160 mM divalent ions) (6,7). The RNase P protein subunits play essential roles in the *in vivo* activity of the RNase P holoenzyme, including optimizing the catalytic activity, enhancing affinity of pre-tRNA substrates for RNase P, stabilizing the RNA·protein complex, and decreasing the metal ion concentration required for activation of RNase P catalysis (8-12). The RNA-dependent RNase P has been

proposed as a remnant from the ancient RNA world. Recently, an RNase P activity composed solely of protein subunits was demonstrated in both human mitochondria and spinach chloroplast (13,14). The newly identified "proteinaceous" RNase P from human mitochondrial (mtRNase P) is composed of three protein subunits called MRPP1, MRPP2 and MRPP3, which are not related to any previously known RNase P protein components (14). The chloroplast RNase P (PRORP1) is suggested to require a single subunit that is homologous to MRPP3.

MRPP1 is a tRNA m^1G methyltransferase, which is a homolog of Trm10p that catalyzes the N^1 methylation of guanosine at position 9 of tRNA. 10 out of 34 *S. cerevisiae* tRNAs, including $tRNA^{Pro}$, $tRNA^{Gly}$, $tRNA^{Trp}$, $tRNA^{Val}$, $tRNA_{ICG}^{Arg}$, two $tRNA_{UCU}^{Arg}$, $tRNA^{Ile}$, $tRNA_i^{Met}$, and $tRNA^{Ala}$ have m^1G modification at position 9 of tRNA (14,16). MRPP2 is a member of the short-chain dehydrogenase/reductase family that has multiple functions *in vivo* (17), including isoleucine degradation, sex steroid and neurosteroid metabolism, and potentially related to Alzheimer's Disease progression (18-21). Specifically, MRPP2 catalyzes the NAD^+-dependent oxidation of 2-methyl-3-hyroxybutryryl-CoA, a metabolite in isoleucine degradation, to form 2-methyl-acetoacetyl-CoA as well as the oxidation of 17β-estradiol, a steroid hormone, to form estrone. 2-methyl-3-hyroxybutryryl-CoA dehydrogenase deficiency has lead to progressive infantile neurodegeneration (22). MRPP1 and MRPP2 form a complex and each contains a RNA binding motif that is proposed to function in recognition of tRNA for the mitochondrial RNase P (23,24). MRPP3 was annotated as a protein of unknown function.

Domain analysis and sequence comparisons indicate that MRPP3 has two pentatricopeptide repeats (PPR motifs) as well as three conserved aspartate and one conserved histidine residues at the C-terminus, which is a characteristic of a metallonuclease enzyme (14). Therefore, MRPP3 is proposed to form a novel metallonuclease family. However, the catalytic function of each of the MRPP subunits in human mtRNase P has not yet been determined. Further investigation is necessary to understand how a protein-only RNase P adopts the functionality of RNA-mediated RNase P enzyme. The catalytic mechanism, requirement for metal ions and the determinants of molecular recognition in human mtRNase P remain to be studied. Here in Chapter 4, we will elucidate metal ion requirement for activating the catalytic activity of human mtRNase P, which is one of the important elements in the RNase P catalysis.

All characterized RNase P enzymes are metal-dependent, requiring magnesium ions to activate cleavage of a phosphodiester bond of pre-tRNA to form mature tRNA with a 5'-phosphate and a leader fragment with 3'-hydroxyl end groups (25,26). Metal ions play multiple roles in the RNA-dependent RNase P. For example, more than 100 magnesium ions interact non-specifically with bacterial RNase P RNA to neutralize charge repulsion between phosphates and to stabilize the formation of tertiary structure. Additionally, at least four specific magnesium binding sites stabilize RNase P RNA folding as well as ground and transition state interactions with pre-tRNA (27). The RNase P protein increases the apparent affinity of magnesium ions that are required for enhancing the affinity of RNase P for pre-tRNA. The enhancement of magnesium affinity is

coupled to a conformational change that allows the 5' leader of pre-tRNA to interact with the P protein subunit of RNase P (12,28,29). Hence, the protein subunit of RNase P protein enhances catalytic activity at physiological magnesium concentrations. Therefore, magnesium ions play multiple essential functions in the ribozyme RNase P catalysis *in vivo*. However, the role of metal ions in activating human mitochondrial RNase P is unclear.

Sequence comparison of MRPP3 homologs show two PPR motifs, that are proposed as RNA binding motifs, and eight highly conserved residues, including 2 cysteine, 4 aspartates and 1 histidine residues, that could potentially function to coordinate metal ions (Figure 4-1). Based on the sequence and structure comparisons, bioinformatic analysis predicted that the *KIAA0391* (MRPP3 gene) contains a NYN domain (5). The NYN domain is proposed to share a protein fold that is similar to two characterized nucleases, including Pilt N-terminal (PIN) and FLAP/5' →3' exonuclease. These proteins both contain a set of four conserved acidic residues, such as aspartate, that coordinate one or two magnesium ions important for catalytic activity at the active site. Proteins containing the NYN domain as well as one or more RNA binding domains, such as PPR motifs, KH, RRM and CCCH domains, are proposed to form a new class of nucleases. Therefore, in this chapter, biochemical studies are performed to determine whether human mtRNase P is activated by metal ions and, if so, the identity of the metal ions that enhance catalysis.

Here, we elucidate the first direct evidence that MRPP3, in the absence of the other two subunits, catalyzes cleavage of pre-tRNA in the presence of 1 mM

$MgCl_2$, illustrating that MRPP3 is the catalytic subunit of the human mtRNase P. Additionally, MRPP3 catalytic activity shows a hyperbolic dependence on magnesium ions in the presence of cobalt hexammine indicating a minimum of one inner sphere magnesium binding site in MRPP3. Furthermore, the stoichimetric zinc bound to MRPP3 enhances catalytic activity relative to the 0.14 mol/mol MRPP3. Domain analysis of MRPP3 identifies a site with homology to a zinc finger, suggesting a structural zinc site in MRPP3. Finally, formation of the MRPP1/MRPP2/MRPP3 protein complex slightly decreases the cleavage rate of the (mt)pre-tRNA compared to the MRPP3 alone, indicating that mitochondrial RNase P activity may require only the MRPP3 subunit, as suggested for the chloroplast enzyme (13).

A

```
Homo sapiens                344 KSGQCSGCGK 353 404 FDVVIDGLNV 413 474 DISEDDPFLL 483 495 FITRDLMRDH 504
Mus musculus                341 KSGQCSGCGR 350 401 FDIVIDGLNV 410 471 NISEDDPFLL 480 492 FITKDLLRDH 501
Gallus gallus               300 DSGQCPVCNH 309 360 FDIVIDGLNI 369 430 NISEDDAFLL 439 451 FVTRDFLRDH 460
Danio rerio                 227 PSGDCRNCKA 236 287 FDIVIDGLNV 296 357 DISEDDPYLL 366 378 FLSRDLMRDH 387
Nasonia vitripennis         292 KRGECSHCSQ 301 352 YDVVIDGLNV 361 421 NISQDDPYLL 430 442 FVSRDLMRQH 451
Drosophila melanogaster     290 GLGKCQSCQQ 299 350 YDCVIDGLNV 359 420 NLSHDDPFLL 429 441 FFSRDLMRSH 450
Oryza sativa                489 RNGACLACGE 498 543 FDAVVDGANV 552 619 TGSNDDWYWL 628 638 MVTNDEMRDH 647
Arabidopsis thaliana        340 ENGVCKCCKE 349 394 FDAVIDGANM 403 470 PGSNDDWYWL 479 489 LVTNDEMRDH 498
Trypanosoma brucei          259 ETGMCCRCST 268 332 YDAVIDGANV 341 437 GFLNDDYCWL 446 457 VVSNDQMRDH 466
Leishmania infantum         275 DDGVCSNCGA 284 348 YDTVIDGANV 357 453 AFLNDDYCWL 462 473 IISNDQMRDH 482
```

B

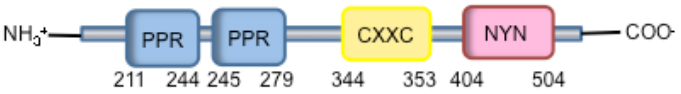

Figure 4-1: (A) Multiple sequence alignment of metazoan, kinetoplastid, and angiosperm MRPP3 protein sequences. Sequences were retrieved from the NCBI database by iterative BLAST searches. Amino acids in red are conserved side chains that could be involved in inner sphere metal ion coordination. (B) Model of MRPP3 domains adapted from Anantharaman, V. et. al., 2006 (5). The PPR, CXXC and NYN domains of the MRPP3 are represented by blue, yellow and red colors, respectively. Pfam analysis (15) indicates two PPR motifs that is proposed to bind RNA, one CXXC motif, which has homology to a structural zinc binding domain (C348 and C351 in (A)), and one NYN domain, where the conserved acidic residues are located (D409, D478, D479, and D499 in (A)).

Materials and Methods

Precursor tRNA substrate

The (mt)pre-tRNA^{Tyr} sequence was PCR and cloned behind a T7 RNA polymerase promoter in the pGEM-1 vector (Promega) containing the BamHI/EcoRI restriction sites. The (mt)pre-tRNA^{Tyr} was linearized using BamHI, transcribed *in vitro* using T7 RNA polymerase (ref) and purified on an 8% polyacrylamide (PAGE) gel. The transcribed (mt)pre-tRNA^{Tyr} consists of the following sequence (tRNA is listed in uppercase letters, while the 5' and 3' trailers are shown in lowercase letters): ggattctagagaatagtcaacggtcggcgaacatcagtgggggtgaGGTAAAATGGCTGAGTGAA GCATTGGACTGTAAATCTAAAGACAGGGGTTAGGCCTCTTTTTACCAgctccga ggtgattttcatattgaattgcaaattggatcc. (mt)pre-tRNA^{Tyr} was body labeled by incusion of [α-^{32}P]GTP in the transcription reaction and 5' end-labeled with [γ-^{32}P]ATP (MP Biomedical) in the presence of T4 polynucleotide kinase (New England Biolabs). The ^{32}P-labeled (mt)pre-tRNA^{Tyr} was gel purified on an 8% PAGE gel, eluted overnight in elution buffer (10 mM Tris-HCl, pH 8.0, 1 mM EDTA, 0.1% SDS and 500 mM NaCl) and extracted with an equal volume of chloroform/phenol followed by ethanol precipitation.

mtRNase P proteins cloning and expression

MRPP1 was cloned behind a T7 polymerase promoter in the JEJ494 vector with a 6x His-tag followed by 3C protease cleavage site at the N-terminus (gift from Dr. Jane Jackman). MRPP2 and MRPP3 were cloned into pETM11 vectors behind a T7 polymerase promoter with a 6x His-tag and a TEV protease cleavage site at

the N-terminus (as described in Chapter 3). The double mutation of D435 and D436 to alanine in MRPP3 was prepared using QuikChange site-directed mutagenesis (Stratagene). MRPP1 was recombinantly expressed in BL21(DE3)pLysS cells transformed with a plasmid encoding MRPP1, while MRPP2, MRPP3 and the D435A/D436A MRPP3 mutant were expressed in the Rosetta(DE3) (Novagen) cells containing the respective plasmids. These *E. coli* cells were grown in Luria broth (LB) media at 37^{o}C and protein expression was induced by addition of 1 mM isopropylthio-β-D-galactopyranoside (IPTG) when OD_{600} = 0.8. At this time, the temperature was reduced to 16^{o}C and the cells were incubated overnight. The cells were harvested by centrifugation (6000g, 15 min at 4^{0}C) and resuspended in the lysis buffer (20 mM Tris-HCl (pH 7.5), 15% glycerol, 150 mM NaCl, 30 mM imidazole, 0.1 mM TCEP, 0.02% Tween 20, 0.1% proteinase inhibitor cocktail (Thermo Fisher) and 0.3 mg/mL phenylmethylsulfonyl fluoride (PMSF)).

mtRNase P proteins purification

E. coli cells expressing RNase P subunits were lysed using a sonicator followed by centrifugation at 16 000g for 30 minutes. The cleared lysate was applied to a $NiSO_4$-charged immobilized metal affinity column (Ni-IMAC; GE Healthcare) and washed with additional lysis buffer. His-tagged MRPP1 and MRPP2 were eluted by a linear gradient of 30 mM to 500 mM imidazole in buffer A (20 mM Tris-HCl (pH 7.5), 15% glycerol, 150 mM NaCl, 0.1 mM TCEP and 0.02% Tween 20). The His-tagged native and D478A/D479A mutant of MRPP3 were eluted with a 30 mM to 300 mM imidazole gradient in buffer A where 20 mM 4-

morpholinepropanesulfonic acid (MOPS, at pH 7.8) replaced 20 mM Tris-HCl (pH 7.5). The 6x His-tagged 3C and TEV proteases were incubated with the purified His-tagged MRPP1, and MRPP2, respectively, and the reaction was dialyzed in buffer B (20 mM Tris-HCl (pH 7.5), 15% glycerol, 150 mM NaCl and 0.1 mM TCEP) at 4^{o}C overnight. The 6x His-tagged MRPP3 was incubated with TEV protease and the reaction was dialyzed in buffer C (20 mM MOPS (pH 7.8), 15% glycerol, 150 mM NaCl and 0.1 mM TCEP) at 4^{o}C overnight. The cleaved recombinant proteins were purified using second Ni(II)-IMAC column to remove the 6x His-tagged proteases and any proteins that nonspecifically bind to this resin. MRPP3 was dialyzed in buffer D (20 mM MOPS (pH 7.8), 15% glycerol, 50 mM NaCl and 0.1 mM TCEP) at 4^{o}C overnight. Then MRPP3 was further purified using DEAE anion-exchange chromatography and was eluted using a linear gradient from 50 mM to 500 mM NaCl. Prior to metal analysis, MRPP1, MRPP2 and MRPP3 were dialyzed in buffer E (30 mM MOPS (pH 7.8), 15% glycerol, 150 mM NaCl, 0.1 mM TCEP and 1 mM EDTA) at 4^{o}C overnight to chelate bound and adventitious divalent metal ions. The recombinant proteins were further dialyzed in the same buffer without 1 mM EDTA at 4^{o}C overnight. The metal ions bound to the recombinant proteins were analyzed by inductively coupled plasma mass spectrometry (ICP-MS) at the Geology ICP Facility.

Human mtRNase P protein complex activity assay

Single turnover experiments were performed using an excess concentration of MRPP3, and MRPP1/MRPP2/MRPP3 complex concentration ([E]/[S] >> 5; [E] ~

50 nM to 440 nM; [S] ≤ 0.1 nM) with limiting radiolabelled (mt)pre-tRNA^{Tyr}. The 5' leader product was separated from the (mt)pre-tRNA^{Tyr} substrate on a 8% denaturing polyacrylamide gel (PAGE) and quantified by PhosphorImager analysis (Amersham Bioscience Corp.). The observed rate constants, k_{obs} were determined by fitting a single-exponential equation to the data (Equation 1). The dependence of k_{obs} on enzyme concentration was evaluated using Equation 2.

Scheme 1 $$E + S \underset{k_{-1}}{\overset{k_1}{\rightleftharpoons}} ES \xrightarrow{k_{max}} E + P$$

Equation 1 $$[P] = [P]_\infty (1 - e^{-k_{obs}t})$$

Equation 2 $$k_{obs} = \frac{k_{\max}[E]}{K_{1/2} + [E]}; K_{1/2} = \frac{k_{\max} + k_{-1}}{k_1}$$

Equation 3 $$k_{obs} = \frac{k_{\max}[E]}{K_{1/2}}$$, assuming that $K_{1/2}$ >>> [E]

Dependence of k_{obs} on magnesium concentration

Single turnover cleavage of pre-tRNA was measured using excess MRPP3 and MRPP1/MRPP2/MRPP3 complex concentration ([E]/[S] >> 5; [E] 100 nM; [S] ≤ 0.1 nM) with limiting 5' end-labelled ^{32}P-(mt)pre-tRNA^{Tyr} at various concentrations of $MgCl_2$ concentration (0 to 3 mM $MgCl_2$). The 5' leader product was separated from the substrate on a 8% PAGE and quantified by PhosphorImager analysis. The observed rate constant, k_{obs}, at each $MgCl_2$ concentration was obtained by fitting Equation 1 to the time-dependent cleavage. The magnesium dependence of k_{obs} was analyzed using the Hill equation (Equation 4) (27) :

$$k_{obs} = \frac{k_{\max}[Mg^{2+}]^{n_H}}{K_{1/2}^{n_H} + [Mg^{2+}]^{n_H}}$$

Equation 4

where k_{obs} is the cleavage rate constant measured at each magnesium concentration, k_{max} is the rate constant at saturating magnesium concentration, $K_{1/2}$ is the magnesium concentration at ½ X k_{max} and n_H is the Hill coefficient.

Circular Dichroism measurement of (mt)pre-tRNA^{Tyr} folding

0.4 μM of (mt)pre-tRNA^{Tyr} was heat denatured at 95^{o}C for 3 min in water, incubated at 37^{o}C for 10-15 min.and then buffer (30 mM MOPS, pH 7.6, 150 mM NaCl) was added and the mixture was incubated at 37^{o}C for 30 min. The CD spectra of (mt)pre-tRNA^{Tyr} was measured as a function of cobalt hexammine chloride (Cohex, $Co(NH_3)_6Cl_3$) addition (0 to 0.25 mM) with a 2 min equilibration at 37^{o}C after each addition. CD spectra were recorded using an AVIV spectropolarimeter and analyzed using Equation 4 to obtain the delta epsilon (Δε) at A_{264}. Equation 5 was fit to the dependence of Δε on Cohex concentration to obtain the $K_{1/2}$ for stabilization of (mt)pre-tRNA^{Tyr} folding by Cohex.

$$\Delta\varepsilon = \frac{\theta}{32980 \times C \times L \times N}$$

Equation 4

$$\Delta\varepsilon = \frac{[Co(NH_3)_6Cl_3]}{K_{1/2} + [Co(NH_3)_6Cl_3]}$$

Equation 5

where θ is the raw CD amplitude in mdeg, C is the concentration of the RNA, L is the cell path length in cm, and N is the number of nucleotides in RNA (30).

Results

MRPP3 alone catalyzes the 5' end maturation of (mt)pre-tRNA

Since there is evidence that RNase P is a metal-dependent enzyme, we measured metal content of the protein using ICP-MS. Using this method, we observed significant metal ion (Mg, Ni and Fe) contamination in MRPP3 with some metals co-eluting with the other two subunits of human mtRNase P protein after the first Ni(II)-IMAC column purification (Table 4-1). This metal contamination in the MRPP proteins could affect the catalytic activity of human mtRNase P. Therefore, as a final step in the purification, MRPP1, MRPP2 and MRPP3 proteins were dialyzed against 1 mM EDTA followed by a PD-10 gel filtration column to remove the EDTA. The ICP-MS results of proteins treated with EDTA indicate that purified MRPP1 contains 0.5 mol Mg/mol protein and 0.2 mol Zn/mol protein while MRPP2 contains ≤ 0.02 mol metal/mol protein. In contrast, ICP-MS data for two different preparations of MRPP3 indicates that one has a ~1:1 ratio of Zn:MRPP3 (0.9 mol Zn/mol MRPP3), while the second preparation has a 0.14:1 ratio of Zn:MRPP3 (0.14 mol Zn/mol MRPP3). The D478A/D479A MRPP3 mutant also has 0.18:1 ratio of Zn: MRPP3 (Table 4-1).

Table 4-1: Metal Content of purified MRPP1, MRPP2 and MRPP3[a]

Protein	Mg (μM)	Fe (μM)	Ni (μM)	Zn (μM)
After first nickel column				
MRPP1[e]	3.02	0.07	0.115	0.598
MRPP2[e]	1.39	0.04	2.43	<0.02[c]
MRPP3[e]	6.66	24.54	6.05	1.30
After 1mM EDTA dialysis				
MRPP1	0.5	0.07	<0.04[b]	0.2
MRPP2	<0.4[c]	0.02	<0.04[b]	<0.001
MRPP3a	<0.4	<0.02[c]	0.03	0.9
MRPP3b	0.1	0.02	0.4	0.14
D478A/479A MRPP3[d]	0.4	<0.02[c]	0.3	0.18

[a] The metal content of MRPP1, MRPP2 and MRPP3 proteins is represented as (mol of metal in protein – mol of metal in buffer)/mol protein.

[b] Measured metal content is below the detection limit of the ICP-MS analysis.

[c] Measured of metal content is lower than the metal content of the buffer (30 mM MOP (pH 7.8), 15% glycerol, 150 mM NaCl, 0.1 mM TCEP). The lower limit for Mg, Fe, Ni and Zn are < 0.4 μM, <0.02 μM, <0.04 μM, and <0.02 μM, respectively.

[d] D435A/436A mutant of MRPP3 protein.

[e] Measurement of metal content of MRPP1, MRPP2 and MRPP3 proteins after the first Ni(II)-IMAC column.

Previous analysis of the MRPP1/MRPP2/MRPP3 complex indicated that magnesium ions were important for the catalytic activity of mtRNase P (14,18). Therefore, to examine whether the purified MRPP3 protein could catalyze cleavage of the mitochondrial pre-tRNA^{Tyr}, activity was assayed in the presence of 1 mM $MgCl_2$ under single turnover condition where [E]/[S] ≥ 5-fold. The results indicates MRPP3 catalyzes complete cleavage of the 5' end-labeled (mt)tRNA^{Tyr} under these conditions to form a leader of 46 nucleotides, which is similar to the (mt)pre-tRNA^{Tyr} cleavage by the MRPP1:MRPP2:MRPP3 complex (k_{obs} = 0.14 ± 0.01 min^{-1}) (Figure 4-2 and Figure 4-9A) (14). Furthermore, double aspartate residues mutation (D478/D479) which is proposed to coordinate catalytic metal ions in the MRPP3, decrease the MRPP3 catalytic activity significantly, with < 20% (mt)pre-tRNA^{Tyr} cleavage. The catalytic activity of PRORP1, a homolog of MRPP3, is also abolished when the same double aspartate residues are mutated to alanine in the PRORP1 (13). There results indicate that containing 0.9 mole Zn/mol protein has the highest activity with a k_{obs} of 0.36 ± 0.01 min^{-1}. Decreasing the bound zinc by 6-fold (0.14 Zn/MRPP3) is also decrease in the value of k_{obs} to 0.01 ± 0.002 min^{-1} (Figure 4-3). These activity data indicate that MRPP3 alone catalyzes cleavage of (mt)pre-tRNA^{Tyr} in the presence of Mg^{2+} ions and, furthermore, suggest that a bound zinc ion is also important for catalytic activity.

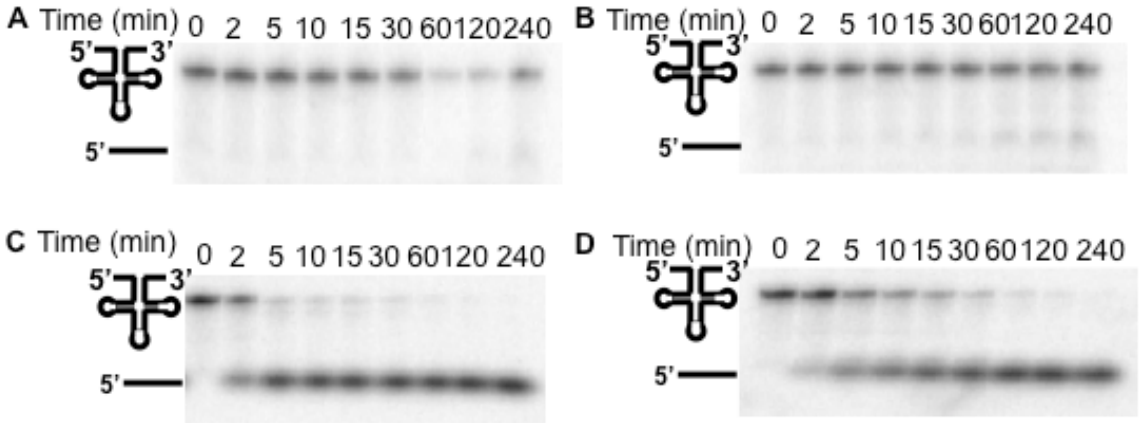

Figure 4-2: Measurement of cleavage of (mt)pre-tRNA^{Tyr} catalyzed by MRPP3, MRPP1:MRPP2:MRPP3 complex and D478/D479 MRPP3 mutant. ^{32}P-labeled (mt)pre-tRNA^{Tyr} (~0.01 nM) was incubated at 37^{o}C for up to 4 hr with: (A) buffer only (30 mM MOPS, pH 7.6, 150 mM NaCl and 1 mM $MgCl_2$); (B) buffer plus 100 nM D345/346 MRPP3 mutant; (C) buffer plus MRPP3 (0.9 mole/ mol MRPP3); and (D) buffer plus MRPP1:MRPP2:MRPP3 complex in 2:4:1 ratio; The reaction was quenched with 50 mM EDTA and the reaction products were separated by PAGE gel and analyzed using a phosphorimager.

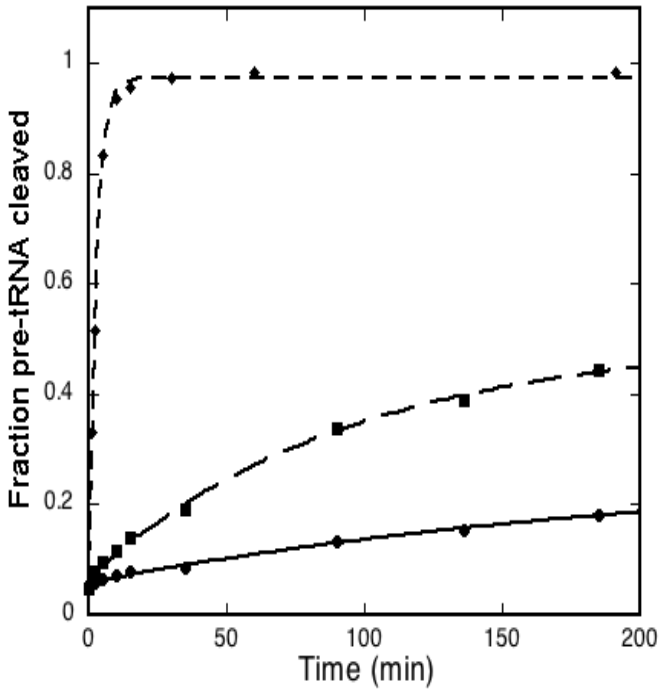

Figure 4-3: Single turnover measurement of (mt)pre-tRNA^{Tyr} cleavage catalyzed by MRPP3 and MRPP3 double D435A/D436A mutant. ^{32}P-labeled (mt)pre-tRNA^{Tyr} (~0.01 nM) was incubated with 100 nM of 0.9 Zn/MRPP3, 0.14 Zn/MRPP3 or D435A/D436A MRPP3 ([E]/[S] ≥ 5-fold) in 30 mM MOPS, pH 7.6, 150 mM NaCl and 1 mM $MgCl_2$ at 37^{o}C. The samples were fractionated on a PAGE and the fraction of pre-tRNA cleaved by MRPP3 as a function of time was quantified by PhosphorImager analysis. Equation 1 was fit to the data to calculate the observed cleavage rate constants, k_{obs} for (mt)pre-tRNA^{Tyr} catalyzed by: 0.9 mol Zn/mol MRPP3 (◆) as 0.36 ± 0.01 min^{-1}; 0.14 mol Zn/mol MRPP3 (■) as 0.01 ± 0.002 min^{-1}; and D478A/D479A MRPP3 (●) as 0.005 ± 0.001 min^{-1}.

Metal-dependence of MRPP3 catalytic activity

The previous data demonstrate that the catalytic subunit of human mtRNase P (MRPP3) has catalytic activity in 1 mM Mg^{2+}. However, it is not clear whether this is either the optimal metal cofactor or concentration. Analysis of metals (using ICP-MS) that co-elute with MRPP3 from the first Ni(II)-IMAC column indicate a high amount of magnesium, iron and zinc (Table 4-1). These data suggest that MRPP3 could bind and/or be activated by iron, zinc or magnesium. The traditional method for measuring the identity of functional metal ions is to prepare enzyme with out metal ions and measure activity as metal ions are added back. However, for MRPP3 this experiment is complicated by the metal-dependent folding of the substrate, (mt)$tRNA^{Tyr}$ (31). Therefore, to investigate the role of inner sphere metal ions in activation of MRPP3 catalysis, metal titration was carried out in the presence of cobalt hexammine chloride (Cohex). Cohex is an outer sphere metal ion that mimics magnesium hexahydrate and stabilizes the tertiary structure of RNA (27,32). To examine whether Cohex stabilizes the tertiary structure of (mt)pre-$tRNA^{Tyr}$, the circular dichroism spectra of (mt)pre-$tRNA^{Tyr}$ was measured as a function of Cohex concentration (Figure 4-4A). These data demonstrate that the spectra of (mt)pre-$tRNA^{Tyr}$ in 250 μM Cohex is comparable to that measured in 1 mM $MgCl_2$ (Figure 4-4C). Furthermore, these data can be reasonably described by a single binding isotherm with an apparent $K_{1/2}$ of 54 ± 1 μM (Figure 4-4B). Therefore, low concentrations of Cohex are sufficient to stabilize the tertiary structure of (mt)pre-$tRNA^{Tyr}$.

Experiments to measure the metal dependence of MRPP3 were carried out in the presence of 100 μM or 250 μM Cohex to fold (mt)pre-tRNA^{Tyr} and the cleavage reaction was initiated by adding MRPP3 (containing 0.9 mol Zn/mol protein). In the presence of 250 μM Cohex alone, cleavage of the 5' end of (mt)pre-tRNA is not observed (Figure 4-5A), suggesting that a divalent cation that can form an inner sphere complex is essential for catalytic activity. Furthermore, < 40% and < 20% cleavage of (mt)pre-tRNA is observed in the presence of MRPP3 and either 100 nM $ZnCl_2$ or $FeCl_2$ (Figure 4-5C and 4-5D). The Fe experiments were done under anaerobic conditions to maintain the Fe(II) in the assay. Activation of cleavage was also not observed upon varying the concentration of $ZnCl_2$ (25 nM to 300 nM) or $FeCl_2$ (200 nM to 1 μM) (Figure 4-6). In the presence of 1 mM $MgCl_2$, cleavage of the 5' end of (mt)pre-tRNA catalyzed by MRPP3 is complete within one hour, with an observed pseudo first order rate constant of k_{max} of 0.14 ± 0.02 min^{-1}. These data indicate that $MgCl_2$ likely functions as a catalytic metal ion to activate MRPP3 (Figure 4-5B). Additionally, the observed rate constant, k_{obs}, for the 5' cleavage of (mt)pre-tRNA by MRPP3 has a hyperbolic dependence (n_H =1.2 ± 0.4) on the $MgCl_2$ concentration with a k_{max} of 0.16 ± 0.02 min^{-1} and a $K_{1/2}^{Mg}$ of 0.3 ± 0.1 mM (Figure 4-7).

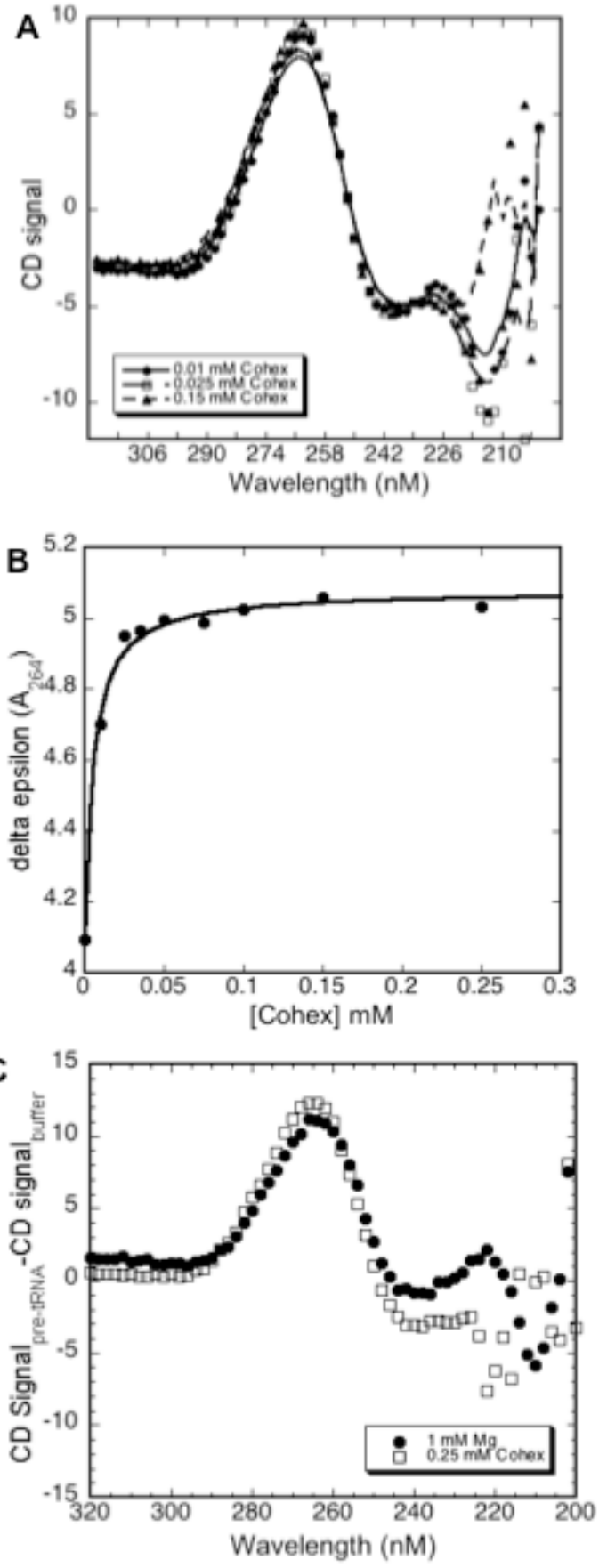
A
CD signal
10
5
0
-5
-10
0.01 mM Cohex
0.025 mM Cohex
0.15 mM Cohex
306 290 274 258 242 226 210
Wavelength (nM)
B
delta epsilon (A264)
5.2
5
4.8
4.6
4.4
4.2
4
0 0.05 0.1 0.15 0.2 0.25 0.3
[Cohex] mM
C
CD Signal pre-tRNA -CD signal buffer
15
10
5
0
-5
-10
-15
1 mM Mg
0.25 mM Cohex
320 300 280 260 240 220 200
Wavelength (nM)

Figure 4-4: (mt)pre-tRNA^{Tyr} folding measurement in the presence of Cohex by performing CD analysis. (A) Representative of CD spectra for (mt)pre-tRNA^{Tyr} folding in the presence of 0.01 mM, 0.025 mM and 0.15 mM Cohex at 37^{o}C. (B) Measurement of 0.4 μM (mt)pre-tRNA^{Tyr} folding in 30 mM MOPS, pH 7.6, 50 mM NaCl and various Cohex concentration (0 to 0.15 mM Cohex). The CD spectra were analyzed using Eq. 4 to obtain the delta epsilon at A_{264}. The delta epsilon at A_{264} was plotted as a function of Cohex concentration and fitted using Eq. 5. The $K_{1/2}^{Cohex}$ for (mt)pre-tRNA^{Tyr} folding is ~ 54 ± 1 μM. (C) Representative of CD spectra of 0.4 μM (mt)pre-tRNA^{Tyr} folding in the presence of 0.25 mM Cohex (□) and 1 mM $MgCl_2$ (●).

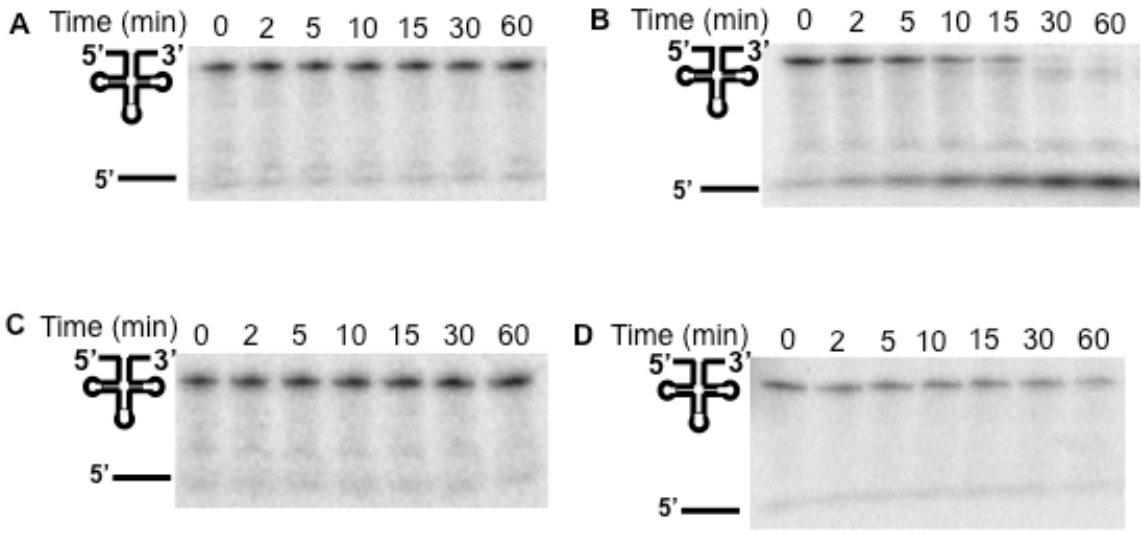

Figure 4-5: Metal-dependence of pre-tRNA cleavage catalyzed by MRPP3. The ^{32}P-labeled (mt)pre-tRNA^{Tyr} (~0.01 nM) was incubated with 100 nM MRPP3 in 30 mM MOPS, pH 7.6, 150 mM NaCl, 250 μM cohex at 37^{o}C for up to one hour in the presence of various metal ions, including: (A) 250 μM Cohex only; (B) 1 mM $MgCl_2$; (C) 100 nM $ZnCl_2$ and (D) 100 nM $FeCl_2$. The (mt)pre-tRNA^{Tyr} cleavage was performed under anaerobic conditions.

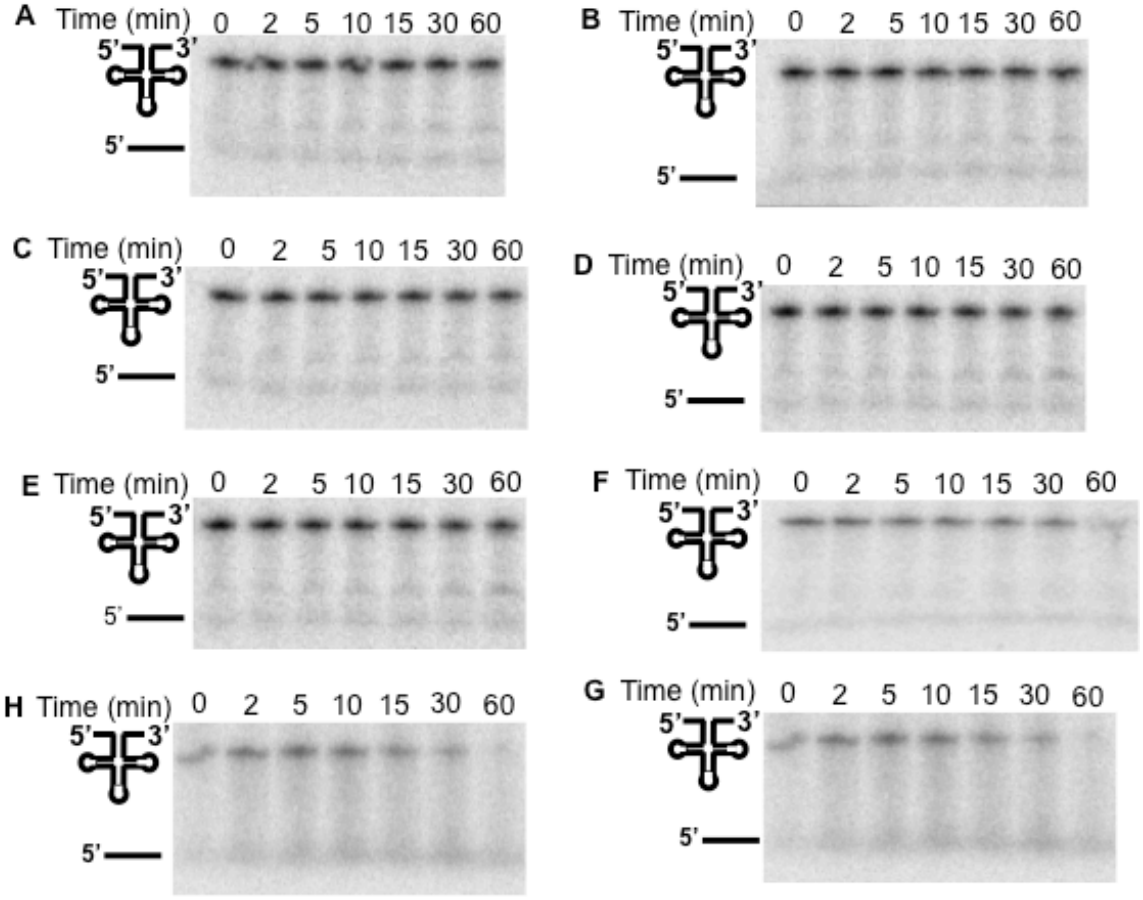

Figure 4-6: Measurement of cleavage of (mt)pre-tRNA^{Tyr} catalyzed by MRPP3 in the presence of $ZnCl_2$ and $FeCl_2$. ^{32}P-labeled (mt)pre-tRNA^{Tyr} (~0.01 nM) was incubated at 37^{o}C for up to 1 hr with 0.9 mol Zn/mol MRPP3 in 30 mM MOPS, pH 7.6, 150 mM NaCl, 250 μM cohex and (A) 25 nM $ZnCl_2$, (B) 37.5 nM $ZnCl_2$, (C) 50 nM $ZnCl_2$, (D) 200 nM $ZnCl_2$, (E) 300 nM $ZnCl_2$, (F) 200 nM $FeCl_2$, (G) 500 nM $FeCl_2$, and (H) 1 μM $FeCl_2$. The reaction was quenched with 50 mM EDTA and the reaction products were separated by PAGE and analyzed using a phosphorimager.

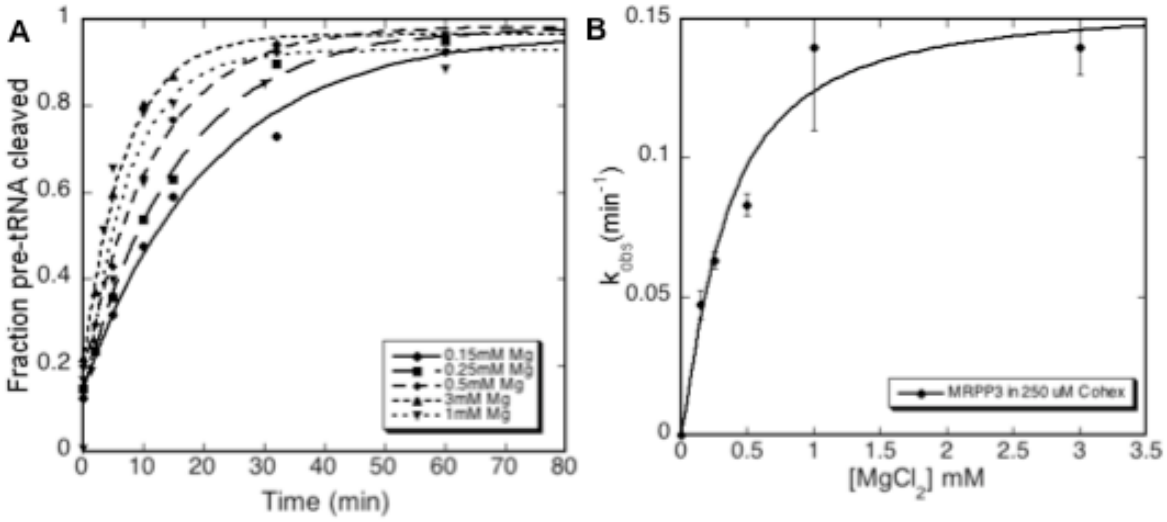

Figure 4-7: Measurement of the magnesium dependence of the observed cleavage rate, k_{obs} catalyzed by MRPP3 for (mt)pre-tRNA^{Tyr}. (A) Cleavage of ^{32}P-labeled (mt)pre-tRNA^{Tyr} (~0.01 nM) was catalyzed by 100 nM MRPP3 in 30 mM MOPS, pH 7.6, 250 µM Cohex, 150 mM NaCl, and varied $MgCl_2$ concentration (0.15 mM to 3 mM $MgCl_2$) at 37^{o}C. The fraction of (mt)pre-tRNA^{Tyr} was determined as described in the legend of Figure 4.3. Eq.1 was fit to the time-dependence of cleavage yielding the following values for k_{obs}: 0.15 mM $MgCl_2$ (●), 0.047 ± 0.005 min^{-1}; 0.25 mM $MgCl_2$ (■), 0.063 ± 0.003 min^{-1}; 0.5 mM $MgCl_2$ (◆), 0.083 ± 0.004 min^{-1} ; 3 mM $MgCl_2$ (▲), 0.14 ± 0.02 min^{-1} ; 1 mM $MgCl_2$ (▼), 0.14 ± 0.01 min^{-1}. (B) Magnesium ion dependence of k_{obs} for cleavage of (mt)pre-tRNA^{Tyr} by MRPP3. The k_{obs} demonstrated a hyperbolic dependence on the magnesium ion concentration; a fit of Eq. 3 to these data yielded values for k_{max} of 0.16 ± 0.02 min^{-1}, $K_{1/2,}^{Mg}$ of 0.3 ± 0.1 mM and n_H of 1.2 ± 0.4.

Mutations in putative Mg^{2+} binding site

A comparison of conserved sequences in MRPP3 and a recently identified homolog from chloroplasts, known as PRORP1, (13) demonstrate a series of conserved aspartate and histidine residues at the C-terminus of these proteins that have been proposed to be important for metal coordination (14,33) (Fig. 4-1). These proteins also have weak homology to a PIN domain where a crystal structure indicates that the aspartate residues coordinate a magnesium ion. In *Arabidopsis thaliana* RNase P (PRORP1) catalytic activity is abolished when two of these adjacent aspartates (D474, D475) are mutated to alanine. To examine whether the homologous aspartate residues in MRPP3 are important for coordinating the catalytic metal ions in the human mtRNase P complex, the D478A/D479A MRPP3 mutant was prepared. This protein co-purifies with substoichiometric concentrations of Zn (0.18 mol/mol protein) and Ni (0.4 μM) (Table 4-1). Furthermore the activity in the presence of 1 mM $MgCl_2$ is decreased significantly compared to the wild-type Zn-bound MRPP3 with a single turnover k_{obs} of 0.005 ± 0.001 min^{-1} (Figure 4-3).

Zinc ions enhance the cleavage rate of the (mt)pre-tRNA by MRPP3

The data in Figure 4.3 indicate that MRPP3 with nearly stoichiometric bound zinc (0.9 mol Zn/mol protein) has a significantly higher cleavage rate constant (k_{obs} = 0.36 ± 0.01 min^{-1}) than MRPP3 containing 0.14 mol Zn/mol protein (k_{obs} = 0.01 ± 0.002 min^{-1}) suggesting that a bound zinc cofactor may be important for catalytic activity in addition to Mg^{2+}. To further evaluate the differential activity of these two enzyme preparations, the dependence of the observed rate constants, k_{obs} on the

concentration of 0.9 mol Zn/mol MRPP3 and 0.14 mol Zn/mol MRPP3 (0 to 300 nM) was measured in the presence of 1 mM $MgCl_2$. For Zn-bound MRPP3, the single turnover rate constant, $k_{obs,}$, has a nearly linear or slightly hyperbolic dependence on the enzyme concentration (Fig. 4-8C). A fit of a Eq. 2 to the data yields values for k_{max}, $K_{1/2}$ and $k_{max}/K_{1/2}$ of 3.0 ± 0.8 min^{-1}, 790 ± 300 nM and 0.004 ± 0.002 $min^{-1}nM^{-1}$ = 2 x 10^6 $M^{-1}min^{-1}$ = 3.3 x 10^4 $M^{-1}s^{-1}$. A linear fit of the data yields a comparable value for $k_{max}/K_{1/2}$ (0.003 ± 0.0001 $min^{-1}nM^{-1}$). The activity of MRPP3 containing limited bound zinc 0.14 mol Zn/mol MRPP3 is significantly decreased. A linear fit of the dependence of k_{obs} on the MRPP3 concentration yields a value for $k_{max}/K_{1/2}$ of 5 ± 0.7 × 10^{-5} $min^{-1}nM^{-1}$ = 5 x 10^4 $M^{-1}min^{-1}$, which is 40-fold lower than the activity of MRPP3 with stoichiometric zinc (Figure 4-8C). The reduction of 0.9 mol Zn/mol MRPP3 activity relative to 0.14 mol Zn/ mol MRPP3 activity does not seem to correlate with the reduction of zinc content (~7-fold). This could be due to the 0.14 zinc could be nonspecifically bound to the MRPP3. These enhanced activity of the zinc-bound MRPP3 demonstrates a bound zinc ion is important for the catalytic activity. Furthermore, these data suggest that the affinity of MRPP3 for pre-tRNA under these conditions is nearly 1 μM, assuming that the value of $K_{1/2}$ approximates the pre-tRNA binding affinity (*i.e.* $k_{-1} > k_{max}$, Scheme 1). This affinity is significantly weaker than the affinity of bacterial RNase P for pre-tRNA, which is in the 10 nM range (11,34).

Function of other proposed subunits in pre-tRNA cleavage activity

Preceding studies have indicated that three subunits (MRPP1, MRPP2 and MRPP3) are essential for catalysis of 5' end cleavage of (mt)pre-tRNA for the mitochondrial RNase P. Our studies indicates that MRPP3 alone is sufficient to catalyze the 5' end of the (mt)pre-tRNA (Figure 4-1), similar to the results obtained for the chloroplast RNase P where PRORP1, the protein homologous to MRPP3 catalyzes pre-tRNA cleavage (13). To examine the role of MRPP1 and MRPP2 in catalysis of pre-tRNA cleavage, the k_{obs} for cleavage of (mt)pre-tRNA catalyzed by a 2:4:1 ratio of MRPP1:MRPP2:MRPP3 (the proposed RNase P complex (14)) as compared to cleavage in the presence of MRPP3 alone in the presence of 1 mM $MgCl_2$ (Figure 4-1). The data demonstrate that the single turnover rate constant for pre-tRNA cleavage catalyzed by the MRPP1/MRPP2/MRPP3 complex (0.14 ± 0.01 min^{-1}) is more than 2-fold slower than cleavage by MRPP3 (0.36 ± 0.01 min^{-1}) indicating that the MRPP1/MRPP2 complex does NOT enhance the cleavage rate of MRPP3 complex. Furthermore, similar results are obtained from a comparison of the magnesium dependence of the k_{obs} of the (mt)pre-$tRNA^{Tyr}$ cleavage catalyzed by the MRPP1/MRPP2/MRPP3 complex and MRPP3 alone; under these conditions both enzymes are maximally activated by 0.25 mM $MgCl_2$ with k_{obs} values of 0.15 ± 0.003 min^{-1} and 0.4 ± 0.002 min^{-1} for the MRPP1/MRPP2/MRPP3 complex and MRPP3 alone, respectively (Figure 4-9). These results demonstrate that observed cleavage rate of MRPP3 is >2-fold faster than the MRPP1/MRPP2/MRPP3 complex. These data indicate that the MRPP3 subunit is sufficient to catalyze the cleavage reaction.

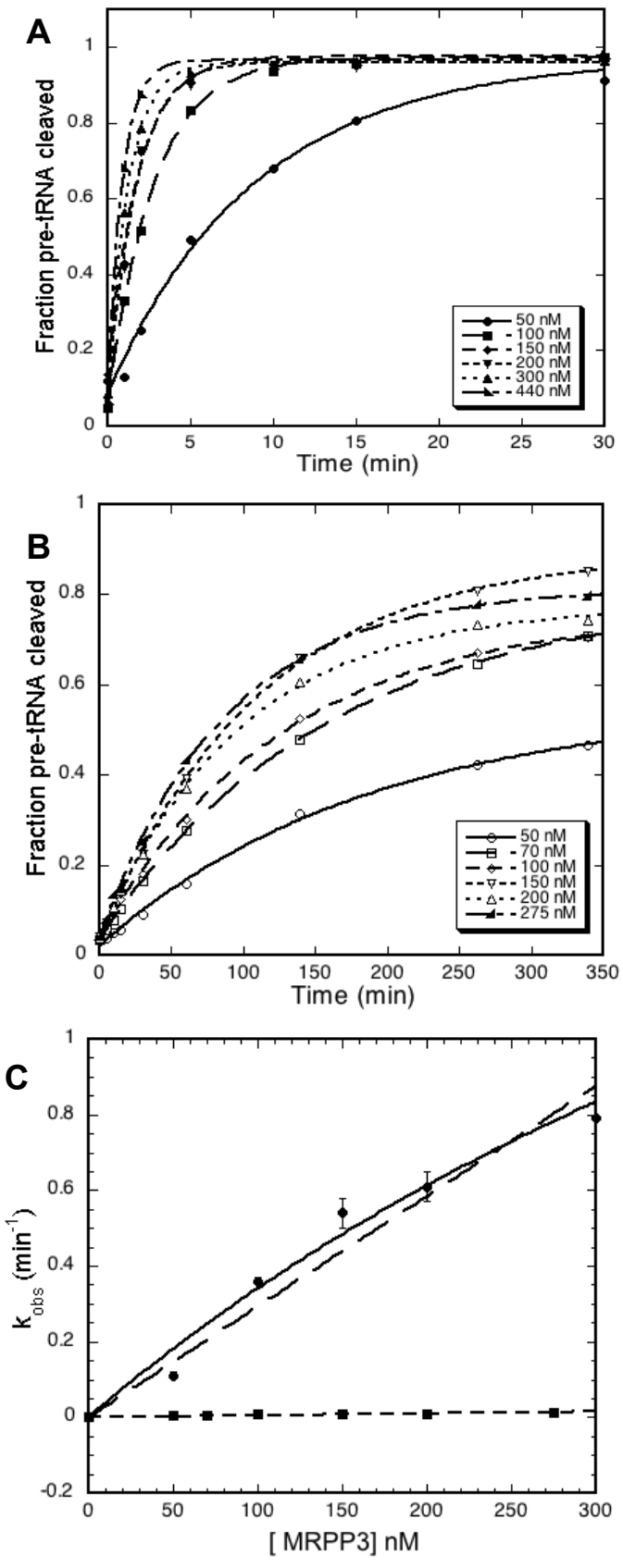
A
Fraction pre-tRNA cleaved
Time (min)
50 nM
100 nM
150 nM
200 nM
300 nM
440 nM
B
Fraction pre-tRNA cleaved
Time (min)
50 nM
70 nM
100 nM
150 nM
200 nM
275 nM
C
k_obs (min^-1)
[MRPP3] nM

Figure 4-8: Catalysis of cleavage of (mt)pre-tRNA^{Tyr} by Zn-MRPP3 under single turnover conditions. (A) The cleavage of ^{32}P-labeled (mt)pre-tRNA^{Tyr} (~0.01 nM) catalyzed by varied concentrations of MRPP3 (0.9 mol zinc/mol MRPP3) in 30 mM MOPS, pH 7.6, 150 mM NaCl, and 1 mM $MgCl_2$ at 37°C. The fraction cleaved is measured as described in the legend of Fig. 4.3. Eq. 1 is fit to the time-dependence of cleavage of (mt)pre-tRNA^{Tyr} yielding the following values of k_{obs}: 50 nM MRPP3 (●), 0.11 ± 0.009 min^{-1}; 100 nM MRPP3 (■), 0.36 ± 0.01 min^{-1}; 150 nM MRPP3 (◆), 0.054 ± 0.04 min^{-1} ; 200 nM MRPP3 (▼), 0.61 ± 0.04 min^{-1} and 300 nM MRPP3 (▲), 0.79 ± 0.04 min^{-1}. (B) The cleavage of ^{32}P-labeled (mt)pre-tRNA^{Tyr} (~0.01 nM) catalyzed by varied concentrations of MRPP3 (0.14 mol zinc/mol MRPP3) in 30 mM MOPS, pH 7.6, 150 mM NaCl, and 1 mM $MgCl_2$ at 37°C. The measured values for k_{obs} are: 50 nM MRPP3 (○), 0.0053 ± 0.0006 min^{-1}; 70 nM MRPP3 (□), 0.0063 ± 0.0001 min^{-1}; 100 nM MRPP3 (◇), 0.0079 ± 0.0003 min^{-1} ; 150 nM MRPP3 (▽), 0.009 ± 0.0003 min^{-1} ; 200 nM MRPP3 (△), 0.01 ± 0.0004 min^{-1} and 275 nM MRPP3 (◢), 0.01 ± 0.0004 min^{-1}. (C) The dependence of the observed rate constant, k_{obs}, for catalysis of (mt)pre-tRNA^{Tyr} cleavage on the MRPP3 concentration. The values for k_{max} and $K_{1/2}$ of 0.9 Zn/MRPP3 (●) are 3.0 ± 0.8 min^{-1} and 790 ± 300 nM respectively, when Eq 2 Is fit to the data. The values for $k_{max}/K_{1/2}$ of 0.003 ± 0.0001 min^{-1}nM^{-1} (0.9 Zn/MRPP3 (●)) and 5 ± 0.7 ×10^{-5} min^{-1}nM^{-1} (0.14 Zn/MRPP3 (■)) are obtained from a fit of Eq. 3 to the data.

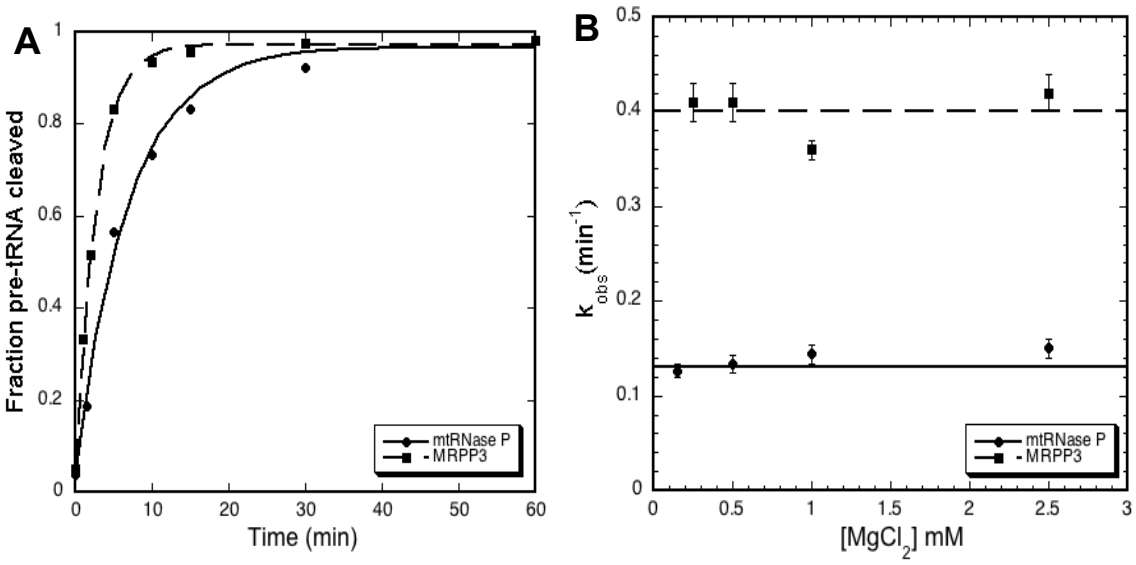

Figure 4-9: (A) Cleavage of (mt)pre-tRNA^{Tyr} catalyzed by MRPP3 and MRPP1:MRPP2:MRPP3 complex in 2:4:1 ratio under single turnover conditions. ^{32}P-labeled (mt)pre-tRNA^{Tyr} (~0.01 nM) was incubated with 100 nM of MRPP3 (0.9 mol Zn/mol protein) and 200:400:100 nM of MRPP1:MRPP2:MRPP3 ([E]/[S] ≥ 5-fold) in 30 mM MOPS, pH 7.6, 150 mM NaCl and 1 mM $MgCl_2$ at 37^{o}C. Eq. 1 was fit to the time-dependence of the fraction of pre-tRNA cleaved catalyzed by MRPP3 or MRPP1:MRPP2:MRPP3 complex. The k_{obs} for (mt)pre-tRNA^{Tyr} catalyzed by MRPP3 (■) is 0.36 ± 0.01 min^{-1} and by the MRPP1:MRPP2:MRPP3 complex (●) is 0.14 ± 0.01 min^{-1}. (B) Magnesium ion dependence of the single turnover rate constant for cleavage of (mt)pre-tRNA^{Tyr} catalyzed by MRPP3 or MRPP1:MRPP2:MRPP3 complex. In the absence of Cohex, the k_{obs} is not dependent on the magnesium concentration (0.25 - 2.5 mM magnesium). The values of k_{obs} are 0.4 ± 0.06 min^{-1} for MRPP3 (■) and 0.13 ± 0.03 min^{-1} for the MRPP1:MRPP2:MRPP3 complex (●).

Discussion

Subunit structure of mtRNase P

The recently discovered human mtRNase P contains one or more protein subunits but does not contain a catalytic RNA subunit, as observed for the well-studied ribonuclear complex RNase P from bacteria, archea and eukaryotes (14,18,35). Rossmanith and coworkers suggest that the three MRPP1, MRPP2 and MRPP3 subunits are essential for human mtRNase P catalysis (14). However, the role of each of these protein subunits in the human mtRNase P is still unclear. During purification of MRPP1 using Ni(II)-IMAC resin, MRPP2 co-eluted with MRPP1, suggesting that these two proteins form a complex. Both the MRPP1 and MRPP2 have putative RNA-binding domains known as Rossmann-fold and are proposed to play a role in substrate recognition. Bioinformatic domain analysis of MRPP3 identifies two PPR motifs, which have been suggested to be important for RNA binding. The PPR motif is a 35 amino acids tandem repeat protein and has 2 to 26 tandem arrays. The PPR have been involved in post transcriptional modification process, including editing events, RNA splicing and maturation and RNA stabilization (36). The gel mobility shift assays indicate that chloroplast PPR proteins such as PPR5 and CRP1 bind to the single stranded 31-mer RNA and unspliced trnG-UCC, a pre-tRNA that associate with group II intron, respectively (37). Furthermore, 9 to 6 nucleotides deletion from the 5' and 3' end of the unspliced trnG-UCC decrease the affinity for PPR5, suggesting that PPR proteins have a RNA binding domain. The PPR motifs are related to TPR motif that form antiparallel α-helices and a superhelix if

> two tandem arrays presence. Therefore, structure prediction of the PPR motif suggested that PPR motif has similar tertiary structure as the TPR motif (36). Additionally, sequence homology identifies several conserved aspartate and histidine residues that are proposed to form a novel metallonuclease family (see Figure 4-1).

Two years after identification of human mtRNase P, a second proteinaceous RNase P from *Arabidopsis thaliana* is unearthed, known as PRORP1 (13). PRORP1 is a single protein subunit that is localized to mitochondrial and chloroplast in plants and is sufficient to catalyze cleavage of the 5' end of the pre-tRNA. Based on sequence homology, PRORP1 is ortholog to the MRPP3 subunit that is also composed of two PPR motifs and conserved aspartates and histidine residues at the C-terminus (Figure 4-1). The discovery of PRORP1 catalysis of pre-tRNA cleavage led to the question as to whether all three subunits are essential for the catalytic activity of the mitochondrial enzyme. In our experiments, under single turnover condition, MRPP3 alone catalyzes cleavage of the 5' end of the (mt)pre-tRNA^{Tyr} to completion within an hour, which is similar to the (mt)pre-tRNA^{Tyr} cleavage by the MRPP1:MRPP2:MRPP3 complex, forming a 46 nucleotides leader (Figure 4-2). In addition, double mutation of the two conserved aspartate residues to alanine (D478A/D479A) in the MRPP3, which proposed to coordinate the catalytic metal ions, significantly decrease the MRPP3 catalytic activity (Figure 4-3). Furthermore, PRORP1 catalytic activity is also abolished when the same double aspartate residues were mutated to alanine (D474A/D475A) (13). These data demonstrate that MRPP3 alone is

sufficient to catalyze (mt)pre-tRNA cleavage, as previously observed for PRORP1.

Additionally we evaluated whether the other two subunits proposed to be essential for the catalytic activity of mtRNase P enhanced the catalytic activity. Contrary to our expectations, addition of the MRPP1/MRPP2 subunit to MRPP3 decreased the single turnover rate constant for cleavage of (mt)pre-tRNA^{Tyr} cleavage by 2 – 3-fold under a variety of conditions. These data indicate that addition of the MRPP1/MRPP2 complex to MRPP3 does NOT enhance the catalytic activity of the human mtRNase P at saturating magnesium ions. The lack of enhancement of activity under the single turnover conditions with sub-saturating enzyme also indicates that MRPP1/MRPP2 does not increase pre-tRNA affinity. Therefore, our data suggest that the human mitochondrial RNase P, like the *Arabidopsis* chloroplast enzyme, requires a single subunit, MRPP3, for catalytic activity. At this point, a role for MRPP1 and MRPP2 in catalysis of pre-tRNA cleavage is unclear. Previous studies suggested that all three MRPP proteins components are required for (mt)pre-tRNA cleavage, however, in our single turnover condition, the MRPP3 is sufficient to catalyze the (mt)pre-tRNA cleavage. The discrepancy between these two results could be due to several factors, such as contaminating metal ions that could potentially inhibit the catalytic activity of MRPP3, lack of zinc metal ions, which is important in enhancing the MRPP3 catalytic activity or nucleic acids contamination in the MRPP3 proteins. Alternatively, it is possible that 2:4:1 ratio of MRPP1:MRPP2:MRPP3 protein is not optimal for mtRNase P catalytic activity

and the ratio of MRPP1:MRPP2:MRPP3 protein need to be optimized or MRPP1 and MRPP2 require cofactors such as SAM and NAD^+ to enhance the mtRNase P catalytic activity. Therefore, the vitality of MRPP1 and MRPP2 in human mtRNase P catalysis need to be carefully examined in the future.

Zinc Dependence of MRPP3

Divalent metal ions play an essential role in metalloprotein catalysis, where they can be either catalytic and/or structural functions. All known ribozyme RNase P require Mg^{2+} ions for RNase P catalysis, *in vivo* (26,32). In other enzymes, conserved aspartate and histidine residues have been shown to coordinate metal ions, such as magnesium, zinc, and iron to form a metal active site of the metalloproteins (33,38). To identify whether MRPP3 contains any high affinity metal binding sites, bound metal ions were measured using ICP-MS. After fractionation using Ni(II)-IMAC, a number of metal ions (Mg, Fe, Ni and Zn) co-elute with MRPP3 (Table 4-1). To remove contaminating metal ions, MRPP3 was dialyzed against EDTA followed dialysis against metal free buffer. This procedure successfully removed all of the contaminating Fe, Mg and Ni; however, fortuitously, the amount of bound zinc resulting from this procedure varied from 0.1 mol Zn/ mol MRPP3 to 0.9 mol Zn/ mol MRPP3. When 0.15 mg of MRPP3 is dialyzed in 1L EDTA buffer, the Zn content of MRPP3 is ~ 0.1 mol, while dialyzing ~ 1.5 mg of MRPP3 in the 1L EDTA buffer, MRPP3 has stoichiometric bound zinc to the protein. Therefore, the amount of bound zinc to MRPP3 could be varied when the dialyzing different MRPP3 concentration in 1L EDTA buffer. Furthermore, the single turnover rate constant measured under standard

conditions (1 mM $MgCl_2$) varies with the zinc content of the enzyme; MRPP3 with nearly stoichiometric bound zinc (0.9 mol Zn/ mol MRPP3) catalyzes cleavage of (mt)pre-$tRNA^{Tyr}$ 36-fold faster than MRPP3 containing 0.14 mol Zn/ mol MRPP3. This is more activation that would be expected from the 6-fold increase in zinc content, suggesting that that the 0.14 mol zinc may not be bound to the correct site, perhaps due to structural alterations of the enzyme. Consistent with this, incubation of the apo-enzyme with zinc was not able to reactivate the enzyme. Frequently it is difficult to reconstituted cysteine-containing zinc sites due to cysteine oxidation in the apo-enzyme. This is the first evidence that the catalytic component of mtRNase P, MRPP3, requires a tightly bound zinc for function that serves either a catalytic and/or structural role.

MRPP3 is Activated by Magnesium

Evaluation of the role of additional divalent cations in activating MRPP3 is complicated by the requirement of divalent cations to stabilize the folded structure of pre-tRNA. To circumvent this difficulty, we used the outer sphere magnesium mimic, cobalt hexammine to stabilize the pre-tRNA structure. Under these conditions, the zinc-bound enzyme does not catalyze cleavage of the 5' end of (mt)pre-$tRNA^{Tyr}$ cleavage in the presence of cohex alone, cohex with Zn^{2+} ions or cohex with Fe^{2+} ions (Figure 4-5A, 5C, 5D). However, in the presence of cohex with Mg^{2+} ions, MRPP3 catalyzes complete cleavage of the 5' end of (mt)pre-$tRNA^{Tyr}$ (Figure 4-5B). These data demonstrate that in addition to the tightly bound zinc ion, Mg^{2+} ions activate the catalytic activity of MRPP3, and this requirement for Mg^{2+} cannot be fulfilled by Zn^{2+} or Fe^{2+} ions. In the presence of

cohex, the k_{obs} for (mt)pre-tRNA cleavage is dependent on the Mg^{2+} ion concentration, with a k_{max} of 0.16 ± 0.02 min^{-1}, $K_{1/2,}^{Mg}$ of 0.3 ± 0.1 mM and a hill constant, n_H = 1.2 ± 0.4, indicating that MRPP3 has a minimum of one magnesium binding site with an apparent affinity of ~ 300 μM (Figure 4-6B). In the absence of cohex, the activity is independent of Mg^{2+} concentration above 250 μM suggesting that the Mg^{2+} affinity is enhanced. These data suggest that cohex competes with the magnesium binding site, as previously observed in for other enzymes (27). The estimate for readily exchangeable Mg(II) in mammalian cells is ~ 1 mM (39-41), which is sufficient to activate MRPP3 activity *in vivo.* Together these results demonstrate that MRPP3 requires both magnesium and zinc cofactors to activate the catalytic activity. Both magnesium and zinc can function to stabilize the catalytic transition state or magnesium could play a catalytic role while the zinc plays a role in stabilizing the MRPP3 structure.

Metal Ion Binding Sites in MRPP3

PFAM analysis of MRPP3 indicates a PPR motif followed by a zinc-binding motif and a nuclease metal binding domain. This putative zinc binding site could explain the catalytic requirement for bound zinc in MRPP3 (Figure 4-1). The proposed zinc-binding domain of the MRPP3 has three cysteine residues that are generally observed in a structural zinc site (33,42). Sequence alignments of MRPP3 homology indicate that two of these three cysteine residues are highly conserved (C348 and C351), while non-conserved cysteine are located at C367 of the MRPP3. However, sequence alignments of MRPP3 homologs also shown a highly conserved cysteine and histidine at C578 and H504 of the MRPP3.

Therefore, the structure zinc site of the MRPP3 could form by either four cysteine or three cysteine and a histidine residues to coordinate the zinc ligand (33,38).

The PFAM analysis predicted that the MRPP3 has a NYN domain, a nuclease metal domain that has four conserved aspartate residues (D409, D478, D479 and D499) (15). The NYN domain is proposed to have similar protein fold as the PIN and FLAP/5' → 3' exonuclease superfamilies and both have four conserved aspartate residues that are proposed to coordinate Mg^{2+} ions (5). Crystal structure of the a PIN domain of human SMG6, a nonsense-mediated mRNA decay (NMD) proteins, indicate three conserved aspartate residues, including D1251, D1353 and D1392 that could coordinate Mg^{2+} ion (corresponding to D409, D478 and D499 in the MRPP3) (43,44). Superimpose of the magnesium binding site of T4 RNase H, a FLAP nuclease family, to the SMG6 structure, suggest that D1251, D1353 and D1392 can form similar magnesium binding site as the T4 RNase H (44). Hence, the conserved aspartate residues (D409, D478 and D499) can form a magnesium binding site of the MRPP3. Furthermore, double mutation at D478 and D479 residues to alanine in the MRPP3 drastically decrease the MRPP3 catalytic activity, suggesting that the mutation of these aspartate residues affect the binding of the magnesium in the magnesium binding site (Figure 4-3). Therefore, we speculate that MRPP3 has at least one magnesium binding site that coordinates a catalytic Mg^{2+} ion as well as a zinc binding site that could be important for structural stabilization of MRPP3 or substrate binding.

In summary, the metal requirement of MRPP3 in human mtRNase P catalysis is explored. Investigation of the function of metal ions in human mtRNase P catalysis has demonstrated that MRPP3 is catalytically active alone *in vitro*, and therefore is the catalytic subunit (and likely the only essential subunit) of the human mtRNase P. Addition of MRPP1 and MRPP2 subunits to MRPP3 subunit moderately decrease the catalytic activity of the human mtRNase P. Furthermore, we have discovered a requirement for two metal ions, including at least one Mg^{2+} ion that activates catalysis and a tightly bound zinc ion that could serve to stabilize the structure of MRPP3 to activate catalysis.

References

1. Frank, D. N., and Pace, N. R. (1998) *Annu Rev Biochem* **67**, 153-180
2. Gopalan, V., Vioque, A., and Altman, S. (2002) *J Biol Chem* **277**, 6759-6762
3. McClain, W. H., Lai, L. B., and Gopalan, V. (2010) *J Mol Biol* **397**, 627-646
4. Guerrier-Takada, C., Gardiner, K., Marsh, T., Pace, N., and Altman, S. (1983) *Cell* **35**, 849-857
5. Anantharaman, V., and Aravind, L. (2006) *RNA Biol* **3**, 18-27
6. Kikovska, E., Svard, S. G., and Kirsebom, L. A. (2007) *Proc Natl Acad Sci U S A* **104**, 2062-2067
7. Pannucci, J. A., Haas, E. S., Hall, T. A., Harris, J. K., and Brown, J. W. (1999) *Proc Natl Acad Sci U S A* **96**, 7803-7808
8. Crary, S. M., Niranjanakumari, S., and Fierke, C. A. (1998) *Biochemistry* **37**, 9409-9416
9. Day-Storms, J. J., Niranjanakumari, S., and Fierke, C. A. (2004) *Rna* **10**, 1595-1608
10. Koutmou, K. S., Day-Storms, J. J., and Fierke, C. A. (2011) *RNA* **17**, 1225-1235
11. Koutmou, K. S., Zahler, N. H., Kurz, J. C., Campbell, F. E., Harris, M. E., and Fierke, C. A. (2010) *J Mol Biol* **396**, 195-208
12. Kurz, J. C., Niranjanakumari, S., and Fierke, C. A. (1998) *Biochemistry* **37**, 2393-2400
13. Gobert, A., Gutmann, B., Taschner, A., Gossringer, M., Holzmann, J., Hartmann, R. K., Rossmanith, W., and Giege, P. (2010) *Nat Struct Mol Biol* **17**, 740-744
14. Holzmann, J., Frank, P., Loffler, E., Bennett, K. L., Gerner, C., and Rossmanith, W. (2008) *Cell* **135**, 462-474
15. Bateman, A., Birney, E., Durbin, R., Eddy, S. R., Howe, K. L., and Sonnhammer, E. L. (2000) *Nucleic Acids Res* **28**, 263-266
16. Jackman, J. E., Montange, R. K., Malik, H. S., and Phizicky, E. M. (2003) *RNA* **9**, 574-585
17. Yang, S. Y., He, X. Y., and Schulz, H. (2005) *Trends Endocrinol Metab* **16**, 167-175
18. Rossmanith, W., and Holzmann, J. (2009) *Cell Cycle* **8**, 1650-1653
19. Yan, S. D., Fu, J., Soto, C., Chen, X., Zhu, H., Al-Mohanna, F., Collison, K., Zhu, A., Stern, E., Saido, T., Tohyama, M., Ogawa, S., Roher, A., and Stern, D. (1997) *Nature* **389**, 689-695
20. Yan, S. D., Shi, Y., Zhu, A., Fu, J., Zhu, H., Zhu, Y., Gibson, L., Stern, E., Collison, K., Al-Mohanna, F., Ogawa, S., Roher, A., Clarke, S. G., and Stern, D. M. (1999) *J Biol Chem* **274**, 2145-2156
21. Oppermann, U. C., Salim, S., Tjernberg, L. O., Terenius, L., and Jornvall, H. (1999) *FEBS Lett* **451**, 238-242

22. Ofman, R., Ruiter, J. P., Feenstra, M., Duran, M., Poll-The, B. T., Zschocke, J., Ensenauer, R., Lehnert, W., Sass, J. O., Sperl, W., and Wanders, R. J. (2003) *Am J Hum Genet* **72**, 1300-1307
23. Lukacik, P., Kavanagh, K. L., and Oppermann, U. (2006) *Mol Cell Endocrinol* **248**, 61-71
24. Anantharaman, V., Koonin, E. V., and Aravind, L. (2002) *J Mol Microbiol Biotechnol* **4**, 71-75
25. Beebe, J. A., and Fierke, C. A. (1994) *Biochemistry* **33**, 10294-10304
26. Beebe, J. A., Kurz, J. C., and Fierke, C. A. (1996) *Biochemistry* **35**, 10493-10505
27. Kurz, J. C., and Fierke, C. A. (2002) *Biochemistry* **41**, 9545-9558
28. Niranjanakumari, S., Day-Storms, J. J., Ahmed, M., Hsieh, J., Zahler, N. H., Venters, R. A., and Fierke, C. A. (2007) *Rna* **13**, 521-535
29. Niranjanakumari, S., Stams, T., Crary, S. M., Christianson, D. W., and Fierke, C. A. (1998) *Proc Natl Acad Sci U S A* **95**, 15212-15217
30. Sosnick, T. R. (2001) *Curr Protoc Nucleic Acid Chem* **Chapter 11**, Unit 11 15
31. Jones, C. I., Spencer, A. C., Hsu, J. L., Spremulli, L. L., Martinis, S. A., DeRider, M., and Agris, P. F. (2006) *J Mol Biol* **362**, 771-786
32. Smith, D., Burgin, A. B., Haas, E. S., and Pace, N. R. (1992) *J Biol Chem* **267**, 2429-2436
33. Dokmanic, I., Sikic, M., and Tomic, S. (2008) *Acta Crystallogr D Biol Crystallogr* **64**, 257-263
34. Zahler, N. H., Christian, E. L., and Harris, M. E. (2003) *Rna* **9**, 734-745
35. Evans, D., Marquez, S. M., and Pace, N. R. (2006) *Trends Biochem Sci* **31**, 333-341
36. Delannoy, E., Stanley, W. A., Bond, C. S., and Small, I. D. (2007) *Biochem Soc Trans* **35**, 1643-1647
37. Williams-Carrier, R., Kroeger, T., and Barkan, A. (2008) *RNA* **14**, 1930-1941
38. Dupureur, C. M. (2008) *Curr Opin Chem Biol* **12**, 250-255
39. Csernoch, L., Bernengo, J. C., Szentesi, P., and Jacquemond, V. (1998) *Biophys J* **75**, 957-967
40. Gattis, S. G., Hernick, M., and Fierke, C. A. (2010) *J Biol Chem* **285**, 33788-33796
41. Petrat, F., de Groot, H., and Rauen, U. (2001) *Biochem J* **356**, 61-69
42. Lovejoy, B., Cleasby, A., Hassell, A. M., Luther, M. A., Weigl, D., McGeehan, G., Lambert, M. H., and Jordan, S. R. (1994) *Ann N Y Acad Sci* **732**, 375-378
43. Eberle, A. B., Lykke-Andersen, S., Muhlemann, O., and Jensen, T. H. (2009) *Nat Struct Mol Biol* **16**, 49-55
44. Glavan, F., Behm-Ansmant, I., Izaurralde, E., and Conti, E. (2006) *EMBO J* **25**, 5117-5125

CHAPTER 5

CONCLUSIONS AND FUTURE DIRECTIONS

The objective of this research is to elucidate the substrate recognition of the pre-tRNA by bacterial RNase P and to investigate the catalytic mechanism of the human mtRNase P complex, including identifying important metal ions. These studies established that in bacterial RNase P, P RNA, P protein and metal ions function collectively to contribute to pre-tRNAs recognition. Additionally, the work presented in this thesis provides the first direct evidence of that MRPP3 is the catalytic subunit of mtRNase P and that catalytic activity requires both a high affinity bound zinc ion and a weaker bound Mg^{2+} ions.

Recognition of the N(-2) and N(-3) nucleotides in the leader of pre-tRNA by bacterial RNase P

Bacterial RNase P recognizes the tertiary structure of pre-tRNA (1-5) and makes sequence-specific contacts with the 3' CCA. Bioinformatics analysis of 161 bacterial pre-tRNA genes also suggest a sequence preference in the 5' leader, with stronger sequence preferences near the cleavage site (6,7). In this work, binding affinity studies of *B. subtilis* RNase P with *B. subtilis* pre-$tRNA^{Asp}$

illustrate a sequence preference for adenosine and purine at N(-2) and N(-3) nucleotides of the 5' leader by 10-fold and 6.5-fold, respectively. Sequence specific interactions between the non-conserved nucleotide, G319 at J18/2 of the P RNA, and the N(-2) nucleotide contribute to the sequence preference at this position. Compensatory mutation data suggest that the G319 forms a trans Watson-Crick-sugar-edge interaction with the base at N(-2) position of pre-tRNA. Additionally, binding affinity data indicate that the N61, R62, and R65 residues at the "RNR" motif of the P protein indirectly affect the N(-3) sequence selectivity.

Pre-tRNA binding to RNase P is a two step mechanism, where the initial collision of E and S forms an E·S complex followed by a conformation change that is stabilized by the addition of divalent metal ions, such as Mg^{2+} and Ca^{2+} ions (8). The N(-2) sequence selectivity is not Ca^{2+}-dependence, indicating that the interaction with the N(-2) base occurs at the initial E·S complex. However, the N(-3) sequence selectivity is dependent on the Ca^{2+} concentration, suggesting that the N(-3) sequence selectivity is coupled to the metal-stabilized conformational change of the E·S complex. The biochemical studies presented in chapter 2 demonstrate that both the sequence specificity of RNase P for the pre-tRNA leader and the metal-stabilized conformational change of the RNase P·pre-tRNA complex contribute to the RNase P substrate recognition.

Expression and purification of MRPP1, MRPP2 and MRPP3 in *E. coli*

Recombinant expression of MRPP1, MRPP2 and MRPP3 are performed using BL21(DE3)pLysS and Rosetta(DE3) cells in *E. coli*. Expression of these

recombinant proteins is induced by addition of high IPTG (1 mM IPTG) at low temperature (≤ 16^{o}C) to increase the protein yield and reduce proteolysis (8,9). The 6xHis-tagged recombinant proteins are purified using Ni(II)-IMAC column chromatography to ≥ 70% purity. The His-tags are cleaved from MRPP1, MRPP2 and MRPP3 using 3C or TEV protease with ≥ 50% efficiency, respectively. The cleaved proteins are further purified using a second Ni(II)-IMAC column. For MRPP3, a final DEAE column is used to remove contaminating nucleic acids. Metal ion contamination was observed in the protein samples after the first Ni(II)-IMAC purification. These metal ions can be eradicated from the recombinant proteins using chelating agents, such as EDTA, by overnight dialysis at 4^{o}C. The work presented in chapter 3 demonstrates that MRPP1, MRPP2, and MRPP3 are successfully expressed in *E. coli* cells and purified using affinity and anion-exchange chromatography.

MRPP3, the catalytic component of human mtRNase P

Previous experiments indicated that three subunits, MRPP1, MRPP2 and MRPP3, are required for catalyzing the 5' end maturation of human (mt)pre-tRNA^{Tyr}. In the published work, about 20% of (mt)pre-tRNA^{Tyr} is cleaved by the human mtRNase P at 5 min under single turnover conditions (10). Sequence conservation and PFAM analysis indicates that MRPP3 contains two PPR motifs, a zinc binding domain, and four highly conserved amino acids (3 aspartates and 1 histidine) that could be important for RNA binding and/or coordinating catalytic or structural metal ions (11). These data suggested that MRPP3 could be a

member of a new family of metallonucleases. Furthermore, PRORP1 from *Arabidopsis thaliana,* a homolog of MRPP3, is a single protein that catalyzes cleavage of the *Arabidopsis thaliana* (mt)pre-tRNA^{Cys} (12). In this work, we demonstrated that MRPP3 alone could also catalyze cleavage of (mt)pre-tRNA^{Tyr} under single turnover conditions with a k_{obs} of 0.36 ± 0.01 min^{-1} at 100 nM MRPP3 in the presence of 1 mM $MgCl_2$. This observed rate constant is not enhanced by the addition of MRPP1 and MRPP2. These data clearly demonstrate that the MRPP3 is the catalytic component and, possibly, only required subunit of human mtRNase P.

Identification of metal ions activating the MRPP3 catalysis

All known RNA-containing RNase P enzymes require Mg^{2+} ions for catalysis, *in vitro* (13-18). However, the metal dependence of the mtRNase P is unclear (10). ICP-MS analysis of MRPP3 after the initial Ni(II)-IMAC column indicated that high iron and zinc co-eluted with the enzyme. MRPP3 has three conserved aspartate and one conserved histidine residues located in the C-terminal domain, which have been proposed to coordinate catalytic metal ions (19,20). To evaluate the role of metal ions in activating MRPP3 compared to stabilizing the structure of the pre-tRNA substrate, the dependence of the catalytic activity of MRPP on divalent metal ions (Mg^{2+}, Fe^{2+} and Zn^{2+}) were measured in the presence of cohex. The pre-tRNA tertiary structure is stabilized by cohex (17). In the presence of cohex, MRPP3 catalytic activity is enhanced only by the addition of Mg^{2+} ions, but not Fe^{2+} and Zn^{2+} ions. These data suggest that catalytic activity

of MRPP3 requires a metal that can form inner sphere coordination with selectivity for Mg^2+. The dependence of the activity of MRPP3 on the Mg^{2+} is hyperbolic with $K_{1/2}^{Mg}$ of 300 ± 100 μM and n_H of 1.2 ± 0.4. Additionally, a ~1:1 ratio of Zn:MRPP3 enhances the catalytic activity of MRPP3 by 36-fold relative to the 0.14:1 ratio of Zn:MRPP3 suggesting that a tightly bound, stoichiometric zinc ion enhances catalytic activity. Addition of MRPP1 and MRPP2 to MRPP3 decreases the k_{obs} by 2- to 3-fold. The metal dependence studies presented in chapter 4 demonstrate that at least two types of metal ions are essential for MRPP3 activity. We speculate that Mg^{2+} ion is the catalytic metal ions, while a structural zinc may stabilize structure required for MRPP3 catalytic activity.

Future Directions

Determine the metal binding site of the MRPP3

Metal-dependent protein nucleases generally possess ≥ 2 highly conserved acidic active site residues that bind metal ion(s) (20,21). These metal ions can have either a structural or catalytic function. For example, the metal ion can activate catalysis by: coordinating the scissile phosphodiester, activating the nucleophile, stabilizing the transition state, and/or protonating the leaving group. Sequence alignments of MRPP3 homologs reveal eight conserved cysteine, aspartate, and histidine residues in the C-terminal domain that commonly coordinate Zn^{2+} (Asp, His, Cys) or Mg^{2+} (Asp) bound to proteins. The results in Chapter 4 demonstrate that MRPP3 contains at least one bound Mg^{2+} and one

bound zinc ion that are essential for efficient catalysis.. Pfam analysis of MRPP3 indicates a zinc binding domain and a NYN domain, which are proposed to coordinate a structural zinc and a catalytic Mg^{2+}, respectively (11,22). Pfam analysis indicates that the zinc binding domain of MRPP3 has three cysteine residues (Cys348, Cys351 and Cys367); however sequence alignments of MRPP3 indicate that only two of the three cysteines (Cys348 and Cys351) are conserved (Figure 4-1), suggesting that these two amino acids likely form 2 of the 3-4 ligands that coordinate a bound zinc ion; a conserved histidine in the NYN domain could be an additional ligand. Additionally, the three conserved aspartate residues could coordinate Mg^{2+} to activate catalysis. The structure of NYN (also called PIN) domains in SMG5 and SMG6, cofactors in Nonsense-mediated decay, visualize Mg^{2+} binding to 3 aspartate residues (23). Alanine substitution of ligands that coordinate catalytic and structural metal ions in metalloenzymes generally decrease the catalytic activity (>100-fold) significantly and/or increase the metal concentration required to activate catalysis (24).

Therefore, we propose to:

(1) Substitute alanine for the conserved aspartate and histidine residues in MRPP3 (D409, D478, D479 and H504) and measure the catalytic activity of MRPP3. The function of these residues in metal binding will be assessed by measuring the dependence of activity on both the magnesium and MRPP3 concentrations as well as the analyzing the metal content bound to the mutant MRPP3 subunits using ICP-MS.

(2) Identify the protein side chains that coordinate zinc in MRPP3. The three

cysteine residues in the zinc binding domain identified by pfam analysis (Cys 348, 351 and 367) will be substituted with alanine and the dependence of the activity of MRPP3 on zinc concentration will be measured. The zinc content of the mutant MRPP3 will be determined by ICP-MS analysis. If these cysteine residues coordinate the zinc metal, alanine mutation will sequester the zinc from the MRPP3 and decreased the MRPP3 catalytic activity. Mutations in other conserved His, Cys and Asp will be prepared and analyzed to identify additional zinc ligands.

Determine the roles of MRPP1 and MRPP2 in human mtRNase P catalysis

Single turnover measurement of the catalytic activity of the MRPP1/MRPP2/MRPP3 complex compared to MRPP3 alone indicates that the two additional subunits moderately decreases the observed cleavage activity. The reasons for this result are not clear. It is possible that MRPP1 and MRPP2 are not essential components on of human mtRNase P. However, this result could be explained by a number of other possibilities, including that ratio of subunits (MRPP1:MRPP2:MRPP3 ratio at 2:4:1) in these experiments is not optimal and/or additional cofactors, such as SAM or NAD^+ are required to see activation. Human mtRNase P activity has not yet been shown to correlate with the precise subunit stoichiometry and the effect of cofactors on activity have also not been explored. Hence, we propose to:

(1) Investigate the stoichiometry of the active mtRNase P complex by measuring the (mt)pre-$tRNA^{Tyr}$ cleavage under single (limiting substrate; k_{SS} and $K_{1/2}$)

and multiple turnover (excess substrate; k_{cat}, K_M, k_{cat}/K_M) conditions as a function of the subunit molar ratios (*e.g.* each subunit alone, 1:1:1, 1:4:1, 2:4:1, 2:2:2) and NaCl concentration.

(2) Measure the dependence of (mt)pre-tRNA^{Tyr} cleavage rate on enzyme concentration after the optimal ratio of MRPP1:MRPP2:MRPP3 is established. In the presence of 1 mM Mg^{2+} ions, the observed cleavage rate, k_{obs} is linearly dependent on MRPP3 concentration, with $k_{max}/K_{1/2}$ of 0.003 ± 0.0001 $min^{-1}nM^{-1}$. The linear dependence of k_{obs} on MRPP3 concentration suggests that the binding affinity of (mt)pre-tRNA^{Tyr} is in the μM range (scheme 1 and eq. 1). If the other subunits (MRPP1/MRPP2/MRPP3) enhance pre-tRNA affinity, then a hyperbolic dependence on the enzyme concentration should be observed under single turnover conditions, assuming that $k_{max} < k_{-1}$. This result would imply that the MRPP1 and MRPP2 contribute to human mtRNase P substrate recognition.

Scheme 1 $$E + S \underset{k_{-1}}{\overset{k_1}{\rightleftarrows}} ES \xrightarrow{k_{max}} E + P$$

Equation 1 $$k_{obs} = \frac{k_{\max} + [E]}{K_{1/2} + [E]}; \; K_{1/2} = \frac{k_{\max} + k_{-1}}{k_1}$$

(3) measure the (mt)pre-tRNA^{Tyr} cleavage by MRPP1:MRPP2:MRPP3 complex in the presence of SAM and NAD^+ cofactors. If the SAM and NAD^+ is essential in the mtRNase P catalysis, addition of SAM and NAD^+ cofactors to

the MRPP1:MRPP2:MRPP3 complex will enhance the cleavage rate of the (mt)pre-tRNA^{Tyr}.

Analyzing molecular recognition of human (mt)pre-tRNA

The secondary structure of all characterized tRNAs have a cloverleaf-shape, including an acceptor stem, D-stem/loop, T-stem/loop, and anticodon stem/loop (Figure 1-7) (25,26). Unlike the canonical nuclear tRNAs, (mt)tRNAs have non-canonical features, such as shortened or deleted stems and loops (27,28). There are only 22 (mt)tRNAs in the human mitochondrial genome and the (mt)pre-tRNAs features important for mtRNase P recognition are unknown. All three subunits, MRPP1, MRPP2 and MRPP3 have been proposed to contribute to human mtRNase P substrate recognition. The MRPP2 has a Rossmann NAD^+-binding fold that has been suggested to function as an RNA binding domain, while MRPP1 and MRPP3 have domains that have homology to RNA binding proteins (29-32). Furthermore, point mutations in human (mt)tRNAs have been linked to human mitochondrial dysfunction, such as mitochondrial myopathy, encephalopathy, lactic acidosis and stroke (MELAS) syndrome (33,34). ≥ 50% of point mutations in tRNA^{Ile}, tRNA^{Leu}, and tRNA^{Lys} have been identified to associate with the pathogenic diseases and are known as pathogenic mutation. Furthermore, pathogenic mutations in (mt)pre-tRNA^{Leu} decrease the cleavage efficiency of human mtRNase P (35). Hence, we will investigate the (mt)pre-tRNA features that are crucial for human (mt)RNase P recognition and examine whether pathogenic mutations in (mt)pre-tRNAs perturb mtRNase P-catalyzed 5'

end maturation. We propose to:

(1) Identify regions of (mt)pre-tRNA that bind to human mtRNase P by hydroxyl radical footprinting. Regions of the (mt)pre-tRNA backbone that contact the human mtRNase P will be protected from reaction with hydroxyl radicals generated from Fe-EDTA-catalyzed Fenton chemistry (36). The products of hydroxyl radical cleavage in the presence and absence of human mtRNase P will be compared and analyzed by PAGE. A decrease in cleavage by hydroxyl radicals will reduce the intensity of electrophoresis band for enzyme-substrate complex relative to the substrate alone. These results will allow us to compare the regions of pre-tRNA that are protected by binding to human mtRNase P complex.

(2) Determine specific regions of (mt)pre-tRNA that contact particular human mtRNase P subunits. Crosslinking experiments will be performed between human mtRNase P and (mt)pre-tRNA^{Tyr} with 4-thiouridine (4-thioU) incorporated at discrete positions, including the 5' leader, acceptor stem, D-stem loop, anticodon stem, and/or T-stem loop, as suggested by hydroxyl-radical footprinting data. 4-thioU is a photoreactive uridine analog that readily forms short-range RNA-RNA and RNA-protein crosslinks (37-39). To incorporate 4-thioU into the (mt)pre-tRNA^{Tyr}, chemically synthesized oligonucleotide containing 4-thioU will be ligated to the rest of the pre-tRNA prepared by *in vitro* transcription. Crosslinking will be initiated by UV irradiation (λ = 300 nm) of the mtRNase P•pre-tRNA complex and the crosslinked products will be isolated on a PAGE gel and

identified by mass spectrometry (MRPP1 ~49 kDa, MRPP2 ~26 kDa, MRPP3 ~65 kDa) after treatment with RNase. An alternative photoactive group, azidophenacyl can be used if no crosslinks are observed with 4-thioU-labeled pre-tRNA (40).

(3) Investigate the effect of (mt)tRNA pathogenic mutations on the efficiency of processing catalyzed by human mtRNase P. (mt)tRNA^{Ile} has one of the highest number of pathogenic mutations among the (mt)tRNAs. Therefore, (mt)pre-tRNA^{Ile} with 3' trailers will be prepared by site-directed mutagenesis with the following nucleotide substitutions: A7G, U12C, U27C, G40A, G51A, A59G, C62U. Single and multiple turnover parameters for cleavage of (mt)pre-tRNA^{Ile} catalyzed by human mtRNase P will be measured to evaluate the effect of these mutants on the (mt)pre-tRNA processing. The cleavage site selection of (mt)pre-tRNA^{Ile} mutants will also be determined from the mobility of the 5′ cleavage products, as described (41).

The future studies proposed in this chapter will elucidate the role of each MRPP subunit in mtRNase P catalysis, identify the binding sites for metal ions that activate human mtRNase P and determine the essential features of (mt)pre-tRNA for human mtRNase P recognition. These studies will provide insight into how the mechanism of this enzyme and into how a "proteinaceous" RNase P could evolve to adopt the functionality and molecular recognition of a RNA-mediated RNase P.

References

1. Hansen, A., Pfeiffer, T., Zuleeg, T., Limmer, S., Ciesiolka, J., Feltens, R., and Hartmann, R. K. (2001) *Mol Microbiol* **41**, 131-143
2. Kahle, D., Wehmeyer, U., and Krupp, G. (1990) *Embo J* **9**, 1929-1937
3. Loria, A., and Pan, T. (1997) *Biochemistry* **36**, 6317-6325
4. McClain, W. H., Guerrier-Takada, C., and Altman, S. (1987) *Science* **238**, 527-530
5. Thurlow, D. L., Shilowski, D., and Marsh, T. L. (1991) *Nucleic Acids Res* **19**, 885-891
6. Koutmou, K. S., Zahler, N. H., Kurz, J. C., Campbell, F. E., Harris, M. E., and Fierke, C. A. (2010) *J Mol Biol* **396**, 195-208
7. Zahler, N. H., Christian, E. L., and Harris, M. E. (2003) *Rna* **9**, 734-745
8. Esposito, D., and Chatterjee, D. K. (2006) *Curr Opin Biotechnol* **17**, 353-358
9. Jahic, M., Wallberg, F., Bollok, M., Garcia, P., and Enfors, S. O. (2003) *Microb Cell Fact* **2**, 6
10. Holzmann, J., Frank, P., Loffler, E., Bennett, K. L., Gerner, C., and Rossmanith, W. (2008) *Cell* **135**, 462-474
11. Bateman, A., Birney, E., Durbin, R., Eddy, S. R., Howe, K. L., and Sonnhammer, E. L. (2000) *Nucleic Acids Res* **28**, 263-266
12. Gobert, A., Gutmann, B., Taschner, A., Gossringer, M., Holzmann, J., Hartmann, R. K., Rossmanith, W., and Giege, P. (2010) *Nat Struct Mol Biol* **17**, 740-744
13. Beebe, J. A., Kurz, J. C., and Fierke, C. A. (1996) *Biochemistry* **35**, 10493-10505
14. Guerrier-Takada, C., Gardiner, K., Marsh, T., Pace, N., and Altman, S. (1983) *Cell* **35**, 849-857
15. Kikovska, E., Svard, S. G., and Kirsebom, L. A. (2007) *Proc Natl Acad Sci U S A* **104**, 2062-2067
16. Koutmou, K. S., Casiano-Negroni, A., Getz, M. M., Pazicni, S., Andrews, A. J., Penner-Hahn, J. E., Al-Hashimi, H. M., and Fierke, C. A. (2010) *Proc Natl Acad Sci U S A* **107**, 2479-2484
17. Kurz, J. C., and Fierke, C. A. (2002) *Biochemistry* **41**, 9545-9558
18. Pannucci, J. A., Haas, E. S., Hall, T. A., Harris, J. K., and Brown, J. W. (1999) *Proc Natl Acad Sci U S A* **96**, 7803-7808
19. Dokmanic, I., Sikic, M., and Tomic, S. (2008) *Acta Crystallogr D Biol Crystallogr* **64**, 257-263
20. Dupureur, C. M. (2008) *Curr Opin Chem Biol* **12**, 250-255
21. McCall, K. A., Huang, C., and Fierke, C. A. (2000) *J Nutr* **130**, 1437S-1446S
22. Anantharaman, V., and Aravind, L. (2006) *RNA Biol* **3**, 18-27
23. Eberle, A. B., Lykke-Andersen, S., Muhlemann, O., and Jensen, T. H. (2009) *Nat Struct Mol Biol* **16**, 49-55

24. Jackman, J. E., Raetz, C. R., and Fierke, C. A. (2001) *Biochemistry* **40**, 514-523
25. Kim, S. H., Suddath, F. L., Quigley, G. J., McPherson, A., Sussman, J. L., Wang, A. H., Seeman, N. C., and Rich, A. (1974) *Science* **185**, 435-440
26. Shi, H., and Moore, P. B. (2000) *RNA* **6**, 1091-1105
27. Messmer, M., Putz, J., Suzuki, T., Sauter, C., Sissler, M., and Catherine, F. (2009) *Nucleic Acids Res* **37**, 6881-6895
28. Putz, J., Dupuis, B., Sissler, M., and Florentz, C. (2007) *RNA* **13**, 1184-1190
29. Anantharaman, V., Koonin, E. V., and Aravind, L. (2002) *J Mol Microbiol Biotechnol* **4**, 71-75
30. Delannoy, E., Stanley, W. A., Bond, C. S., and Small, I. D. (2007) *Biochem Soc Trans* **35**, 1643-1647
31. Lukacik, P., Kavanagh, K. L., and Oppermann, U. (2006) *Mol Cell Endocrinol* **248**, 61-71
32. Small, I. D., and Peeters, N. (2000) *Trends Biochem Sci* **25**, 46-47
33. Florentz, C., Sohm, B., Tryoen-Toth, P., Putz, J., and Sissler, M. (2003) *Cell Mol Life Sci* **60**, 1356-1375
34. Wittenhagen, L. M., and Kelley, S. O. (2003) *Trends Biochem Sci* **28**, 605-611
35. Rossmanith, W., and Karwan, R. M. (1998) *FEBS Lett* **433**, 269-274
36. Brenowitz, M., Chance, M. R., Dhavan, G., and Takamoto, K. (2002) *Curr Opin Struct Biol* **12**, 648-653
37. Christian, E. L., and Harris, M. E. (1999) *Biochemistry* **38**, 12629-12638
38. Moore, M. J., and Sharp, P. A. (1992) *Science* **256**, 992-997
39. Niranjanakumari, S., Stams, T., Crary, S. M., Christianson, D. W., and Fierke, C. A. (1998) *Proc Natl Acad Sci U S A* **95**, 15212-15217
40. Schwartz, I., and Ofengand, J. (1974) *Proc Natl Acad Sci U S A* **71**, 3951-3955
41. Brannvall, M., and Kirsebom, L. A. (1999) *J Mol Biol* **292**, 53-63